Supplementary Material

Synthesis and photophysical evaluation of isoleptic Pt(II) and Pd(II) complexes utilizing N^N^N ligands as luminophoric chelators with different ancillary ligands

Silpa Padmakumar Sheelakumari,[1][2]‡ María Victoria Cappellari,[1][2]‡ María Belen Rivas Aiello,[1][2] Alexander Hepp,[1] Cristian A. Strassert[1][2]*

[1] Institut für Anorganische und Analytische Chemie, Universität Münster, Corrensstraße 28/30, D-48149 Münster, Germany.

[2] CeNTech, CiMIC, SoN, Universität Münster, Heisenbergstraße 11, D-48149 Münster, Germany

*Corresponding author e-mail: ca.s@uni-muenster.de (Cristian A. Strassert) ł

These authors have equally to contributed this work (shared first authorship).

Content

1. Synthesis of pyridine-2,6-bis(carboximidamide) dihydrochloride (1)

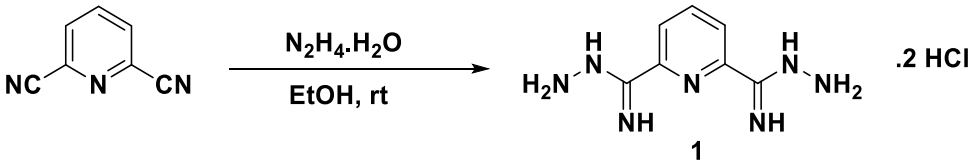

To obtain the intermediate **1**, we followed the procedure reported in the literature.[1] Firstly, pyridine-2,6-dicarbonitrile (5.0 g, 25.9 mmol, 1.0 eq) was dissolved in ethanol (EtOH) (120 mL) and hydrazine monohydrate (39 mL, 517.8 mmol, 20 eq) was slowly added. The reaction mixture was stirred at room temperature (RT) for 24 h, yielding a pale-yellow precipitate in a pale-yellow solution. The precipitate was filtered off, washed twice with cold EtOH, and dried to yield a pale-yellow solid, namely the pyridine-2,6-bis(carboximidhydrazide) (6.3 g, 83%).

2. Synthesis of 2,6-bis(3-(trifluoromethyl)-1*H*-1,2,4-triazol-5-yl)pyridine (CF_3)

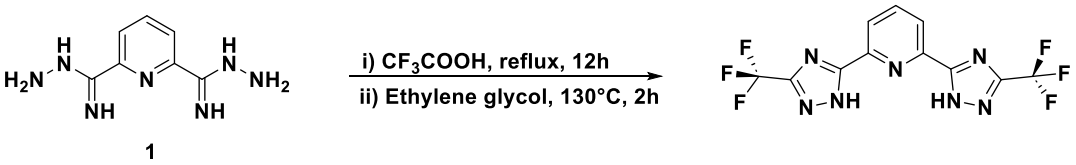

Pyridine-2,6-bis(carboximidhydrazide) (**1**) (5.0 g, 25.9 mmol, 1 eq) was dissolved in 30 mL (excess) of trifluoroacetic acid (TFA) and the mixture was refluxed for 18 h. TFA was then removed under reduced pressure and ethylene glycol (30 mL) was added. The mixture was heated to 150°C for 4 h and cooled down to RT to obtain a brown solution. To the solution, 20 mL H_2O was added and the mixture was stirred for 30 minutes to yield a brown solid. After filtration, the solid was washed three times with H_2O followed by EtOH to yield a white powder, the desired product (7.2 g, 80%).[1]

^{1}H-NMR (400 MHz, DCM-d_2/CD_3OD): δ (ppm) = 8.26 (d, 2H, H_2), 8.15 (t, 3H, H_1).

^{19}F-NMR (376 MHz, DCM-d_2): δ (ppm) = -65.73.

EM-MS-ESI (MeOH, $C_{11}H_5F_6N_7$, *m/z*): calcd. for $[M+H]^+$ = 350.0584, found for $[M+H]^+$ = 350.0584; calcd. for $[M+Na]^+$ = 373.0425, found $[M+Na]^+$ = 373.0425.

3. Synthesis of 2,6-bis(3-(*tert*-butyl)-1*H*-1,2,4-triazol-5-yl)pyridine (^{t}bu)

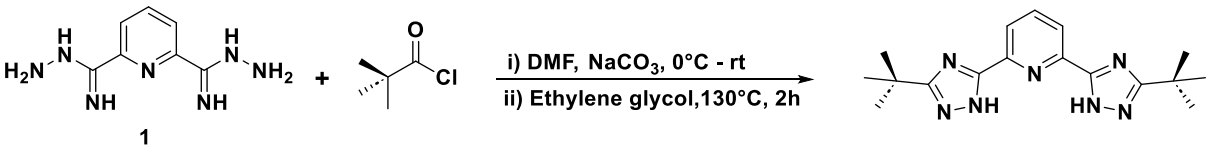

1

With the exception of a few minor modifications, this ligand precursor was synthesized according to literature procedures.[2] A flame-dried, nitrogen-purged Schlenk tube was loaded with 1 (4 g, 20.7 mmol) and anhydrous $NaCO_3$ (4.6 g, 43.5 mmol). 40 mL of dry *N,N*-dimethylformamide (DMF) were added and the suspension was cooled to 0°C. After cooling the suspension, $(CH_3)_3CCOCl$ (41.5 mmol, 5.1 mL) was slowly added under vigorous stirring to the same tube. Upon allowing the reaction mixture to warm up to reach room temperature overnight, a precipitate was formed. The suspension was then filtered off and rinsed with H_2O. The solid was dried under vacuum and used without further purification for the next step, in which it was heated in ethylene glycol (40 mL) to 160°C and cooled down to room temperature within 4 h. A precipitate was formed after adding the excess H_2O (40 mL) to the reaction mixture, then filtered off and dried. The crude product was purified by column chromatography on silica gel with *n*-hexane / ethylacetate (EtOAc) (8:2) as the eluent to give the ligand precursor with ^{t}bu-substitution as a white solid (2.2 g, 32 %).

^{1}H-NMR (400 MHz, DCM-d_2/CD_3OD): δ(ppm) = 8.15 (d, 2H, H_2), 7.95 (t, 3H, H_1), 1.45 (s, 18H, H_3).

EM-MS-ESI (MeOH, $C_{17}H_{23}N_7$, *m/z*): calcd. for $[M+H]^+$ = 326.2095, found for $[M+H]^+$ = 326.2095; calcd. for $[M+Na]^+$ = 348.1907, found for $[M+Na]^+$ = 348.1907.

4. Synthesis of the Pt(II) complexes [CF_3-Pt-AmPy], [^{t}bu-Pt-AmPy] and [^{t}bu-Pt-CNR]

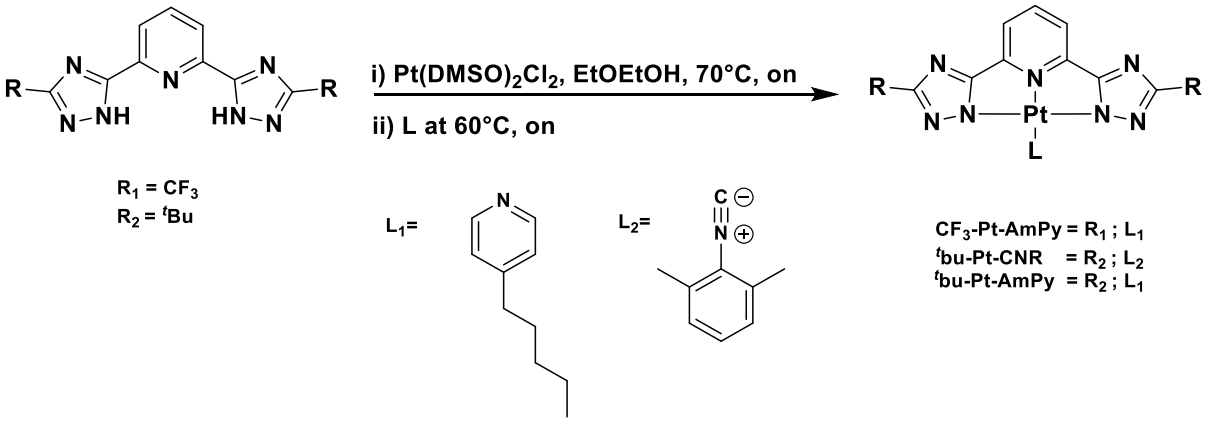

The complexation of the tridentate 2,6-bis(3-(*tert*-butyl/trifluoromethyl)-1*H*-1,2,4-triazol-5-yl)pyridine luminophores was performed using $Pt(DMSO)_2Cl_2$ by adapting literature

procedures.[2] $Pt(dmso_2)Cl_2$ (100 mg, 0.23 mmol, 1 eq) and the ligand precursors (1 eq) were suspended in 2-ethoxyethanol (EtOEtOH) (20 mL). The solution was purged by bubbling with argon for 10 min and subsequently stirred at 70 °C overnight. Once the intermediate was formed, the specific ancillary ligands **L_1** and **L_2** (amyl pyridine or 2,6-dimethyl phenyl isocyanide, 1 eq) were added to the reaction mixture at 60° C and stirred overnight. After cooling down to room temperature, H_2O was added to form a coloured precipitate. After filtering off, washing with H_2O and drying, the compound was purified by silica gel column chromatography with DCM/MeOH as the eluent to yield the complexes.

CF_3-Pt-AmPy:

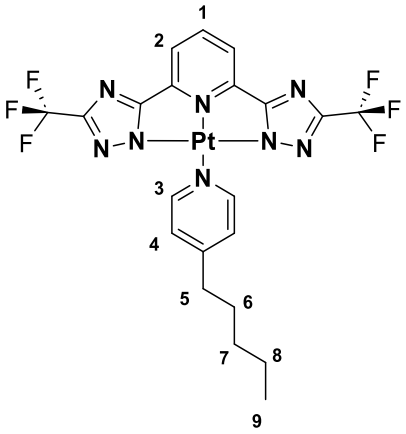

Greenish-yellow solid (128 mg, 64.7 %).

^{1}H-NMR (400 MHz, DCM-d_2): δ (ppm) = 9.31 (d, J = 6.1 Hz, 2H, H_3), 8.04 (t, J = 7.9 Hz, 1H, H_1), 7.75 (d, J = 7.9 Hz, 2H, H_2), 7.37 (d, J = 6.0 Hz, 2H, H_4), 3.35 (d, 2H, H_3), 3.25 (br., 6H, H_5), 2.75 (t, J = 7.9 Hz, 2H, H_6), 1.41 – 1.33 (m, 4H, $H_{7\text{-}8}$), 0.91 (br., J = 6.9 Hz, 3H, H_9).

^{19}F-NMR (376 MHz, DCM-d_2): δ (ppm) = -64.75.

EM-MS-ESI (MeOH, $C_{21}H_{18}F_6N_8Pt$, *m/z*): calcd. for $[M+H]^+$ = 691.1261, found for $[M+H]^+$ = 691.1261; calcd. for $[M+Na]^+$ = 714.1261, found for $[M+Na]^+$ = 714.1261.

^{t}bu-Pt-AmPy:

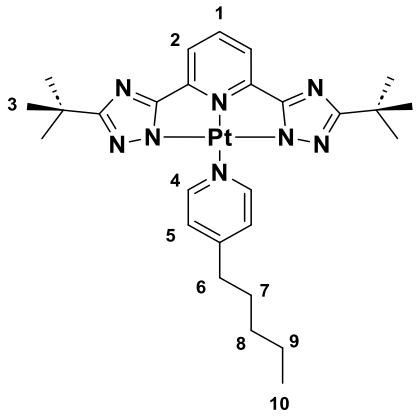

Yellowish solid (152 mg, 74%).

^{1}H-NMR (400 MHz, DCM-d_2): δ (ppm) = 10.00 – 9.87 (m, 2H, H_4), 7.84 (t, J = 8.1 Hz, 1H, H_1), 7.55 (dd, J = 9.6, 7.9 Hz, 2H, H_2), 7.37 (d, J = 6.9 Hz, 2H, H_5), 2.73 (d, J = 7.7 Hz, 2H, H_6), 1.82 – 1.68 (m, 2H, H_7), 1.44 (s, 17H, H_3), 1.38 (td, J = 3.7, 1.7 Hz, 4H, $H_{9\text{-}8}$), 0.99 – 0.87 (m, 3H, H_{10}).

EM-MS-ESI (MeOH, $C_{27}H_{36}N_8Pt$, *m/z*): calcd. for $[M+H]^+$ = 668.2790, found for $[M+H]^+$ = 668.2790; calcd. for $[M+Na]^+$ = 672.231, found for $[M+Na]^+$ = 672.231.

^{t}bu-Pt-CNR:

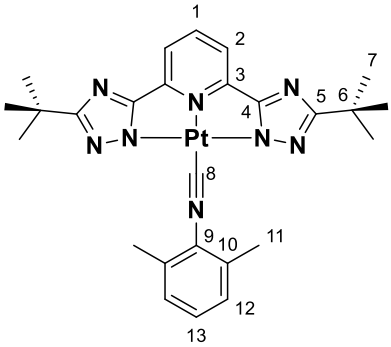

Yellowish solid (145 mg, 73%).

^{1}H-NMR (500 MHz, DCM-d_2/CD_3OD): δ (ppm) = 8.07 (t, J = 8.0 Hz, 1H, H_1), 7.82 (d, J = 8.0 Hz, 2H, H_2), 7.31 (m, 1H, H_{12}), 7.20 (d, 2H, H_{11}), 2.62 (s, 6H, H_{13}), 1.39 (s, 18H, H_7).

^{13}C-NMR (101 MHz, DCM-d_2): δ (ppm) = 174.31 (C_5), 163.9 (C_4),150.09 (C_8), 145.19 (C_1), 145.2 (C_3) 137.38 (C_{10}), 130.81 (C_{13}), 128.55 (C_{12}), 126.4 (C_9), 118.04 (C_2), 33.5 (C_6), 29.84 (C_7), 18.68 (C_{11}).

EM-MS-ESI (MeOH, $C_{26}H_{30}N_8Pt$, *m/z*): calcd. for $[M+H]^+$ = 649.2310, found for $[M+H]^+$ = 649.2310; calcd. for $[M+Na]^+$ = 690.2790, found for $[M+Na]^+$ = 668.2790.

5. Synthesis of the Pd(II) complexes [CF_3-Pd-AmPy], [^{t}bu-Pd-AmPy] and [^{t}bu-Pd-CNR]

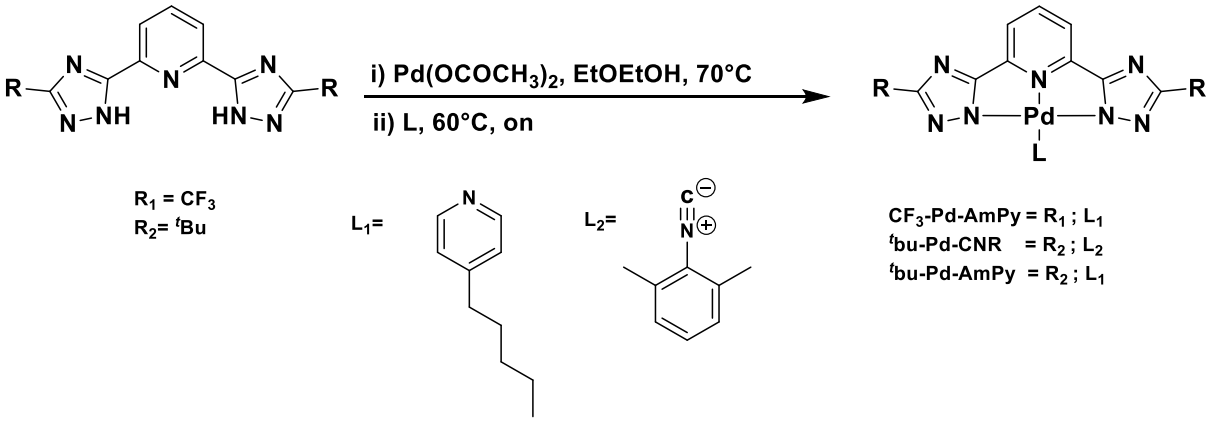

The complexation of Pd(II) with the tridentate luminophores 2,6-bis(3-(*tert*-butyl/trifluoromethyl)-1*H*-1,2,4-triazol-5-yl)pyridine was performed using palladium acetate ($Pd(CH_3COO)_2$). $Pd(CH_3COO)_2$ (100 mg, 0.44 mmol, 1 eq) and the N^N^N ligand precursors (1 eq) were suspended in EtOEtOH (20 mL). The solution was purged by bubbling with argon for 10 min and subsequently stirred at 70 °C overnight. Once the intermediate is formed, the specific ancillary ligands **L_1** and **L_2** (amyl pyridine or 2,6-dimethyl phenyl isocyanide, 1 eq) were added to the reaction mixture at 60° C and kept stirring overnight at 60° C. Next day, after cooling down to room temperature, H_2O was added to the mixture and a coloured precipitate was formed. After filtering off, washing with H_2O and drying, the compound was purified by silica gel column chromatography with MeOH:DCM (1:99) as the eluent to collect the complexes.

CF_3-Pd-AmPy:

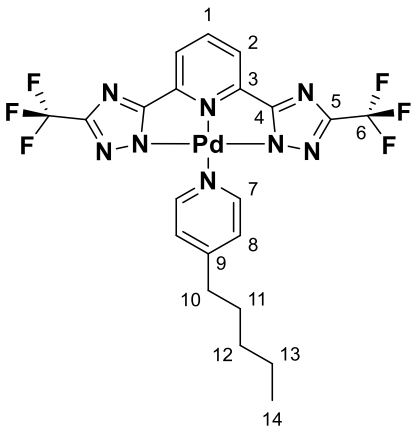

Yellowish solid (123 mg, 72 %).

^{1}H-NMR (400 MHz, DMF-d_7): δ (ppm) = 9.02 – 8.96 (br., 2H, H_7), 8.31 (t, J = 7.9 Hz, 1H, H_1), 8.02 (s, 1H), 7.75 (d, J = 7.9 Hz, 2H, H_2), 7.53 – 7.47 (br., 2H, H_8), 2.85 – 2.71 (m, 2H, H_{13}), 1.80 – 1.68 (br., 2H, H_{10}), 1.40 (br., J = 3.6 Hz, 4H, $H_{11\text{-}12}$), 0.98 – 0.90 (m, 3H, H_{14}).

^{13}C-NMR (126 MHz, DMF-d_7): δ (ppm) = 163.60 (C_4), 158.16 (C_9), 152.52 (C_7), 151.93 (C_5), 147.80 (C_3), 145.19 (C_1), 126.76 (C_8), 121.76 (C_6), 119.62 (C_2), 35.75 (C_{10}), 35.59 (C_{11}), 31.75 (C_{12}), 22.70 (C_{13}), 14.01 (C_{14}).

^{19}F-NMR (376 MHz, DMF-d_7): δ (ppm) = -64.16 (d, J = 1.9 Hz).

EM-MS-ESI (MeOH, $C_{21}H_{18}F_6N_8Pd$, *m/z*): calcd. for $[M+H]^+$ = 603.0674, found for $[M+H]^+$ = 603.0677.

^{t}bu-Pd-AmPy:

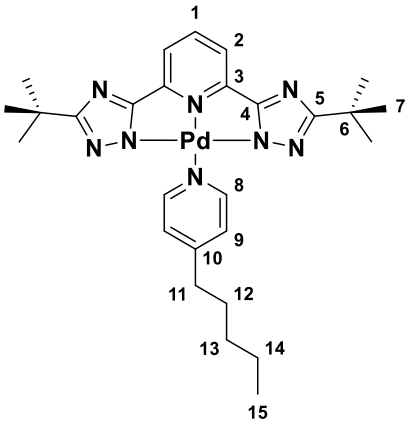

Greenish-yellow solid (123 mg, 72 %).

^{1}H-NMR (500 MHz, DCM-d_2): δ (ppm) = 9.69 – 9.64 (m, 2H, H_8), 7.89 (t, J = 7.8 Hz, 1H, H_1), 7.54 (d, J = 7.8 Hz, 2H, H_2), 7.39 – 7.34 (m, 2H, H_9), 2.74 (t, J = 7.8 Hz, 2H, H_{11}), 1.73 (m, J = 10.5, 4.8 Hz, 2H, H_{12}), 1.43 (s, 18H, H_7), 1.38 (m, J = 7.2, 3.3 Hz, 4H, $H_{13\text{-}14}$), 0.97 – 0.90 (t, 3H, H_{15}).

^{13}C-NMR (101 MHz, DCM-d_2): δ (ppm) = 171.46 (C_5), 161.96 (C_4), 156.61 (C_{10}), 152.94 (C_8), 149.77 (C_3), 142.64 (C_1), 126.04 (C_9), 117.11 (C_2), 50.43 (C_{11}), 35.68 (C_{12}), 33.63 (C_{13}), 31.73 (C_6), 30.21 (C_7), 30.01 (C_{14}), 22.84 (C_{15}).

EM-MS-ESI (MeOH, $C_{27}H_{36}N_8Pd$, *m/z*): calcd. for $[M+H]^+$ = 579.22, found for $[M+H]^+$ = 579.2184 .

^{t}bu-Pd-CNR:

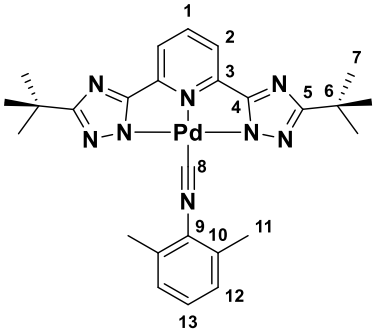

Yellowish solid (120 mg, 67 %).

^{1}H-NMR (400 MHz, DCM-d_2/CD_3OD): δ (ppm) = 8.13 (t, J = 7.9 Hz, 1H, H_1), 7.85 (d, J = 7.9 Hz, 2H, H_2), 7.33 (t, J = 8.3, 7.0 Hz, 1H, H_{13}), 7.22 (d, J = 7.7 Hz, 2H, H_{12}), 2.66 (s, 6H, H_{11}), 1.42 (s, 18H, H_7).

^{13}C-NMR (101 MHz, DCM-d_2): δ (ppm) = 173.53 (C_5), 163.25 (C_4), 149.45 (C_8), 144.46 (C_3), 143.43 (C_1), 137.55 (C_{10}), 135.33 (C_{13}), 131.23 (C_9), 128.59 (C_{12}), 118.55 (C_2), 33.52 (C_6), 29.96 (C_7), 18.71(C_{11}).

EM-MS-ESI (MeOH, $C_{26}H_{30}N_8Pd$, *m/z*): calcd. for $[M+H]^+$ = 561.17, found for $[M+H]^+$ = 561.1722; calcd. for $[M+Na]^+$ = 583.15, found for $[M+Na]^+$ = 583.1540.

6. Synthesis of Pt(II) complexes [CF_3-Pt-PPh_3] and [^{t}bu-Pt-PPh_3]

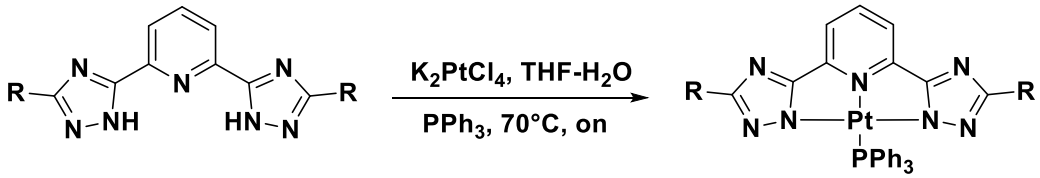

The reaction was performed according to a procedure previously reported in the literature.[2,3] To a mixture of THF:H_2O (3:1, 10 mL), the tridentate N^N^N ligand precursor (75 mg) and K_2PtCl_4 (118 mg, 1 eq) were added. Following this step, triethylamine (2 eq) was added. Stirring was performed at 70°C under a nitrogen atmosphere for 30 minutes. As the next step, triphenylphosphane (**PPh_3**) (1.2 eq) was added, and the reaction mixture was stirred overnight at 70° C. After cooling to RT, DCM (3 x 100 mL) was used to extract the reaction mixture. The combined organic phases were washed with H_2O (3 x 100 mL) and brine (100 mL), dried with $NaSO_4$, and filtered. Then, the solvent was removed, and the crude compound was adsorbed

onto silica gel to perform a column chromatography separation with MeOH:DCM (1:99) as the eluent to yield **CF_3-Pt-PPh_3** and **^{t}bu-Pt-PPh_3**.

CF_3-Pt-PPh_3:

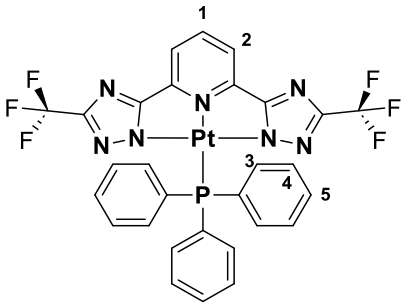

Yellowish solid (142 mg, 62%).

^{1}H-NMR (500 MHz, DMF-d_7): δ (ppm) = 8.53 (t, J = 7.9 Hz, 1H, H_1), 8.14 (dd, J = 7.9, 1.5 Hz, 2H, H_2), 7.88 (m, J = 12.7, 7.0 Hz, 6H, H_3), 7.64 (m, J = 2.6 Hz, 3H, H_5), 7.55 (m, J = 9.7, 8.5 Hz, 6H, H_4).

^{19}F-NMR (471 MHz, DMF-d_7): δ (ppm) = -64.62.

EM-MS-ESI (MeOH, $C_{29}H_{18}F_6N_7PPt$, *m/z*): calcd. for $[M+H]^+$ = 805.10, found for $[M+H]^+$ = 805.0990; calcd. for $[M+Na]^+$ = 827.08, found for $[M+Na]^+$ = 827.0809.

^{t}bu-Pt-PPh_3:

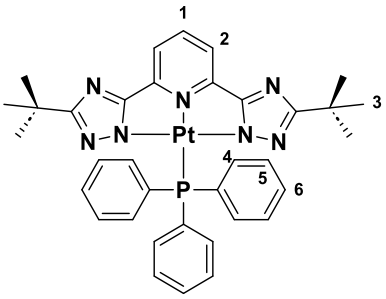

Yellowish solid (144 mg, 60%).

^{1}H-NMR (400 MHz, DCM-d_2): δ (ppm) = 7.94 (t, J = 7.9 Hz, 1H, H_1), 7.78 (m, J = 12.4, 8.4, 1.4 Hz, 6H, H_4), 7.64 (dd, J = 7.9, 1.5 Hz, 2H, H_2), 7.50 (m, J = 2.7 Hz, 3H, H_6), 7.41 (m, J = 11.6, 3.0 Hz, 6H, H_5), 1.14 (s, 18H, H_3).

EM-MS-ESI (MeOH, $C_{35}H_{36}N_7PPt$, *m/z*): calcd. for $[M+H]^+$ = 781.21, found for $[M+H]^+$ = 781.2474; calcd. for $[M+Na]^+$ = 803.23, found for $[M+Na]^+$ = 804.48.

7. Synthesis of the Pd(II) complexes [CF_3-Pd-PPh_3] and [^{t}bu-Pd-PPh_3]

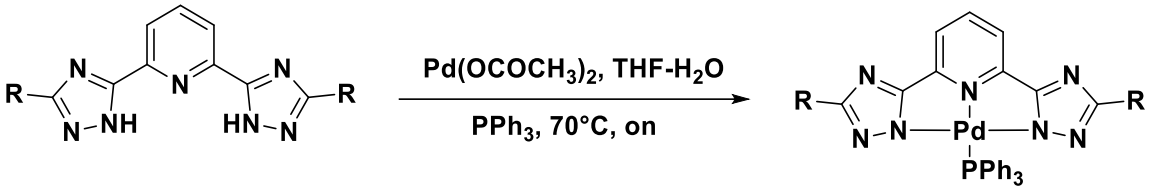

A mixture of the tridentate N^N^N ligand precursor (100 mg) and of $Pd(OCOCH_3)_2$ (1 eq) were dissolved in a mixture of THF:H_2O (3:1, 10 mL). Subsequently, triethylamine (2 eq) was added. The reaction mixture was stirred at 70°C under nitrogen atmosphere for 30 minutes. This was followed by the addition of triphenylphosphane (**PPh_3**) (1.2 eq) and then the reaction mixture was stirred overnight at 70° C. After cooling down to RT, the reaction mixture was extracted with DCM (3 x 100 mL). The combined organic phases were washed with H_2O (3 x 100 mL) and brine (100 mL), dried with $NaSO_4$, and filtered. Later, the solvent was evaporated, and the crude compound was loaded onto a column packed with silica gel to perform a column chromatography separation with MeOH:DCM (1:99) as the eluent to yield **CF_3-Pd-PPh_3** and **^{t}bu-Pd-PPh_3**.

CF_3-Pd-PPh_3:

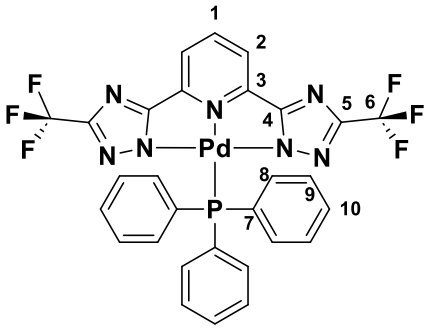

Yellowish solid (126 mg, 62%).

^{1}H-NMR (400 MHz, DCM-d_2): δ (ppm) = 8.19 (d, J = 7.9 Hz, 1H, H_1), 7.96 – 7.90 (m, 2H, H_2), 7.82 – 7.71 (m, 6H, H_8), 7.61 – 7.53 (m, 3H, H_{10}), 7.45 (td, J = 7.5, 2.6 Hz, 6H, H_9).

^{13}C-NMR (101 MHz, DCM-d_2): δ (ppm) = 165.22 (C_4), 153.38 (C_5), 147.45 (C_3), 144.55 (C_1), 135.38 (C_8), 135.26 (C_{10}), 132.41 (C_7), 127.64 (C_9), 121.43 (C_2), 119.83 (C_6).

^{19}F-NMR (376 MHz, DCM-d_2): δ (ppm) = -65.08.

^{31}P-NMR (162 MHz, DCM-d_2): δ (ppm) = 28.53.

EM-MS-ESI (MeOH, $C_{29}H_{18}F_6N_7PPd$, *m/z*): calcd. for $[M+H]^+$ = 716.04, found for $[M+H]^+$ = 716.0393.

^{t}bu-Pd-PPh$_3$:

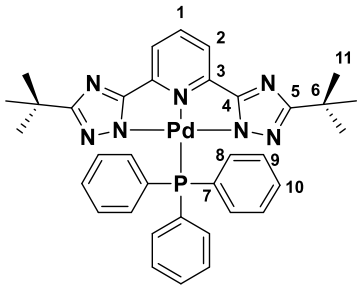

Yellowish solid (129 mg, 61%).

^{1}H-NMR (400 MHz, DCM-d_2): δ (ppm) = 7.98 (t, J = 7.9 Hz, 1H, H_1), 7.80 (m, J = 11.9 Hz, 6H, H_8), 7.62 (dd, J = 7.9, 1.5 Hz, 2H, H_2), 7.56 – 7.50 (m, 3H, H_{10}), 7.43 (m, J = 11.4 Hz, 6H, H_9), 1.15 (s, 18H, H_{11}).

^{13}C-NMR (101 MHz, DCM-d_2): δ (ppm) = 172.28 (C_5), 163.80 (C_4), 148.94 (C_3), 143.04 (C_1), 135.54 (C_8), 135.42 (C_{10}), 131.61 (C_9), 128.75 (C_7), 116.96 (C_2), 33.12 (C_6), 30.04 (C_{11}).

^{31}P-NMR (162 MHz, DCM-d_2): δ (ppm) = 27.66.

EM-MS-ESI (MeOH, $C_{35}H_{36}N_7PPd$, *m/z*): calcd. for $[M+H]^+$ = 692.19, found for $[M+H]^+$ = 692.1899.

8. Synthesis of the Pt(II) complex [^{t}bu-Pt-PTA]

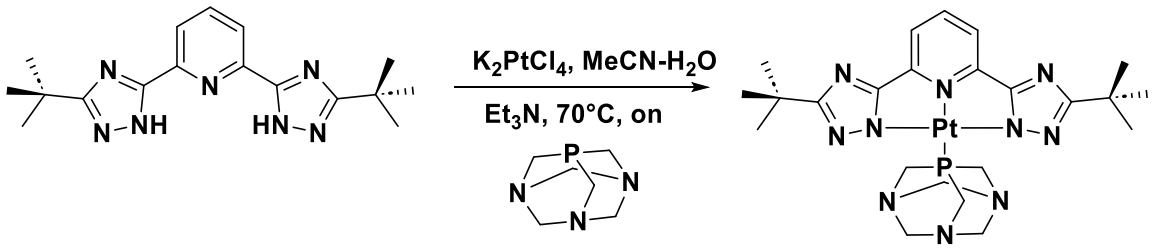

The tridentate N^N^N ligand precursor 2,6-bis(3-(*tert*-butyl)-1*H*-1,2,4-triazol-5-yl)pyridine (**^{t}bu**) (100 mg) and K_2PtCl_4 (127 mg, 1 eq) were dissolved in a mixture of MeCN:H_2O (3:1, 10 mL). Subsequently, triethylamine (2 eq) was added. The reaction mixture was stirred at 70°C under a nitrogen atmosphere for 30 minutes. Further, 1,3,5-triaza-7-phosphaadamantane (**PTA**) (1 eq) was added and the reaction mixture was stirred overnight at 85° C. After cooling down to room temperature, the reaction mixture was extracted with DCM (3 x 100 mL). The combined organic phases were washed with H_2O (3 x 100 mL) and brine (100 mL), dried with $NaSO_4$,

and filtered. Later, the solvent was removed, and the crude compound was adsorbed onto silica gel. This was loaded onto a column packed with silica gel to perform a column chromatography separation with acetone:DCM (1:9) as the eluent to yield a greenish-yellow solid (166 mg, 80%).

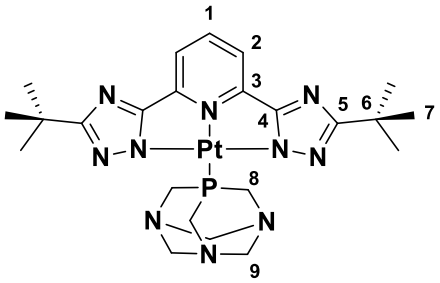

^{1}H-NMR (400 MHz, DCM-d_2): δ (ppm) = 7.92 (t, J = 7.9 Hz, 1H, H_1), 7.60 (dd, J = 7.9, 1.3 Hz, 2H, H_2), 4.64 (br., 6H, H_9), 4.58 (m, J = 2.1 Hz, 6H, H_8), 1.40 (s, 18H, H_7).

^{13}C-NMR (101 MHz, DCM-d_2): δ (ppm) = 174.21 (C_5), 164.49 (C_4), 149.39 (C_3), 143.66 (C_1), 117.03 (C_2), 73.83 (C_9), 51.63 (C_8), 33.44 (C_6), 30.11 (C_7).

^{31}P-NMR (162 MHz, DCM-d_2): δ (ppm) = -53.48, -64.52, -75.55.

^{195}Pt-NMR (86 MHz, DCM-d_2): δ (ppm) = -3836.66.

EM-MS-ESI (MeOH, $C_{23}H_{33}N_{10}PPt$, *m/z*): calcd. for $[M+H]^+$ = 676.24, found for $[M+H]^+$ = 676.2354; calcd. for $[M+Na]^+$ = 698.22, found for $[M+Na]^+$ = 698.4605.

9. Synthesis of the Pd(II) complex [^{t}bu-Pd-PTA]

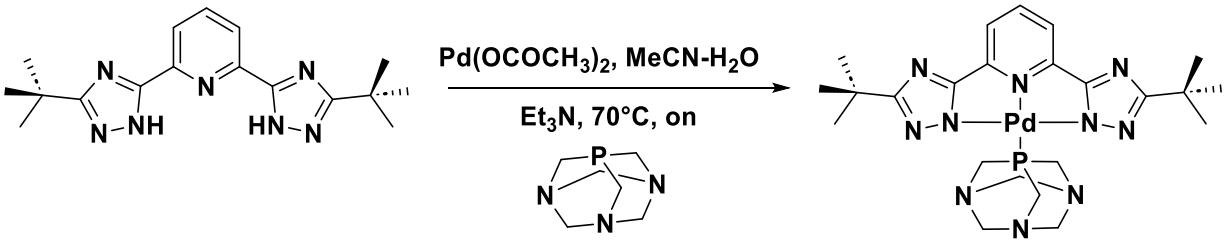

A mixture of the tridentate N^N^N ligand precursor 2,6-bis(3-(*tert*-butyl)-1*H*-1,2,4-triazol-5-yl)pyridine (**^{t}bu**) (100 mg) and of $Pd(OCOCH_3)_2$ (68 mg, 1 eq) were dissolved in a mixture of MeCN:H_2O (3:1, 10 mL). Subsequently, triethylamine (2 eq) was added. The reaction mixture was stirred at 70°C under a nitrogen atmosphere for 30 minutes. Afterwards, 1,3,5-triaza-7-phosphaadamantane (**PTA**) (1 eq) was added and the reaction mixture was stirred overnight at 70° C. The reaction mixture was then extracted with DCM (3 x 100 mL). The combined

organic phases were washed with H_2O (3 x 100 mL) and brine (100 mL), dried with $NaSO_4$, and filtered. Later, the solvent was removed, and the crude compound was adsorbed onto silica gel. This was loaded onto a column packed with silica gel to perform a column chromatography separation with MeOH:DCM (1:99) as the eluent to yield a yellow solid.

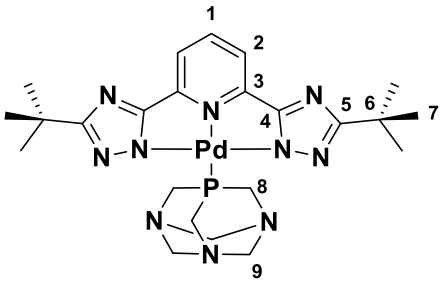

^{1}H-NMR (400 MHz, DCM-d_2): δ (ppm) = 7.93 (t, J = 7.9 Hz, 1H, H_1), 7.61 (dd, J = 7.9, 1.5 Hz, 2H, H_2), 4.77 – 4.58 (m, 12H, H_{8-9}), 1.39 (s, 18H, H_7).

^{13}C-NMR (101 MHz, DCM-d_2): δ (ppm) = 173.63 (C_5), 164.21 (C_4), 148.79 (C_3), 143.11 (C_1), 117.58 (C_2), 73.78 (C_9), 51.69 (C_8), 33.45 (C_6), 30.15 (C_7).

^{31}P-NMR (162 MHz, DCM-d_2): δ (ppm) = -42.27.

EM-MS-ESI (MeOH, $C_{25}H_{41}N_{10}PPd$, *m/z*): calcd. for $[M+H]^+$ = 587.17, found for $[M+H]^+$ = 587.1754.

NMR spectra of the ligand precursors and of the complexes

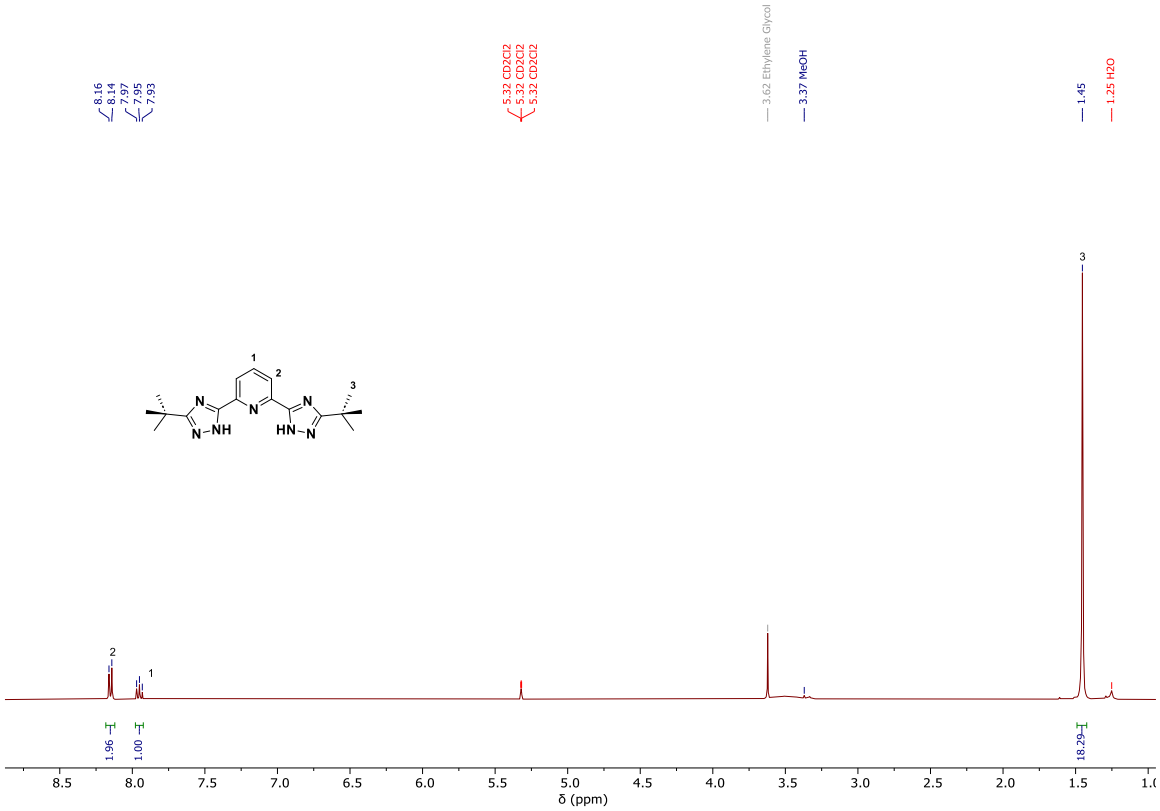

Figure S1. ^{1}H-NMR spectrum (400 MHz, DCM-d_2/CD_3OD) of 2,6-bis(3-(*tert*-butyl)-1*H*-1,2,4-triazol-5-yl)pyridine (**^{t}bu**).

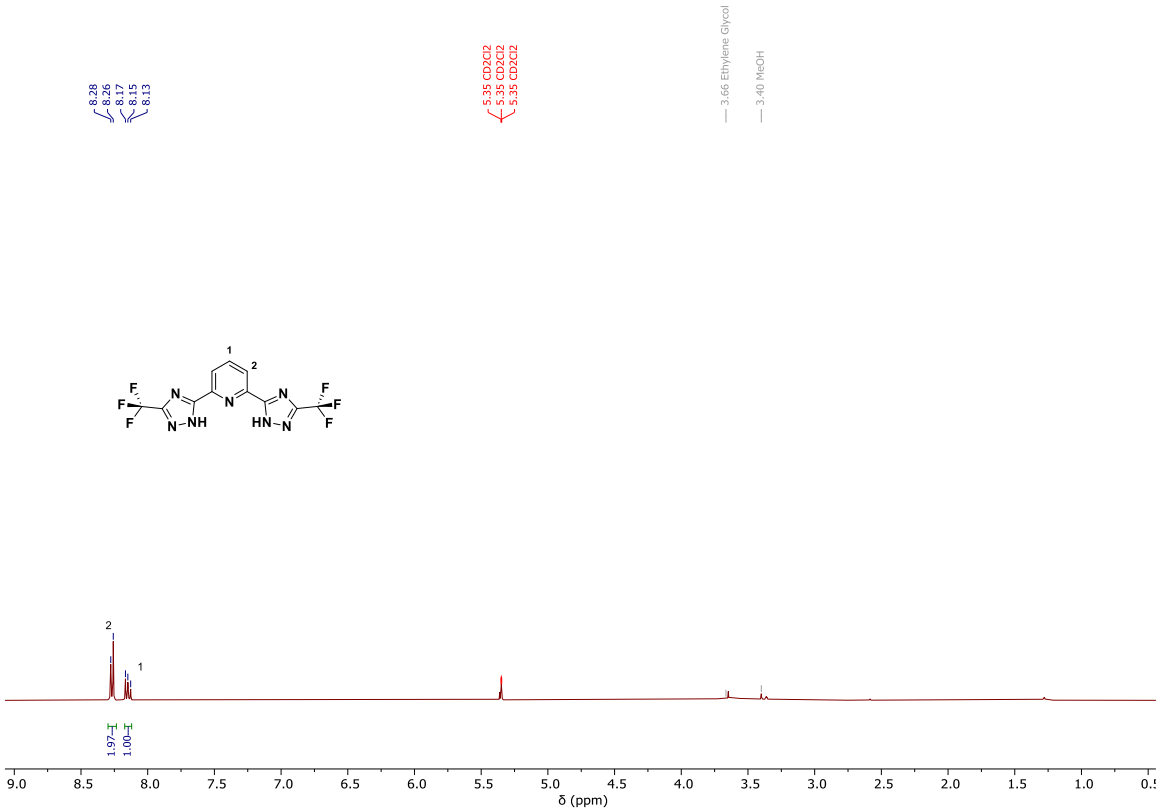

Figure S2. ^{1}H-NMR spectrum (400 MHz, DCM-d_2/CD_3OD) of 2,6-bis(3-(trifluoromethyl)-1*H*-1,2,4-triazol-5-yl)pyridine (**CF_3**).

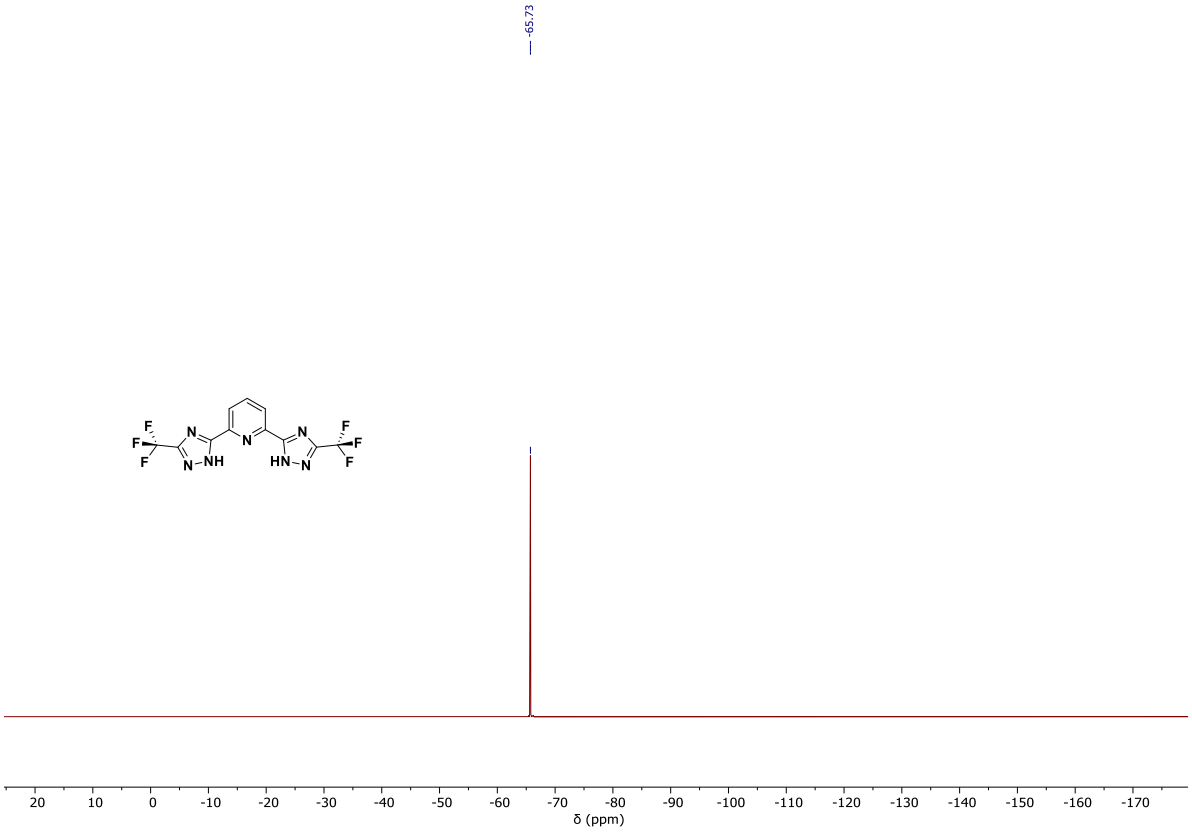

Figure S3. ^{19}F-NMR spectrum (400 MHz, DCM-d_2/CD_3OD) of 2,6-bis(3-(trifluoromethyl)-1*H*-1,2,4-triazol-5-yl)pyridine (**CF_3**).

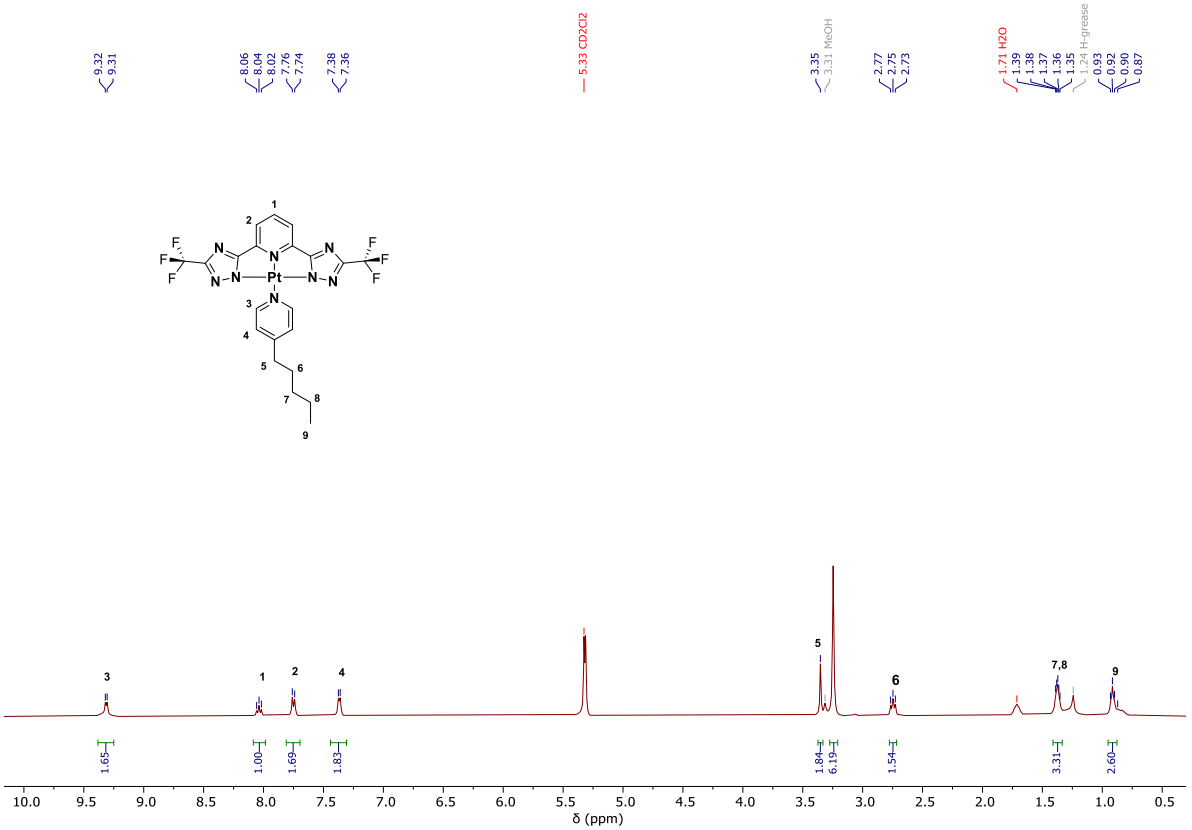

Figure S4. ^{1}H-NMR spectrum (400 MHz, DCM-d_2) of **CF_3-Pt-AmPy**.

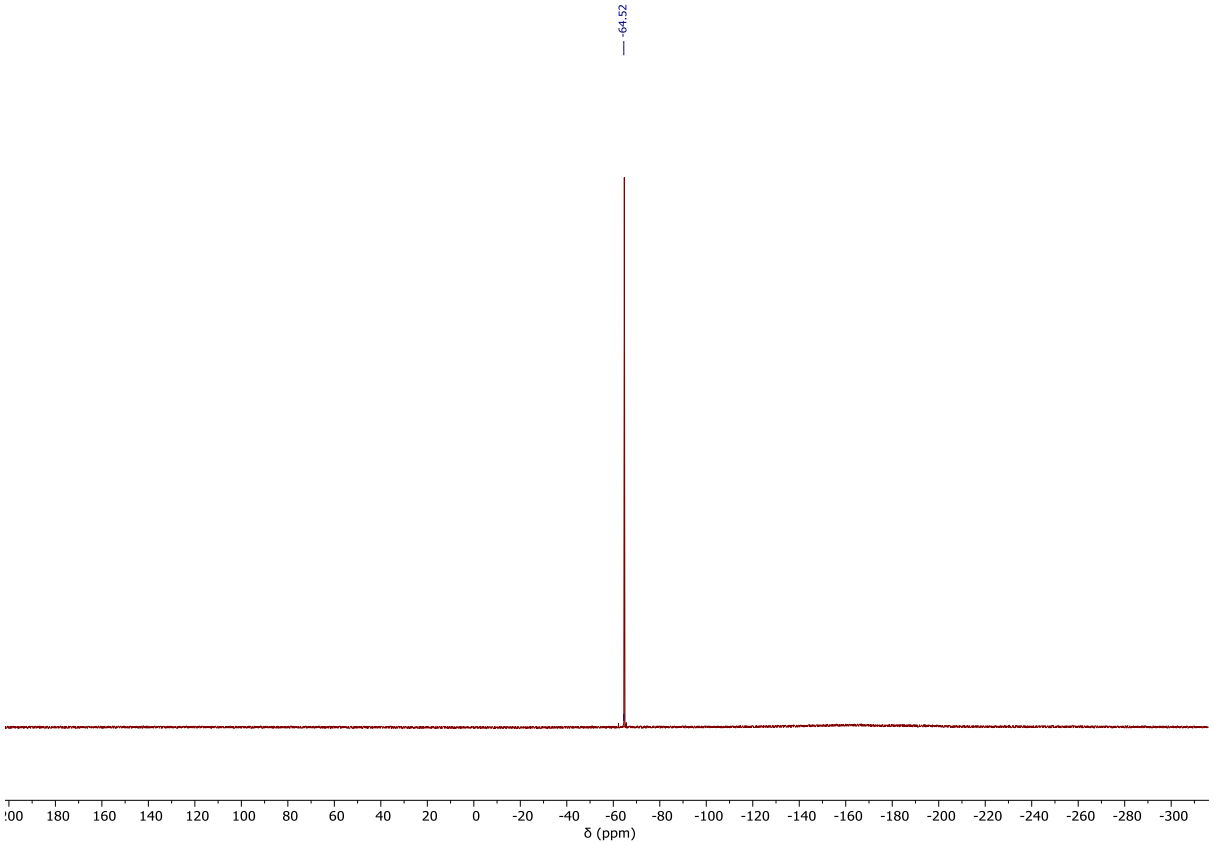

Figure S5. ^{19}F-NMR spectrum (376 MHz, DCM-d_2) of **CF_3-Pt-AmPy**.

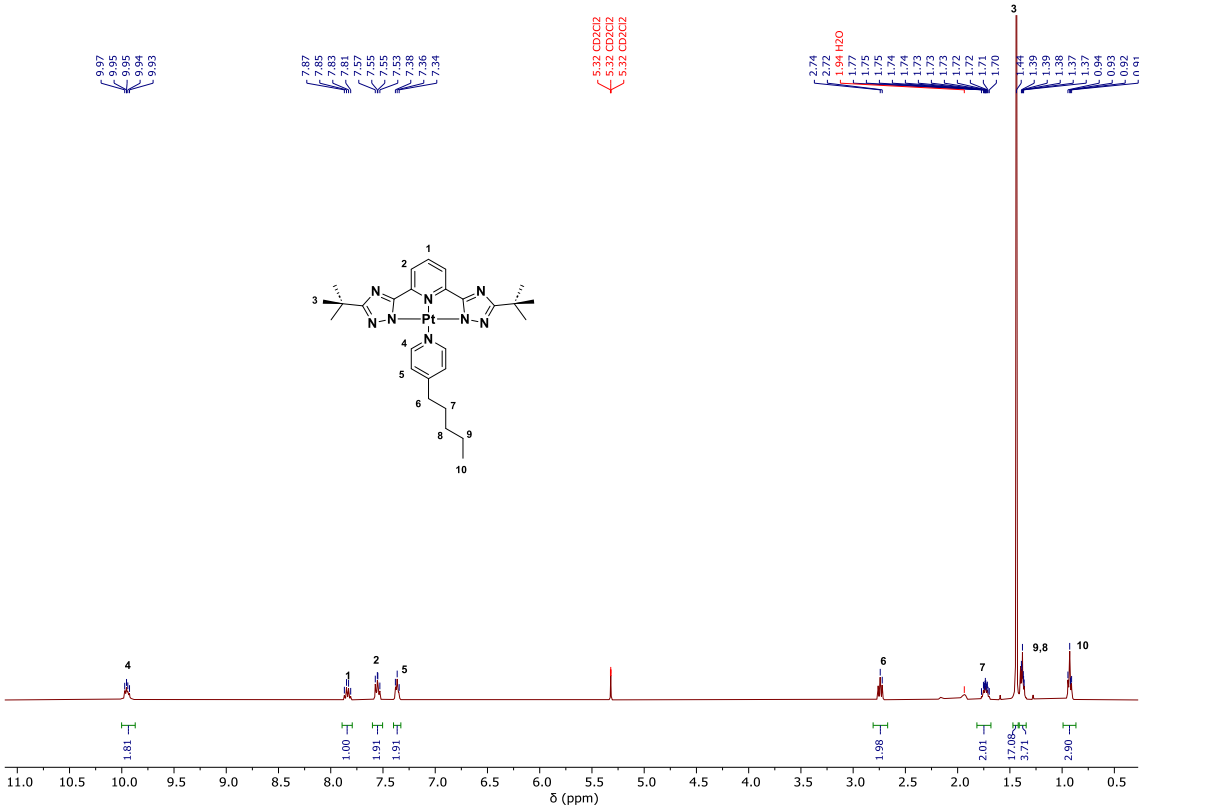

Figure S6. ^{1}H-NMR spectrum (400 MHz, DCM-d_2) of **^{t}bu-Pt-AmPy**.

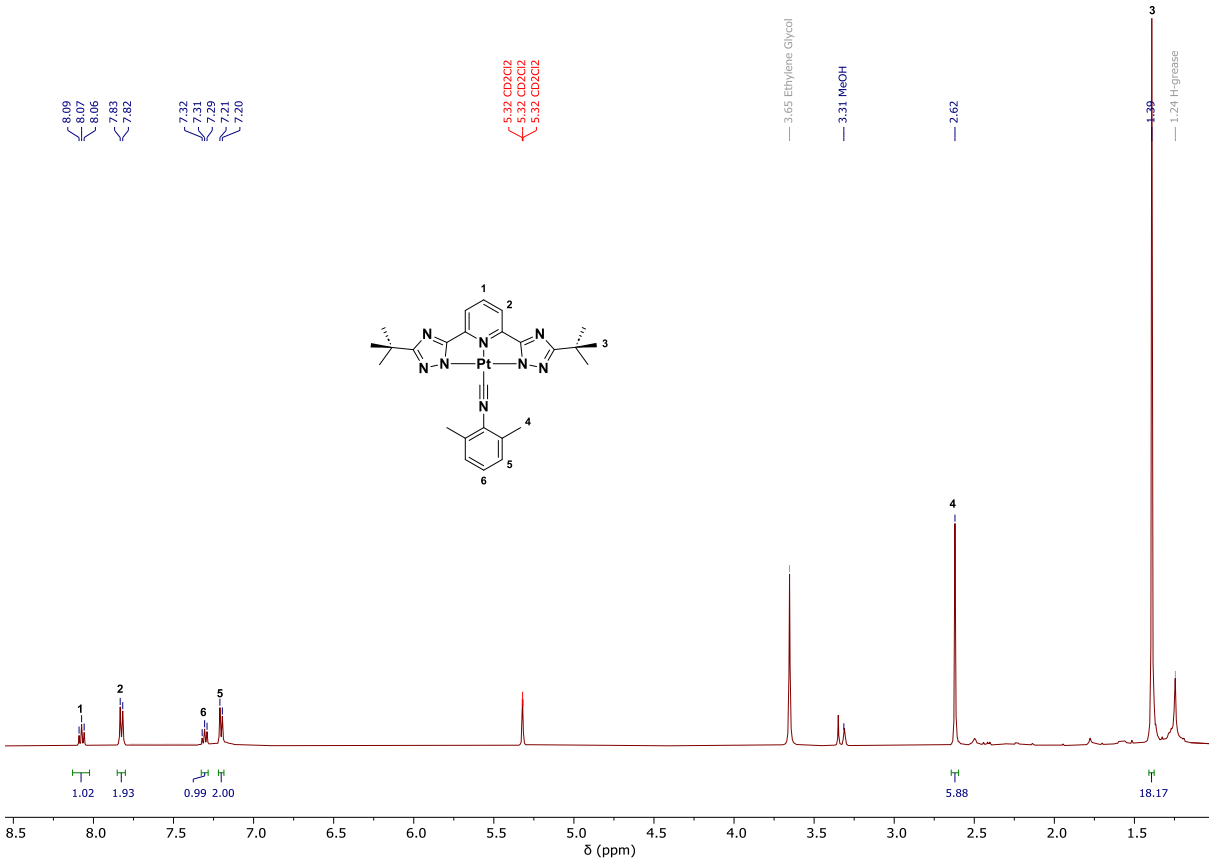

Figure S7. ^{1}H-NMR spectrum (500 MHz, DCM-d_2/CD_3OD) of **^{t}bu-Pt-CNR**.

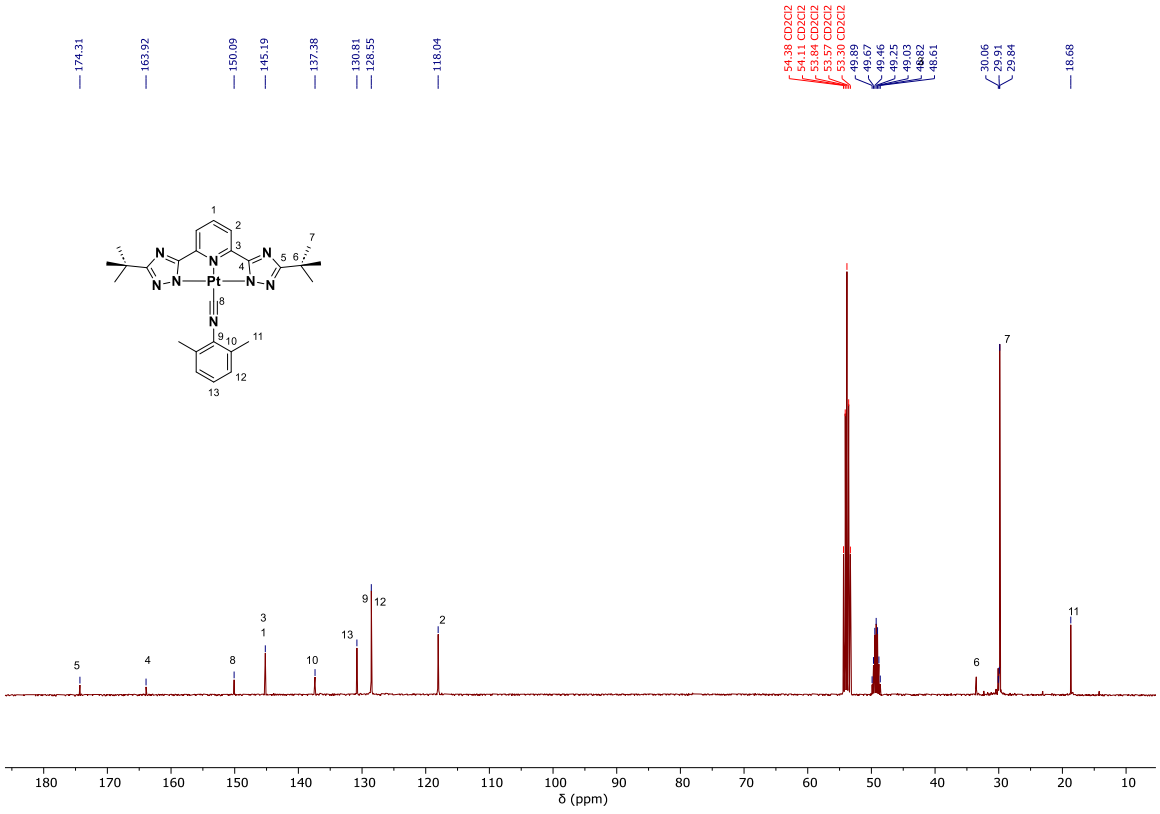

Figure S8. ^{13}C-{^{1}H} NMR spectrum (500 MHz, DCM-d_2/CD_3OD) of **^{t}bu-Pt-CNR**.

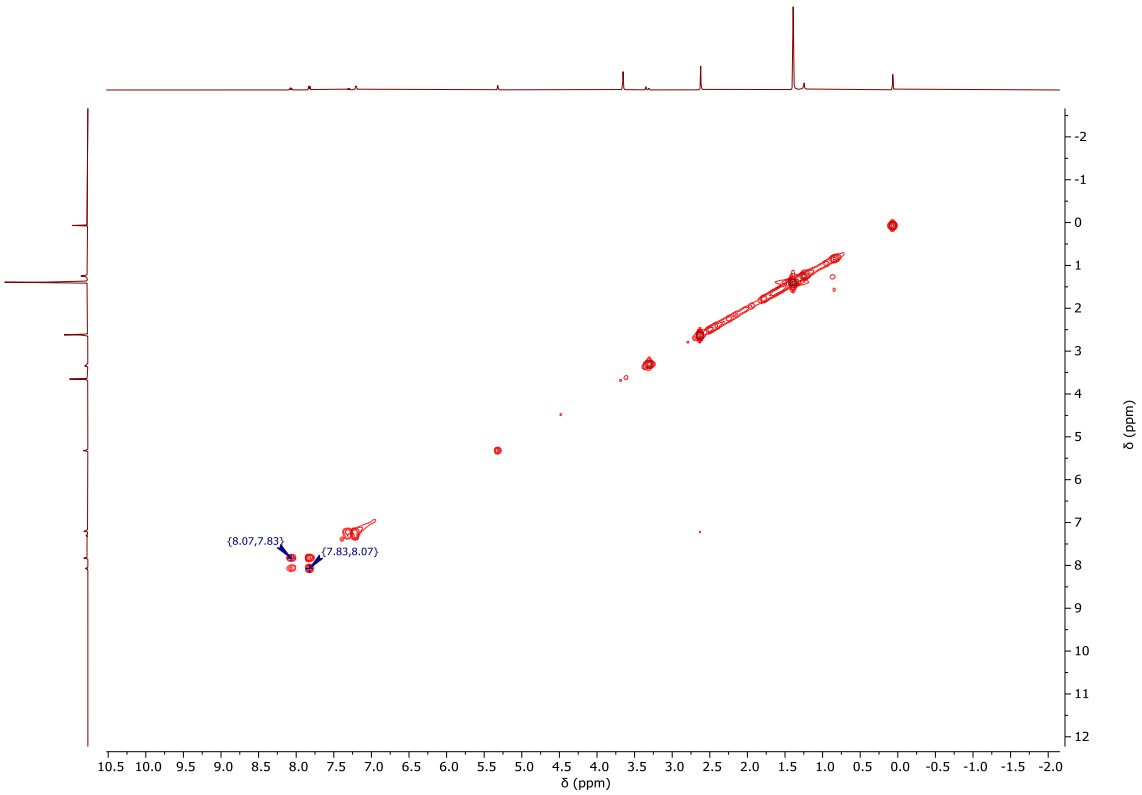

Figure S9. ^{1}H,^{1}H-COSY-NMR spectrum (500 MHz, DCM-d_2/CD_3OD) of **^{t}bu-Pt-CNR**.

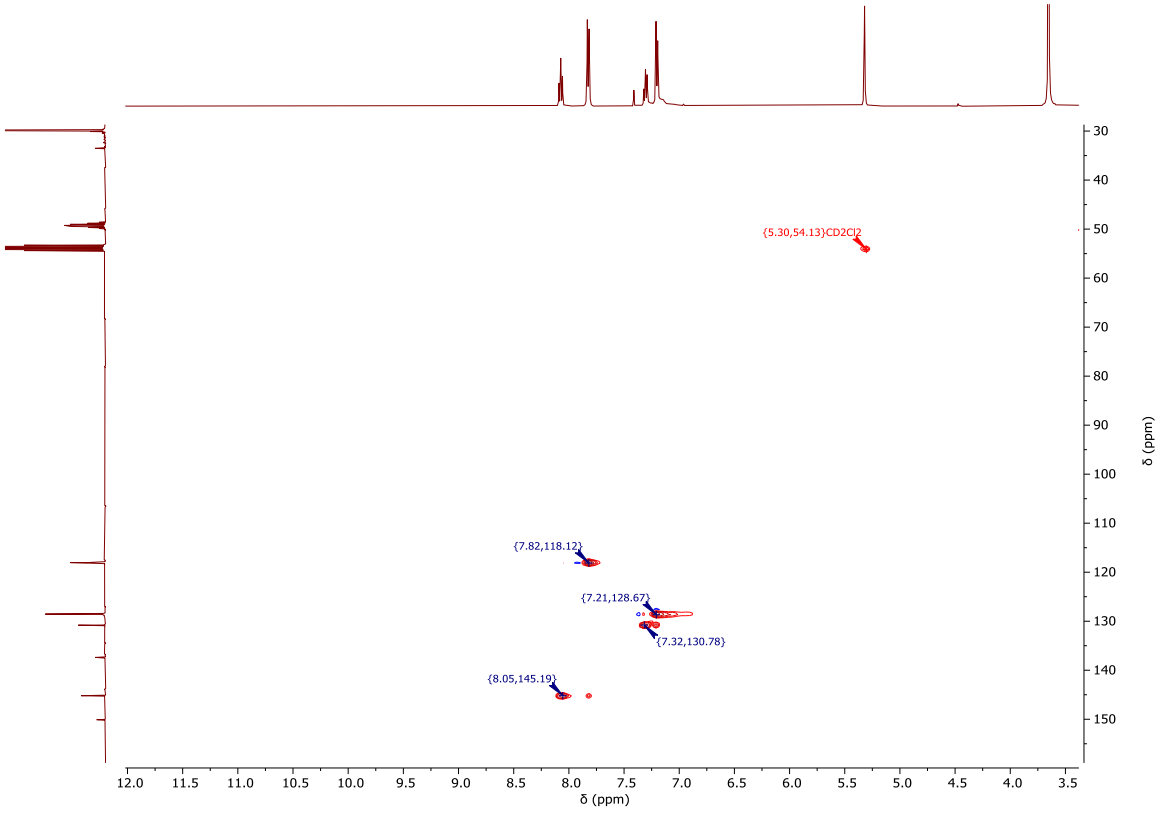

Figure S10. ^{1}H,^{13}C-gHSQC-NMR spectrum (400 MHz, 101 MHz, DCM-d_2/CD_3OD) of **^{t}bu-Pt-CNR**.

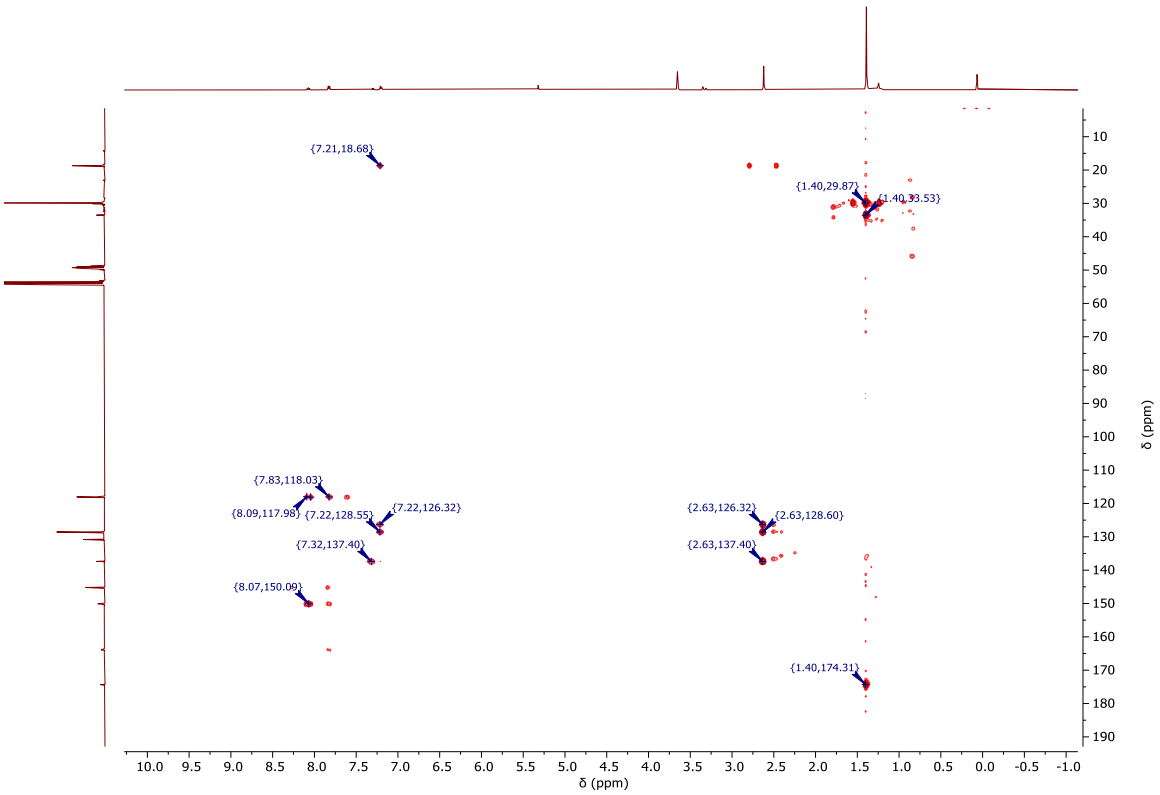

Figure S11. $^{1}H,^{13}C$-gHMBC-NMR spectrum (400 MHz, 101 MHz, DCM-d_2/CD_3OD) of **^{t}bu-Pt-CNR**.

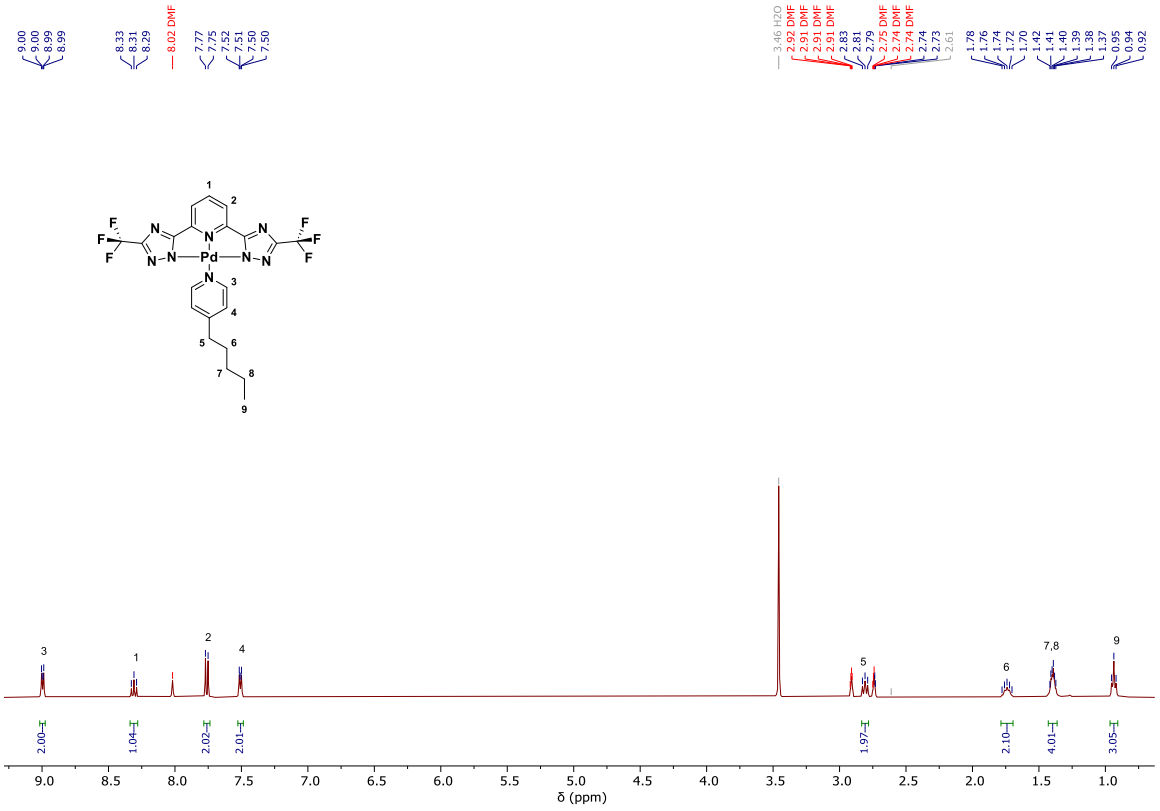

Figure S12. ^{1}H-NMR spectrum (400 MHz, DMF-d_7) of **CF_3-Pd-AmPy**.

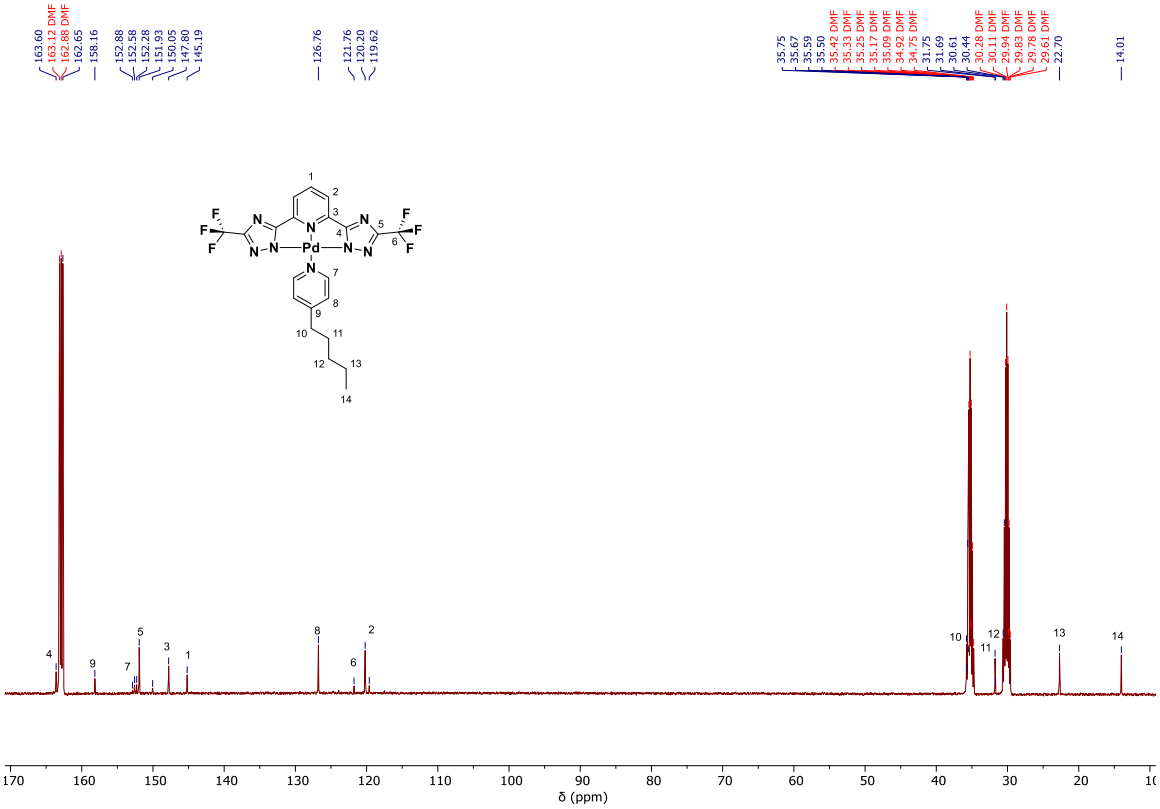

Figure S13. ^{13}C-{^{1}H} NMR spectrum (126 MHz, DMF-d_7) of **CF_3-Pd-AmPy**.

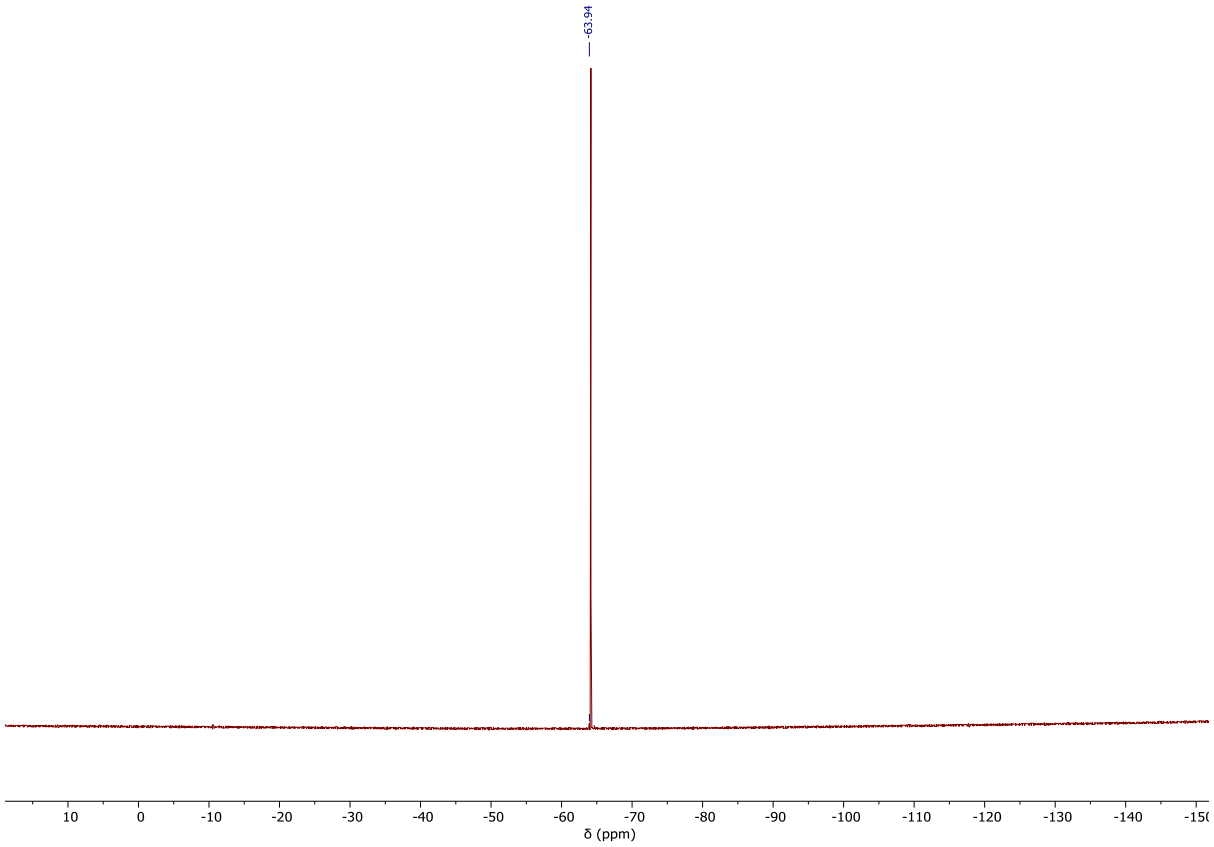

Figure S14. ^{19}F-NMR spectrum (376 MHz, DMF-d_7) of **CF_3-Pd-AmPy**.

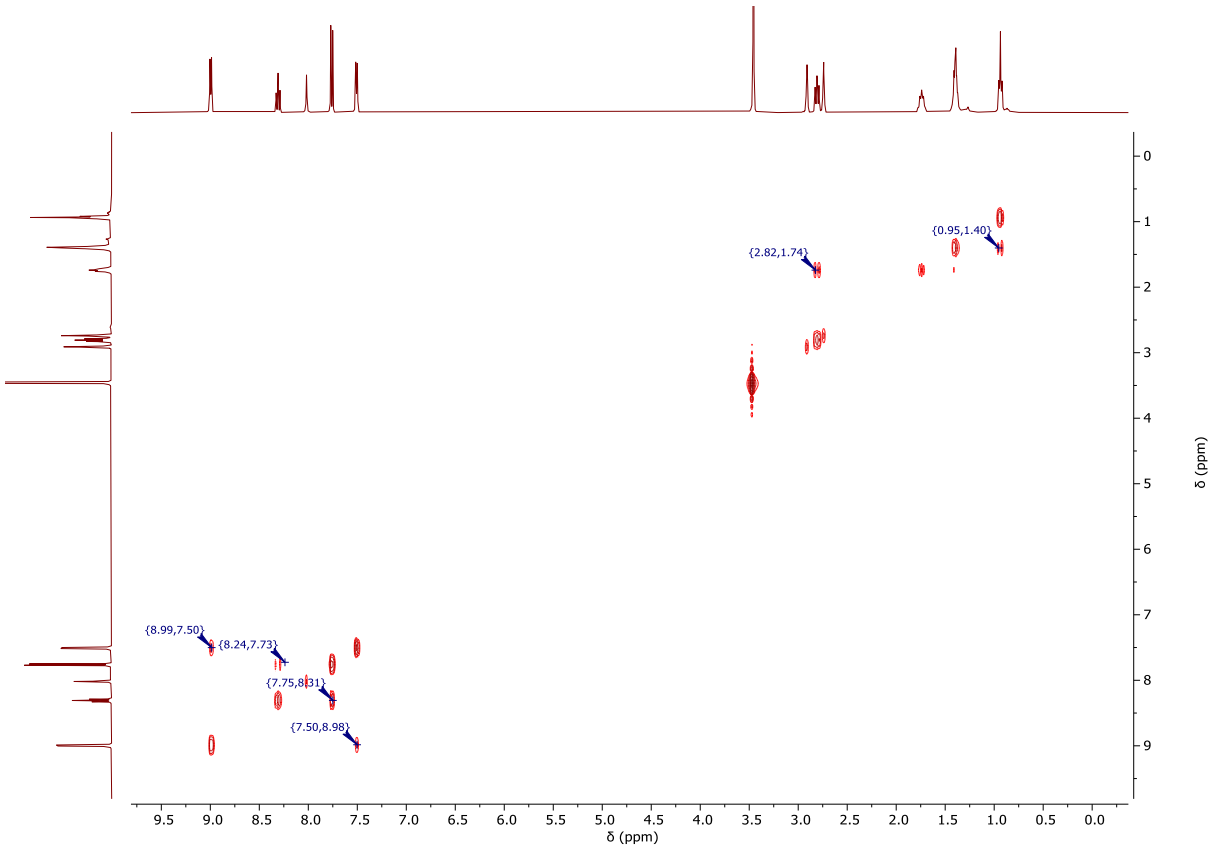

Figure S15. ^{1}H,^{1}H-COSY-NMR spectrum (400 MHz, DMF-d_7) of **CF_3-Pd-AmPy**.

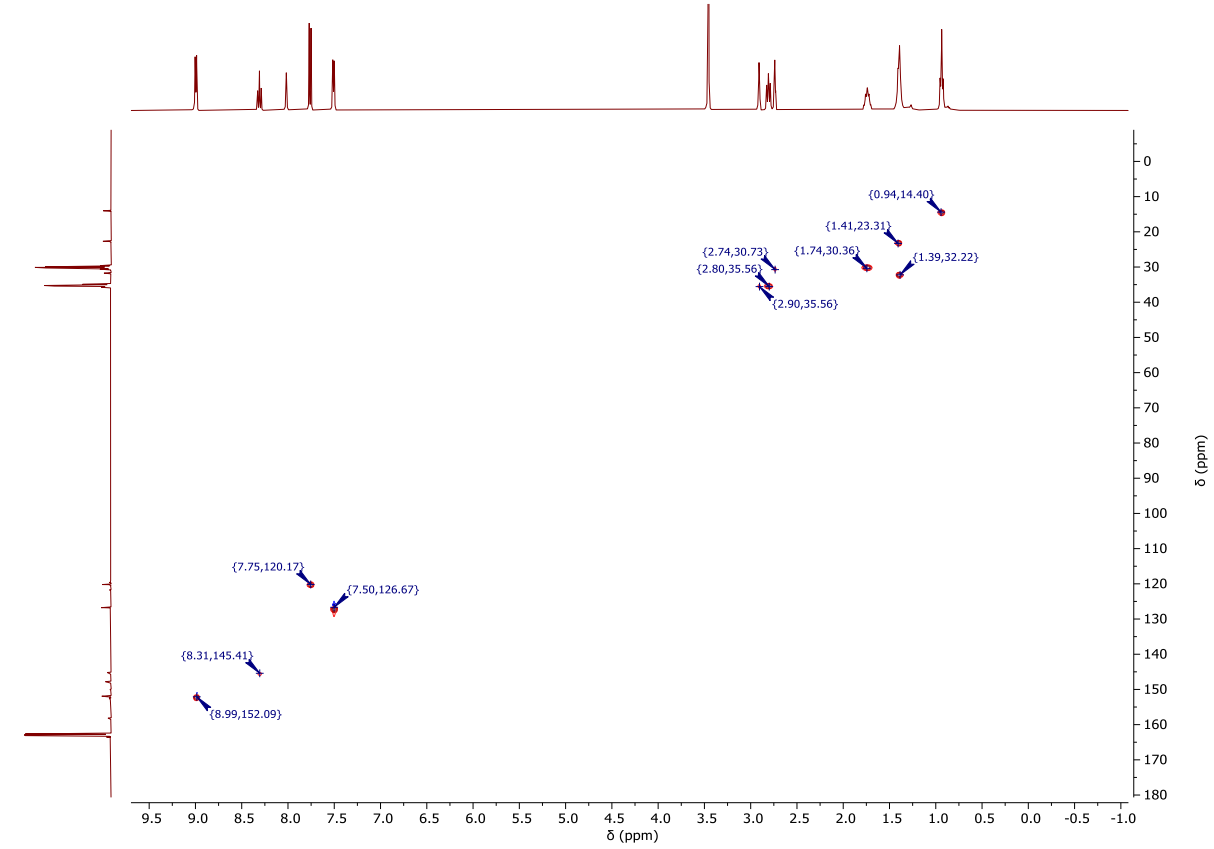

Figure S16. ^{1}H,^{13}C-gHSQC-NMR spectrum (400 MHz, DMF-d_7) of **CF_3-Pd-AmPy**.

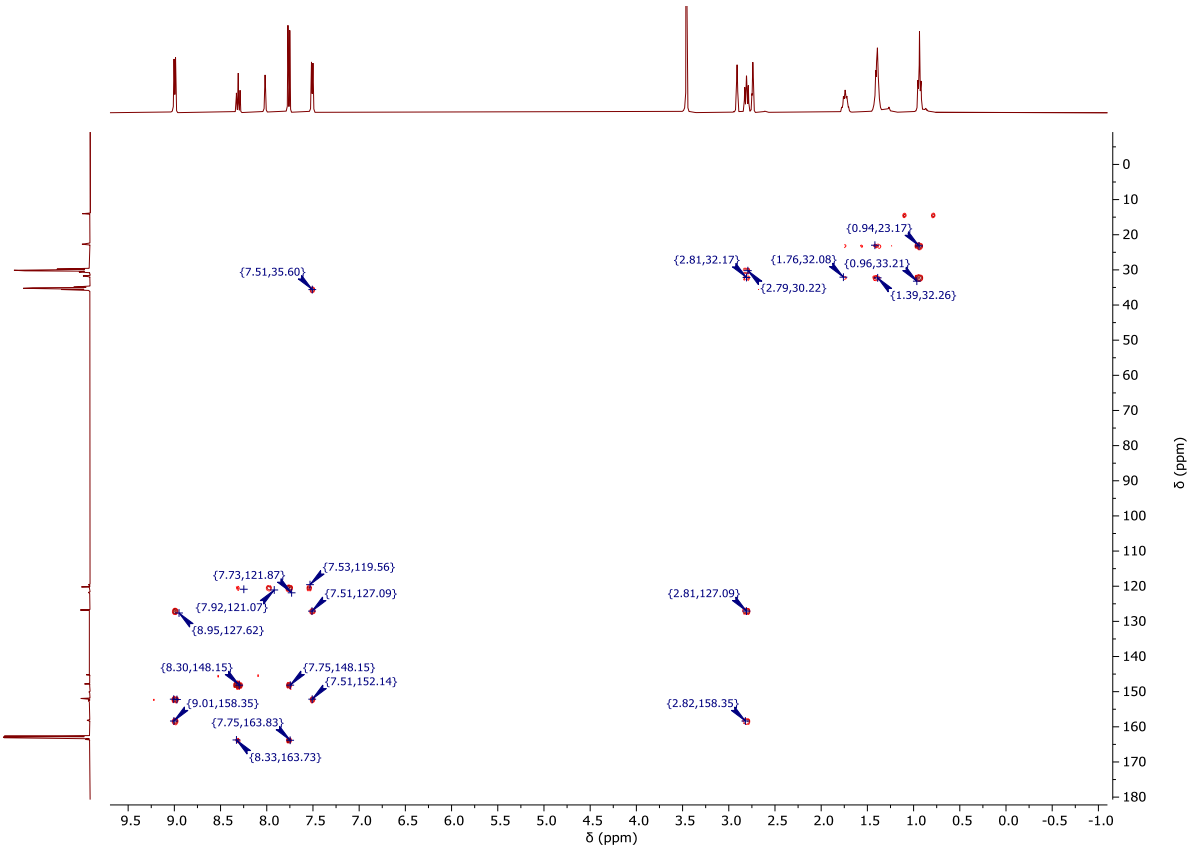

Figure S17. $^{1}H,^{13}C$-gHMBC-NMR spectrum (400 MHz, DMF-d_7) of **CF_3-Pd-AmPy**.

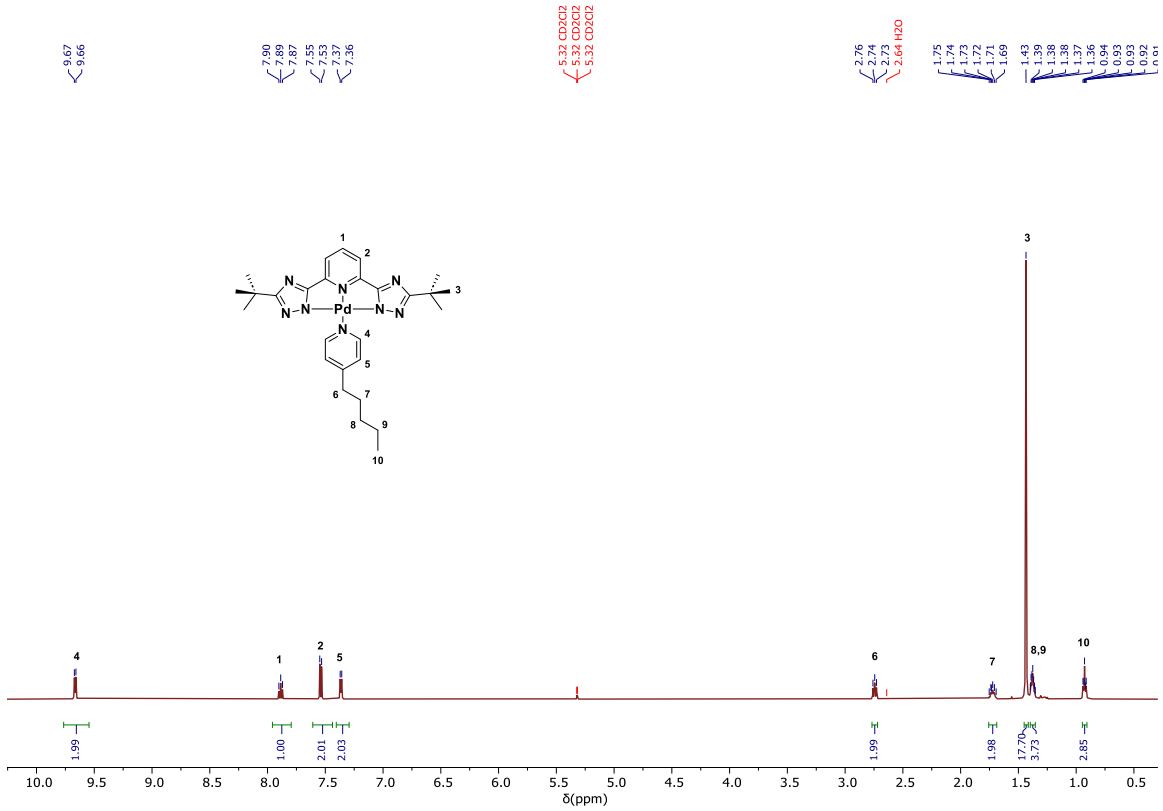

Figure S18. ^{1}H-NMR spectrum (500 MHz, DCM-d_2) of **^{t}bu-Pd-AmPy**.

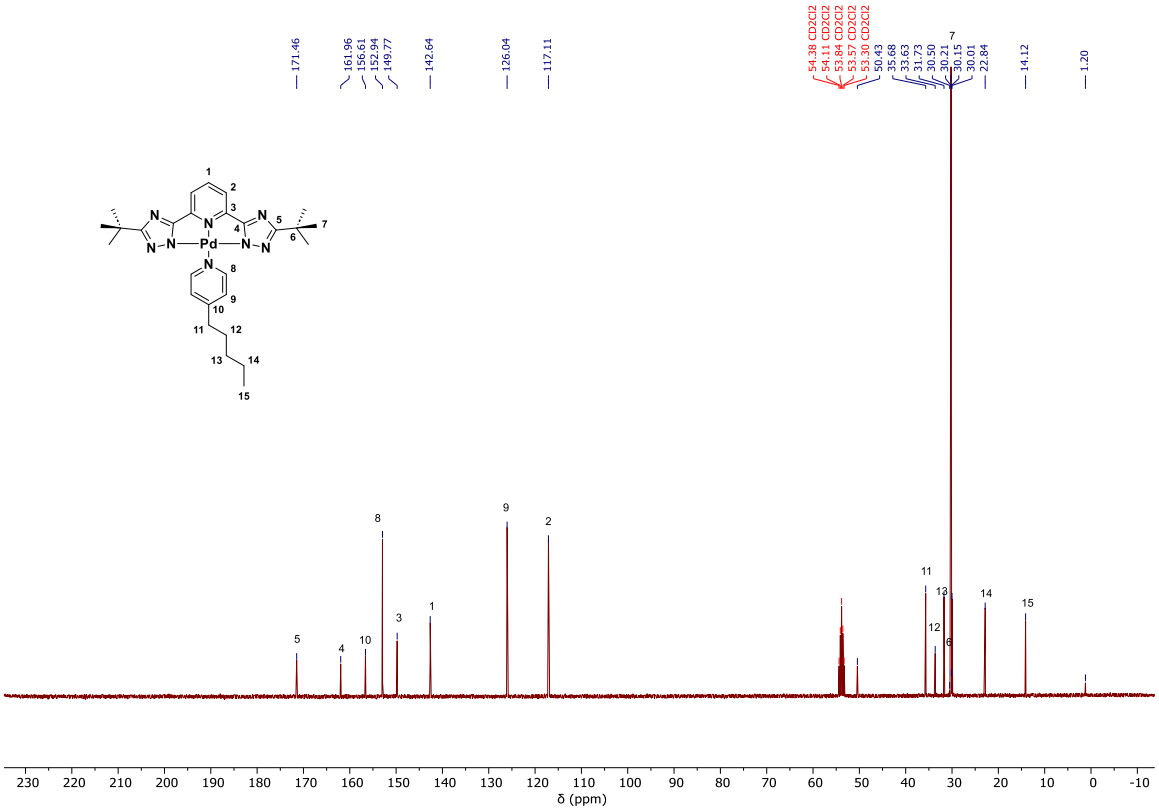

Figure S19. ^{13}C-{^{1}H}-NMR spectrum (101 MHz, DCM-d_2) of **^{t}bu-Pd-AmPy**.

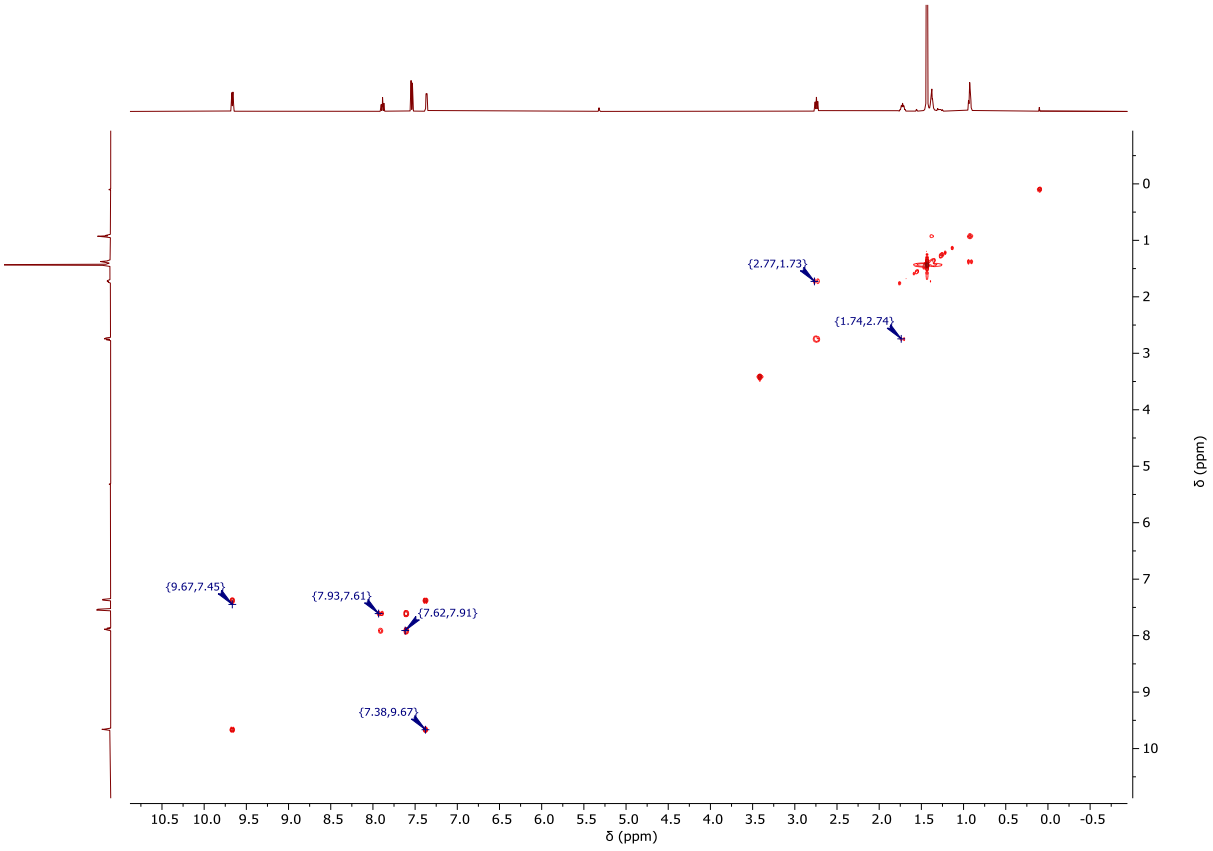

Figure S20. ^{1}H,^{1}H-COSY-NMR spectrum (500 MHz, DCM-d_2) of **^{t}bu-Pd-AmPy**.

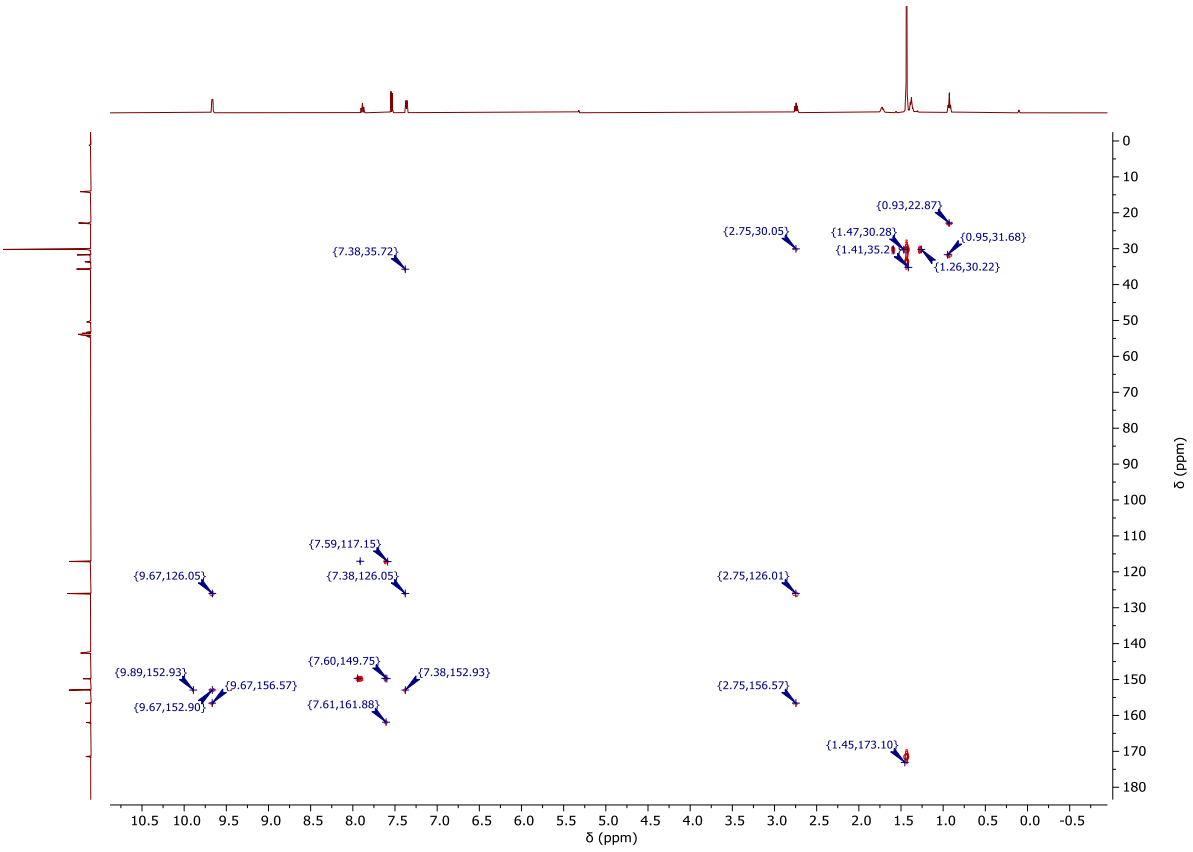

Figure S21. $^{1}H,^{13}C$-gHMBC-NMR spectrum (400 MHz, 101 MHz, DCM-d_2) of **^{t}bu-Pd-AmPy**.

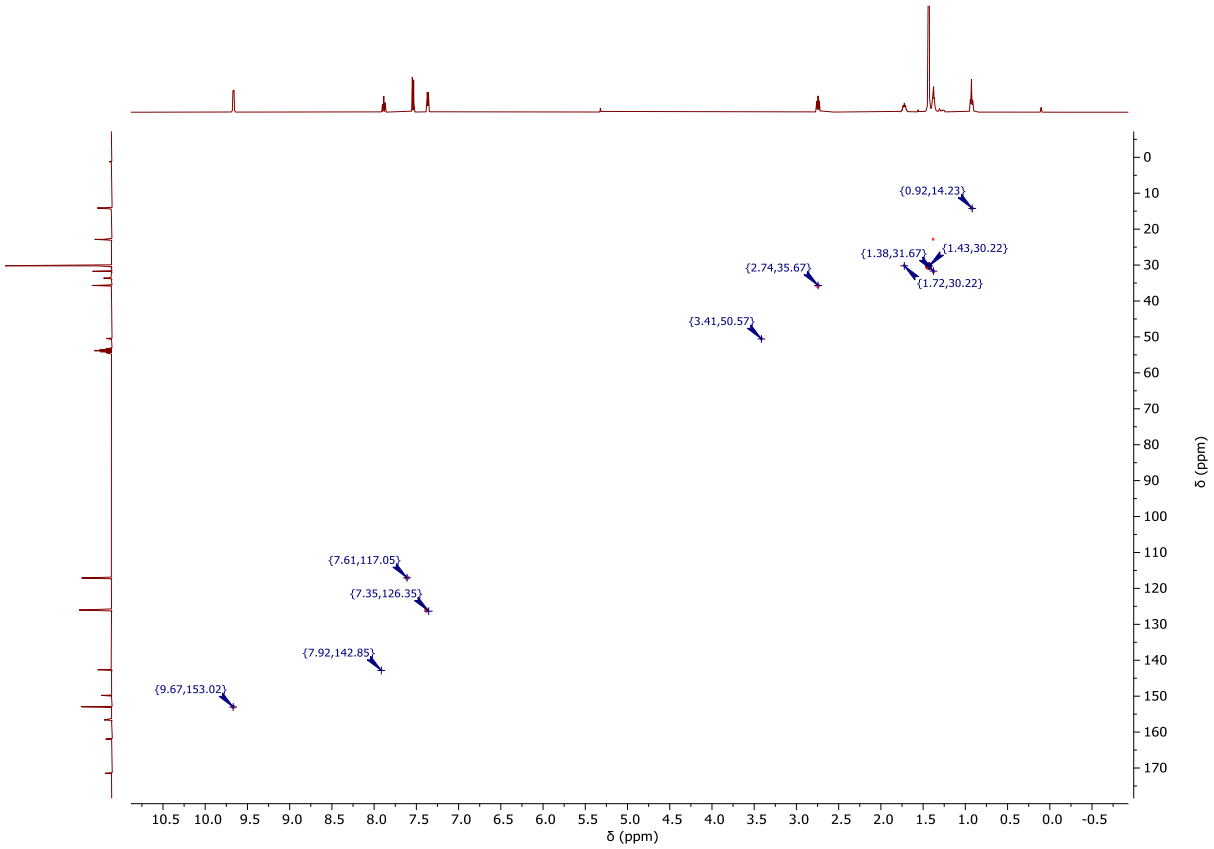

Figure S22. $^{1}H,^{13}C$-gHSQC-NMR spectrum (400 MHz, 101 MHz, DCM-d_2) of **^{t}bu-Pd-AmPy**.

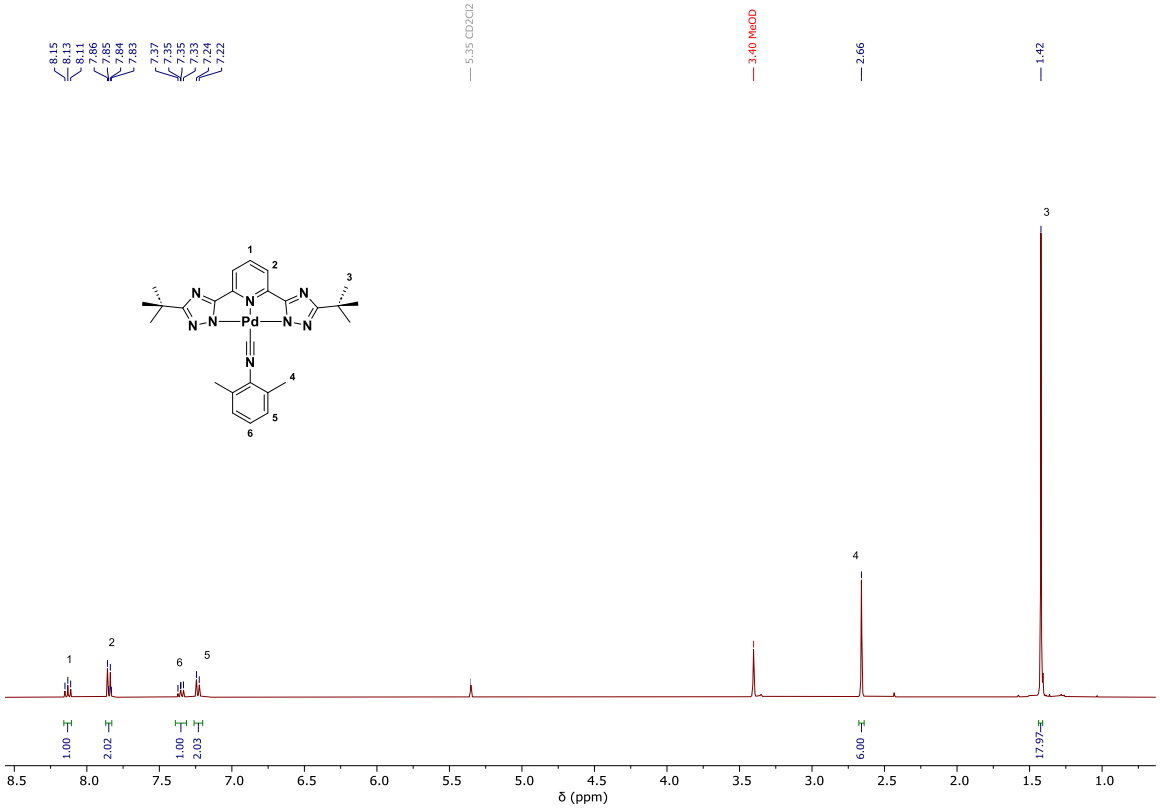

Figure S23. ^{1}H-NMR spectrum (400 MHz, CD_3OD) of **^{t}bu-Pd-CNR**.

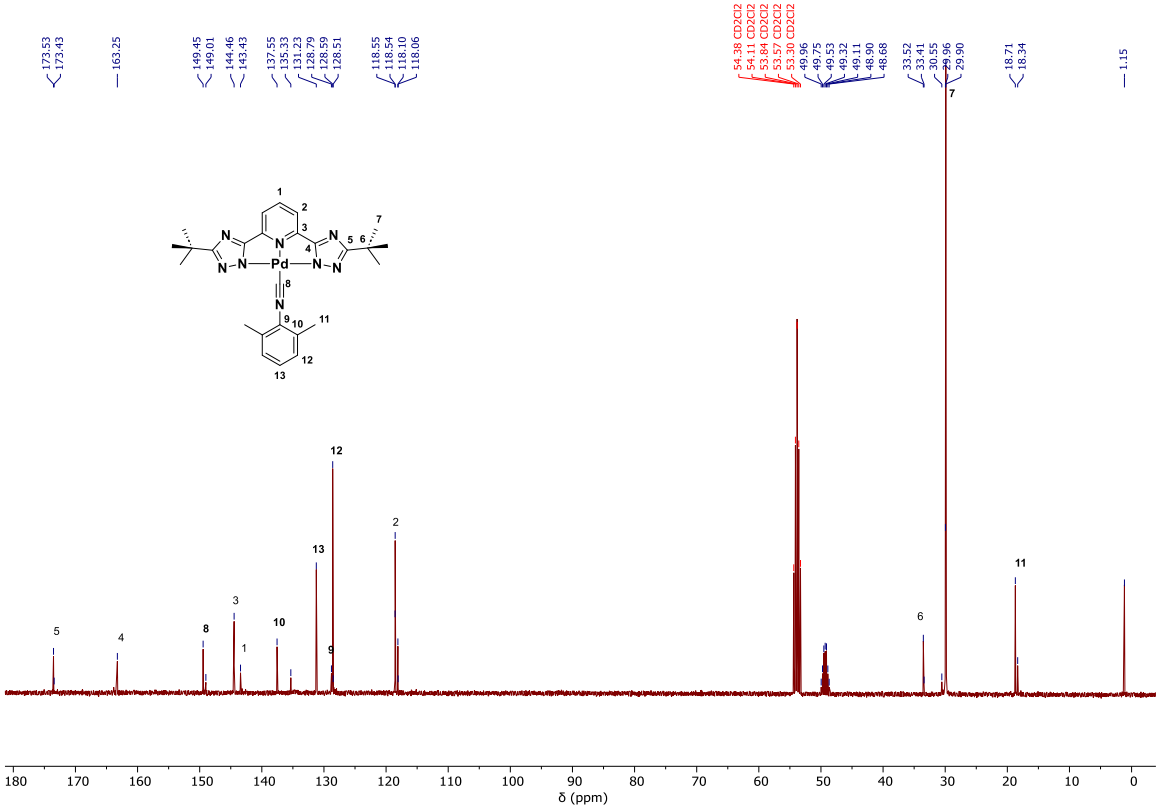

Figure S24. ^{13}C-{^{1}H}-NMR spectrum (101 MHz, DCM-d_2) of **^{t}bu-Pd-CNR**.

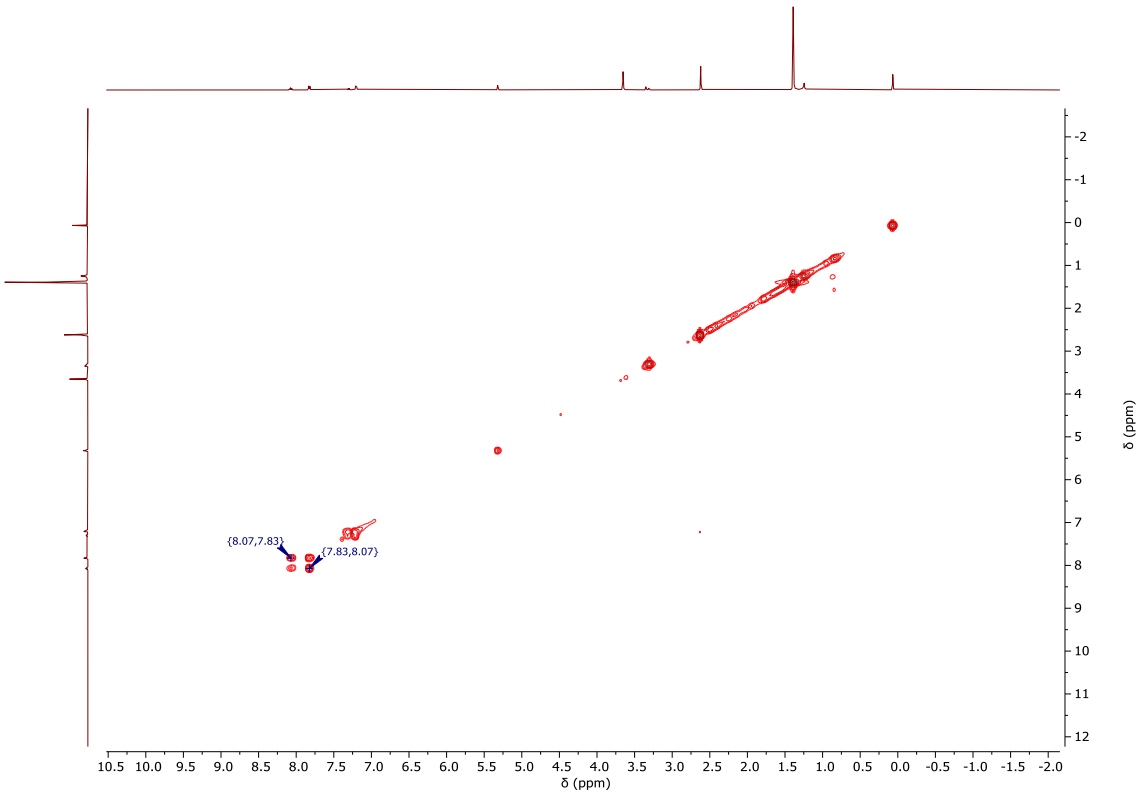

Figure S25. ^{1}H,^{1}H-COSY-NMR spectrum (400 MHz, CD_3OD) of **^{t}bu-Pd-CNR**.

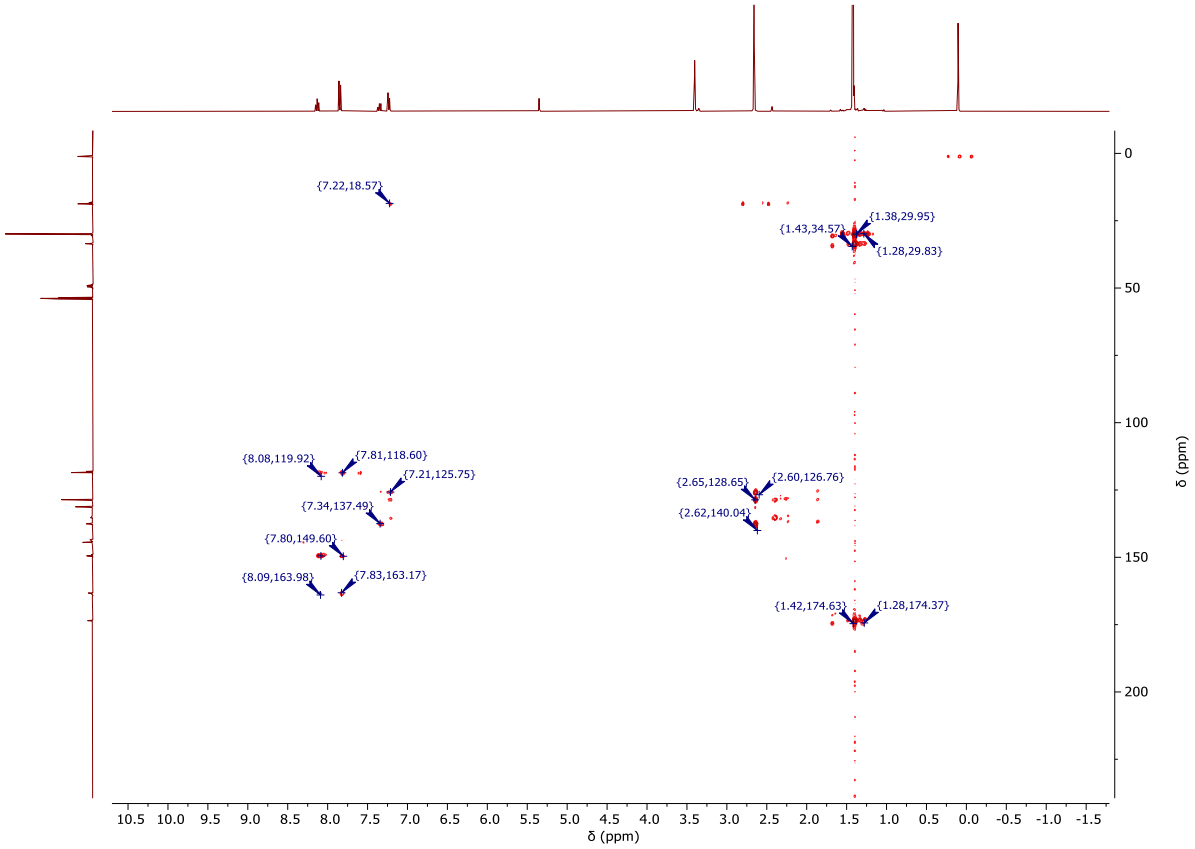

Figure S26. ^{1}H,^{13}C-gHMBC-NMR spectrum (400 MHz, 101 MHz, DCM-d_2/CD_3OD) of **^{t}bu-Pd-CNR**.

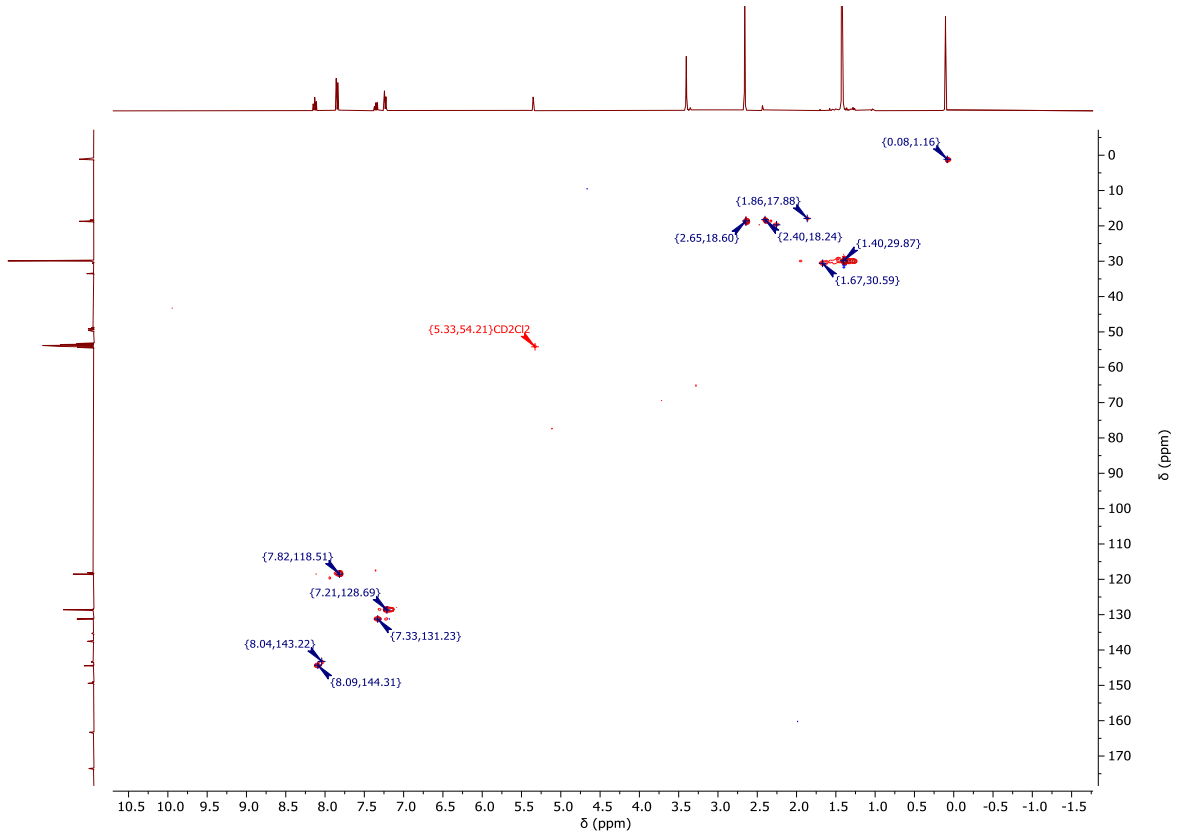

Figure S27. ^{1}H,^{13}C-gHSQC spectrum (400, 101 MHz, DCM-d_2/CD_3OD) of **^{t}bu-Pd-CNR**.

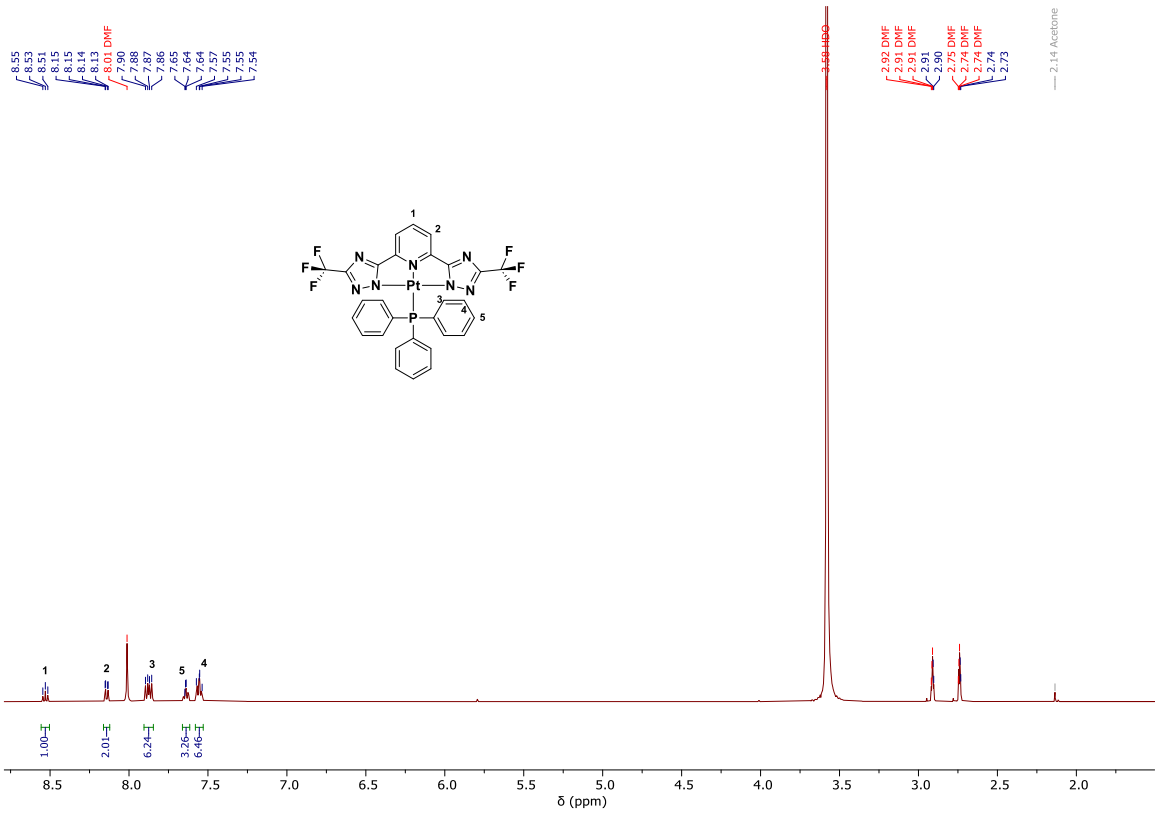

Figure S28. 1H-NMR spectrum (500 MHz, DMF-d_7) of **CF_3-Pt-PPh_3**.

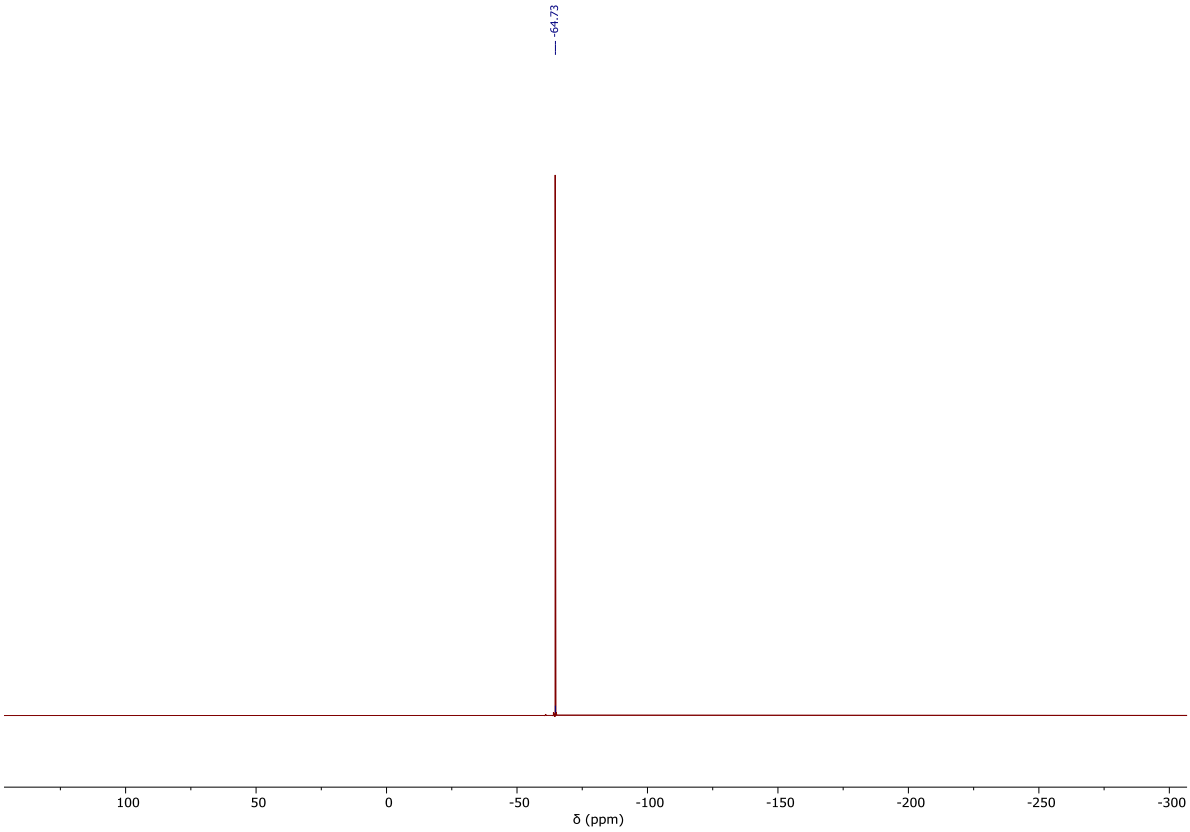

Figure S29. ^{19}F-NMR spectrum (471 MHz, DMF-d_7) of **CF_3-Pt-PPh_3**.

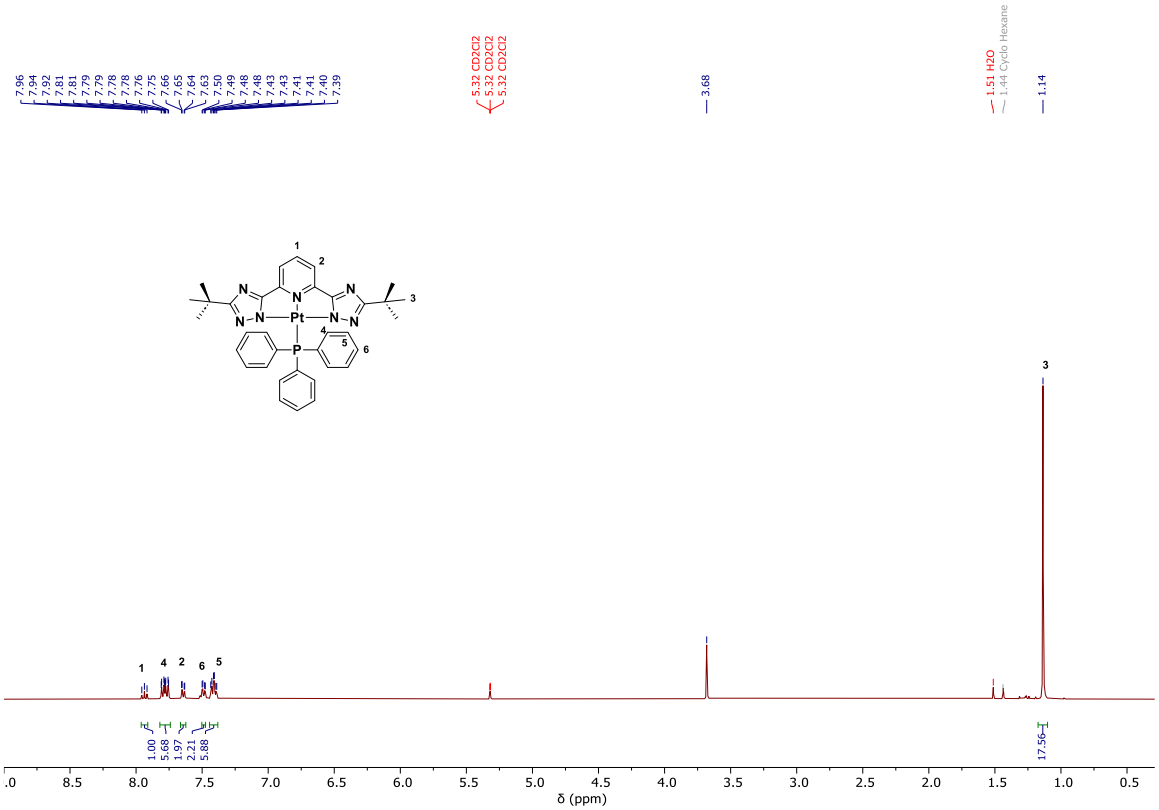

Figure S30. ^{1}H-NMR spectrum (400 MHz, DCM-d_2) of **^{t}bu-Pt-PPh_3**.

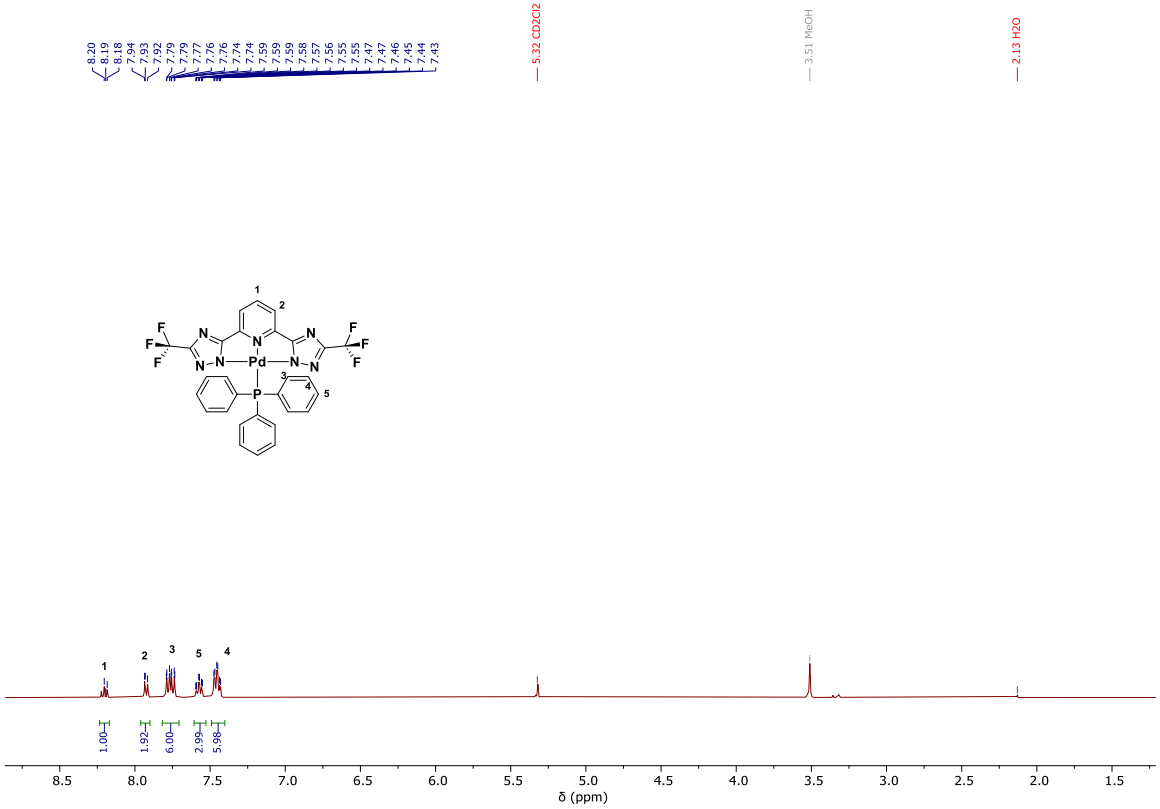

Figure S31. ^{1}H-NMR spectrum (400 MHz, DCM-d_2) of **CF_3-Pd-PPh_3**.

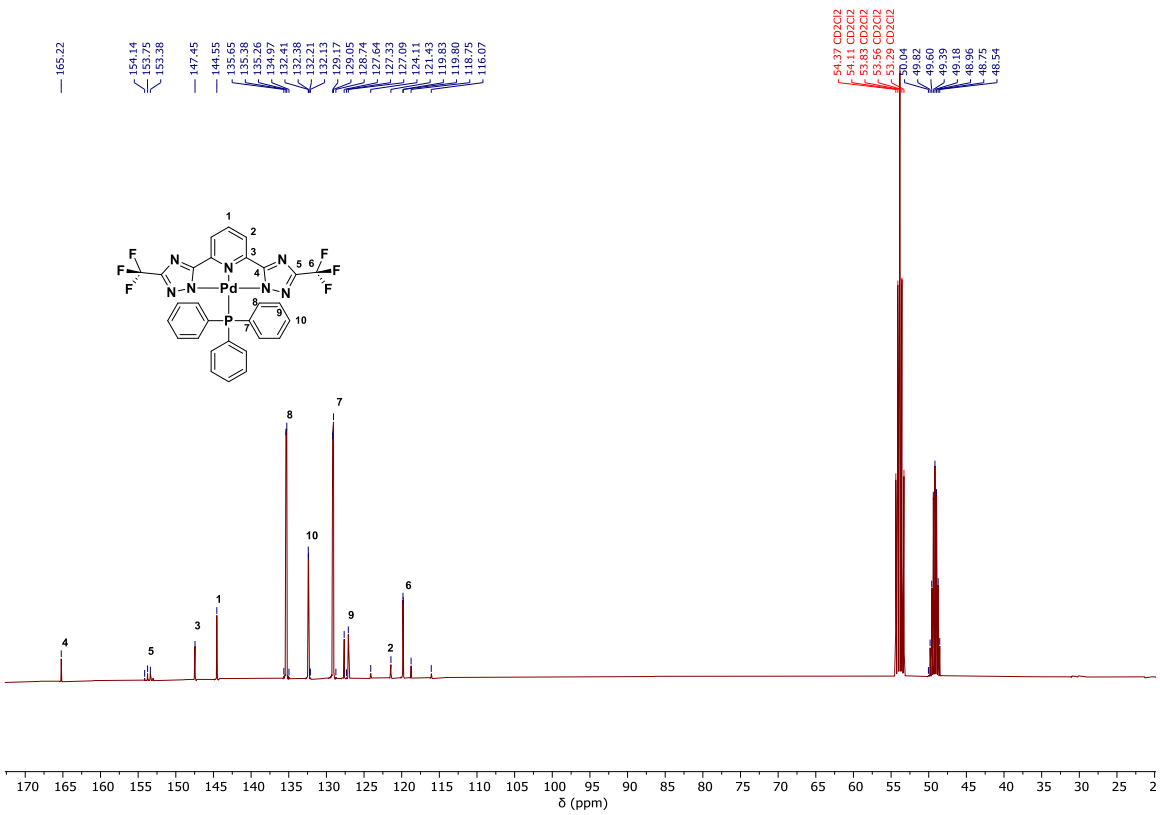

Figure S32. ^{13}C-{^{1}H}-NMR spectrum (101 MHz, DCM-d_2) of **CF_3-Pd-PPh_3**.

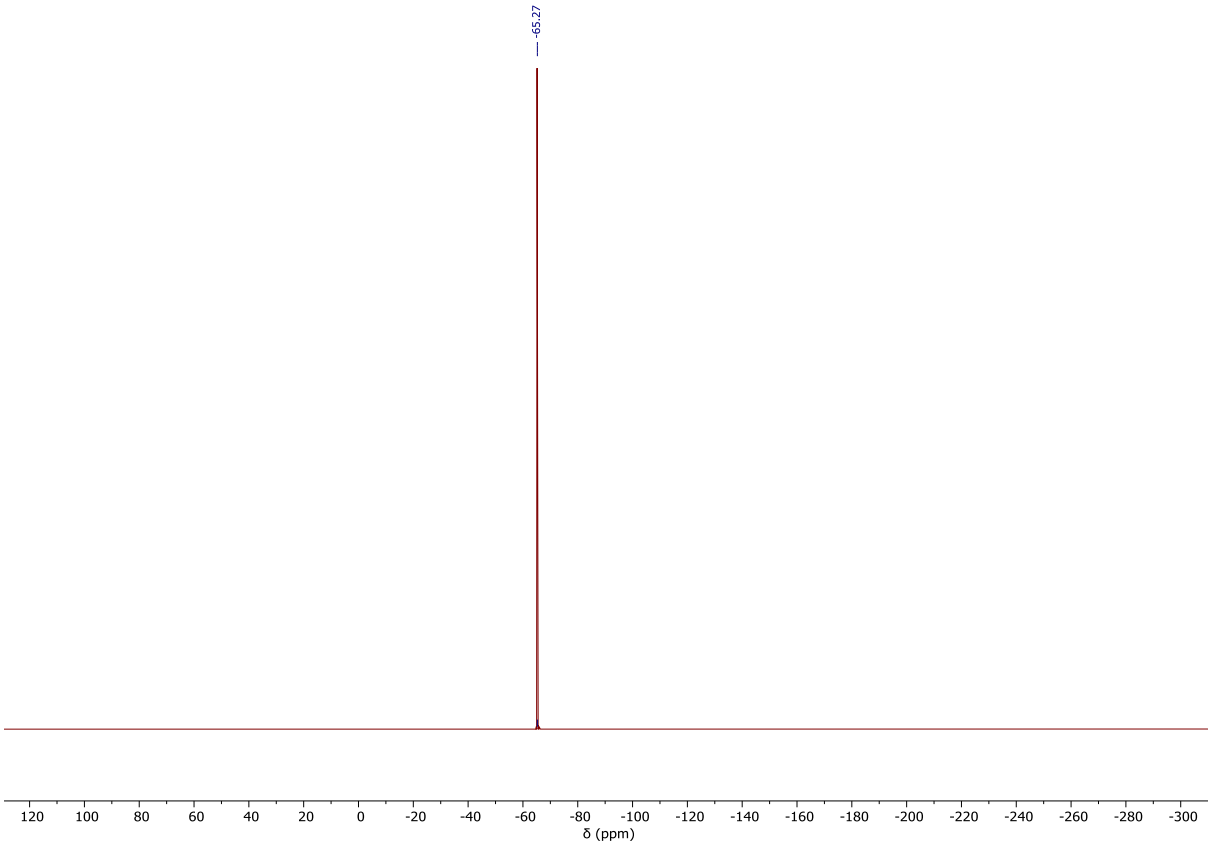

Figure S33. ^{19}F-NMR spectrum (376 MHz, DCM-d_2) of **CF_3-Pd-PPh_3**.

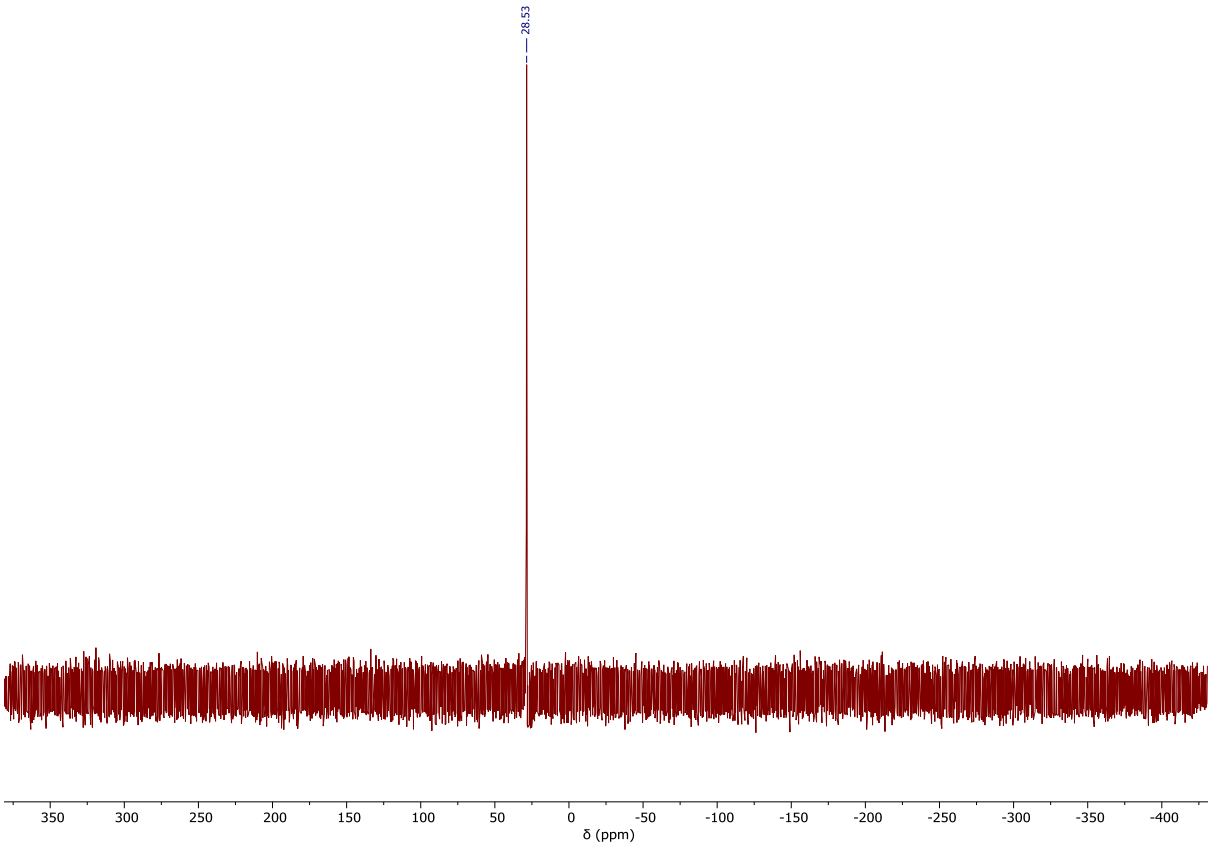

Figure S34. ^{31}P NMR spectrum (162 MHz, DCM-d_2) of **CF_3-Pd-PPh_3**.

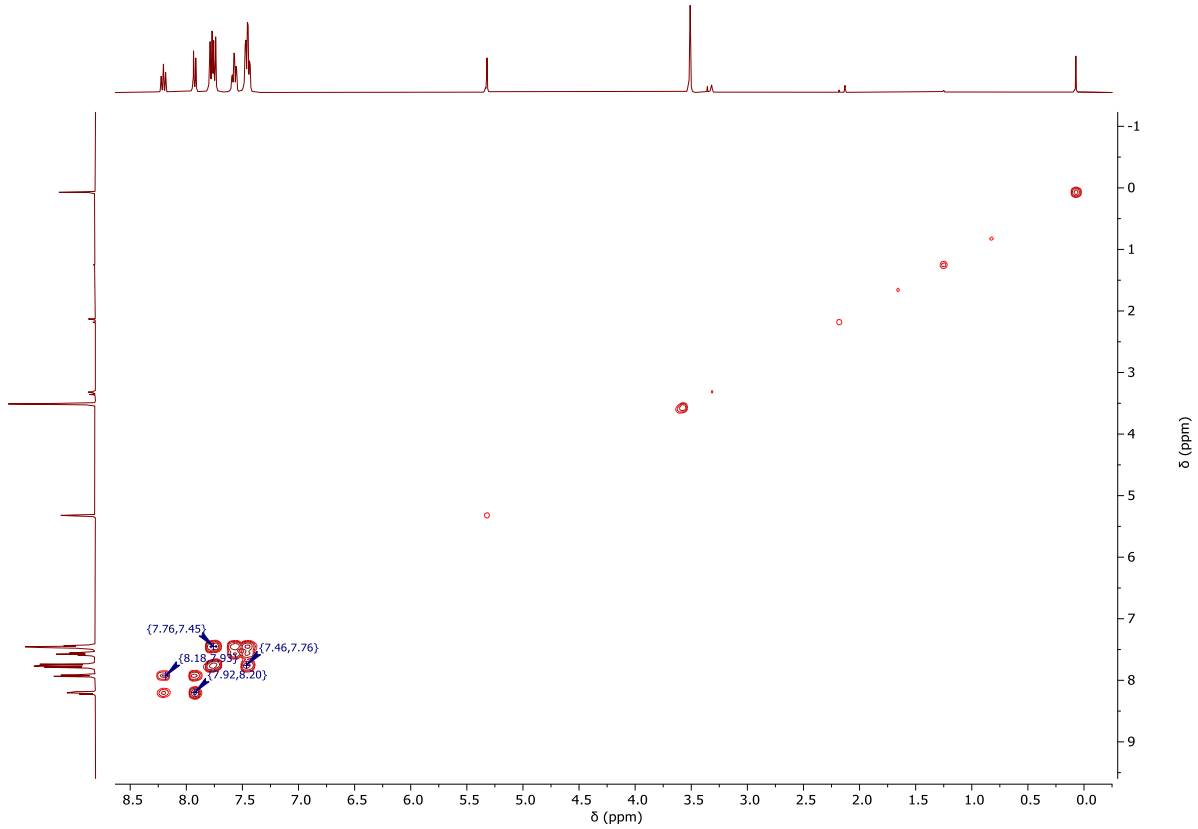

Figure S35. ^{1}H,^{1}H-COSY-NMR spectrum (400 MHz, DCM-d_2) of **CF_3-Pd-PPh_3**.

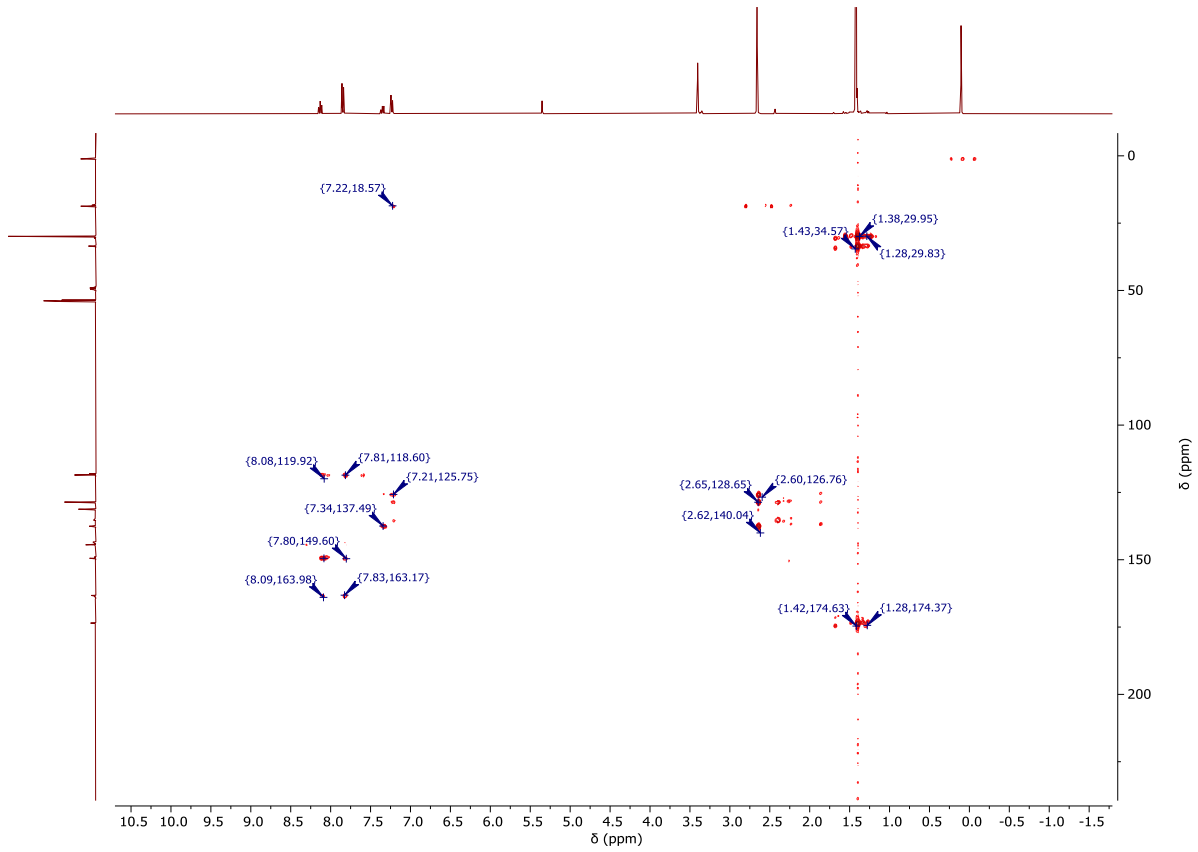

Figure S36. ^{1}H,^{15}N-gHMBC-NMR spectrum (400 MHz, 101 MHz, DCM-d_2) of **CF_3-Pd-PPh_3**.

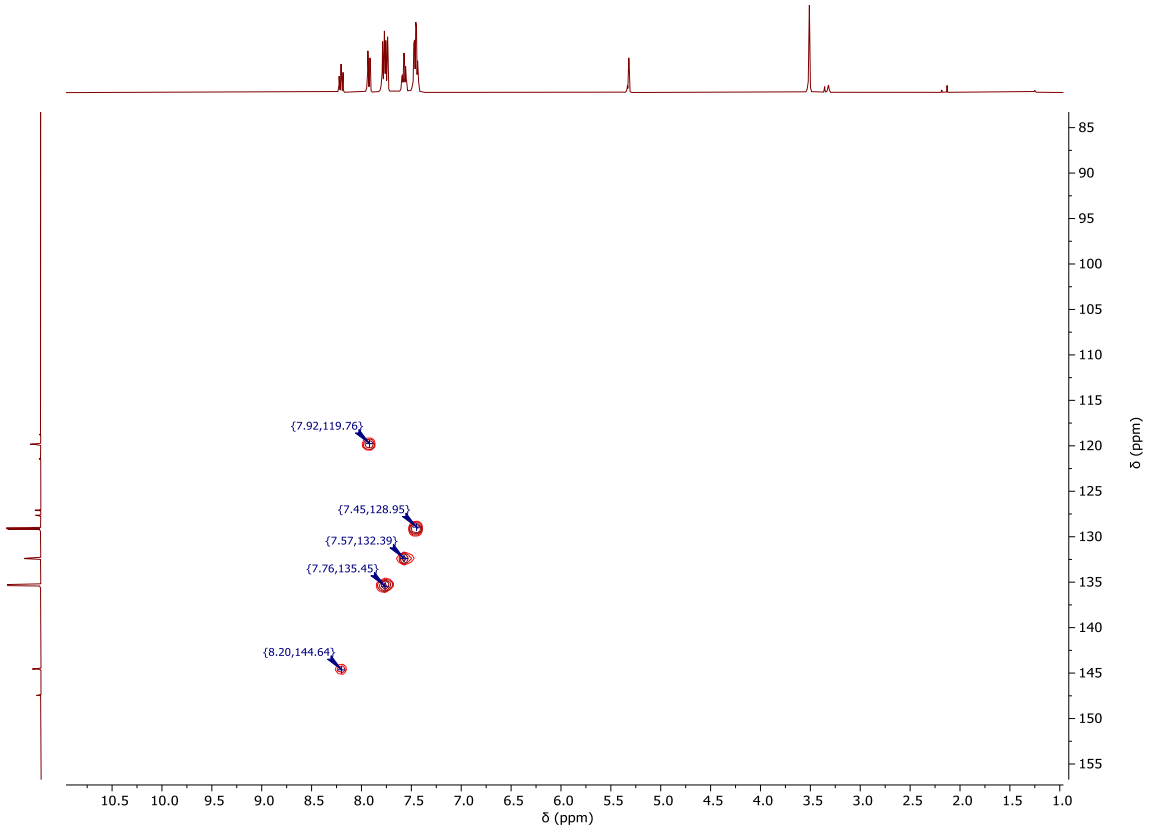

Figure S37. ^{1}H,^{13}C-gHSQC-NMR spectrum (400 MHz, 101 MHz, DCM-d_2) of **CF_3-Pd-PPh_3**.

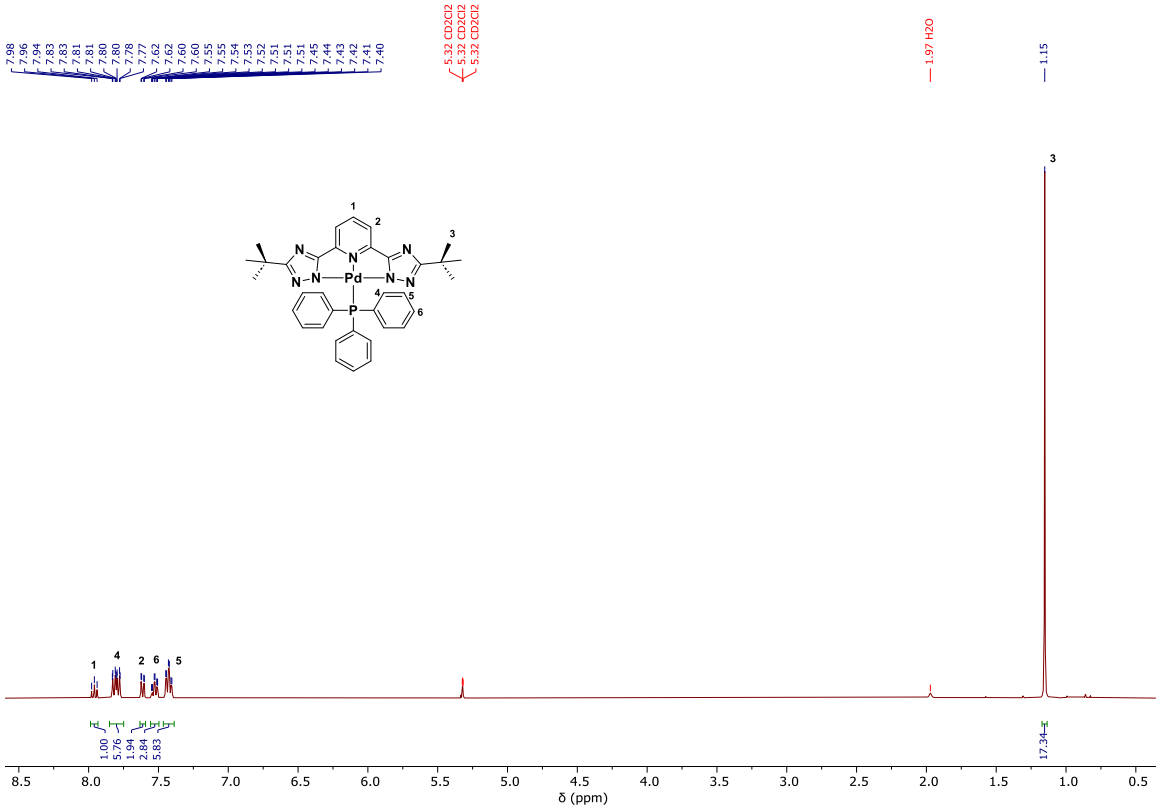

Figure S38. ^{1}H-NMR spectrum (400 MHz, DCM-d_2) of **^{t}bu-Pd-PPh_3**.

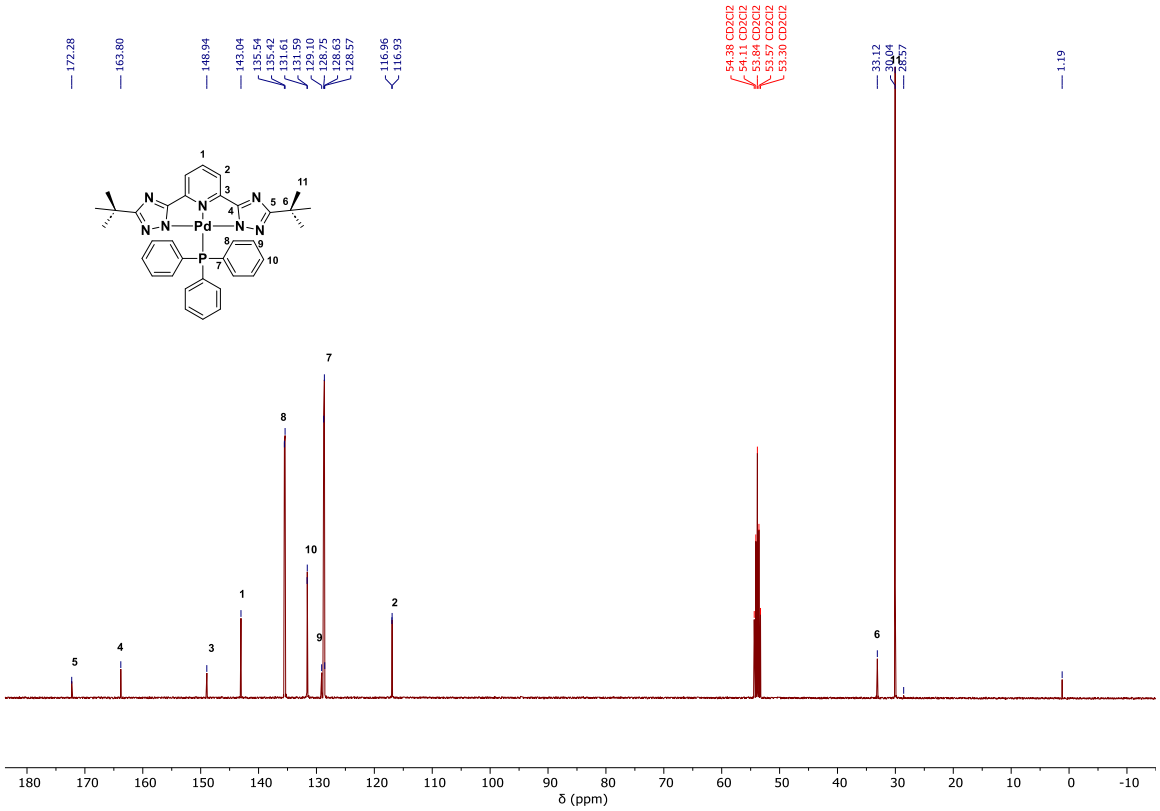

Figure S39. ^{13}C-{^{1}H}-NMR spectrum (101 MHz, DCM-d_2) of **^{t}bu-Pd-PPh$_3$**.

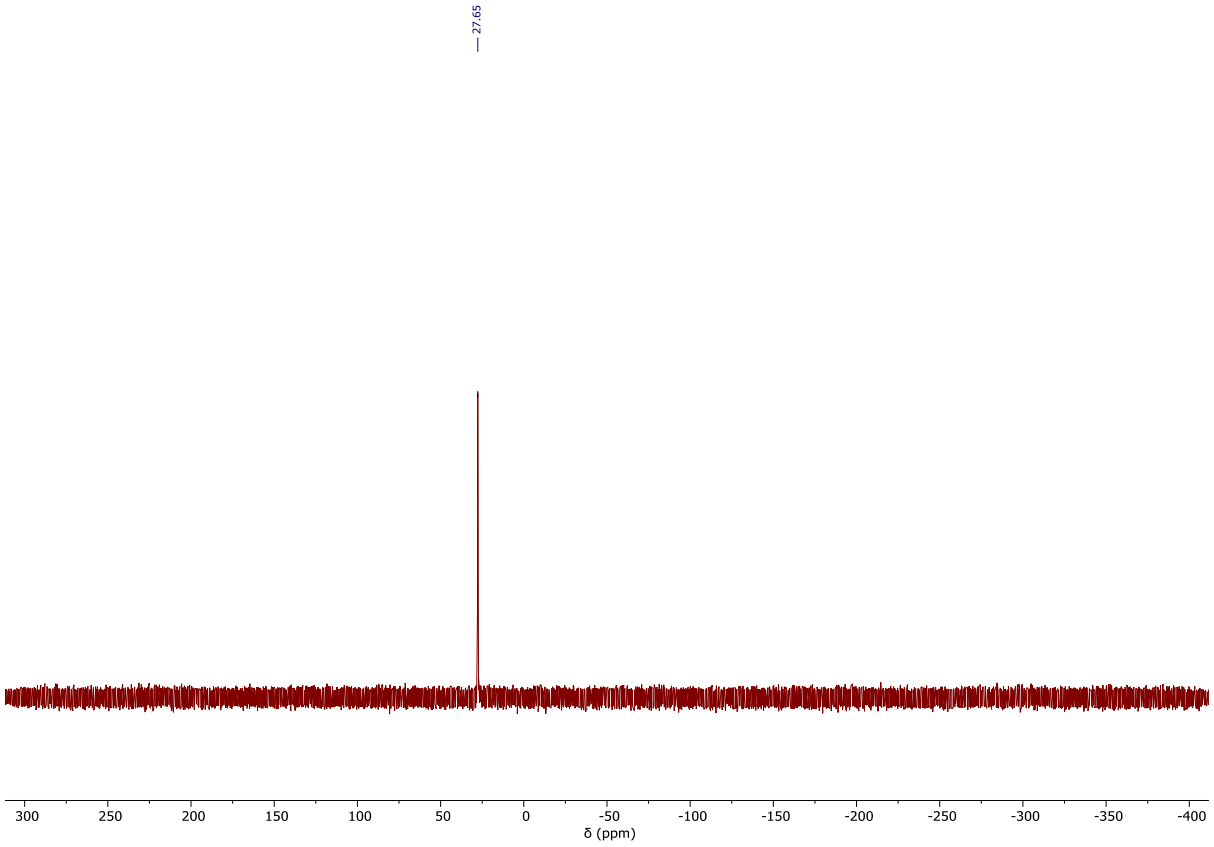

Figure S40. ^{31}P NMR spectrum (162 MHz, DCM-d_2) of **^{t}bu-Pd-PPh$_3$**.

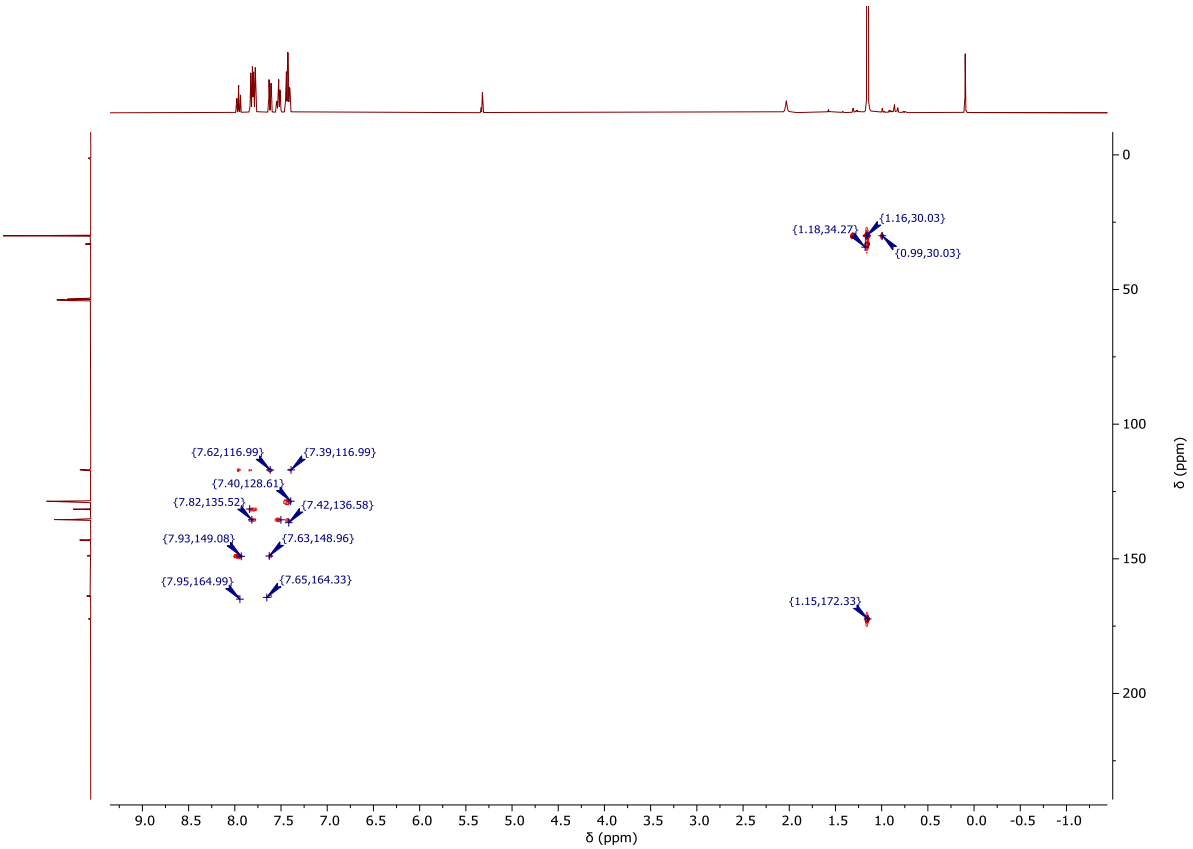

Figure S41. $^{1}H,^{13}C$-gHMBC-NMR spectrum (400 MHz, 101 MHz, DCM-d_2) of **^{t}bu-Pd-PPh$_3$**.

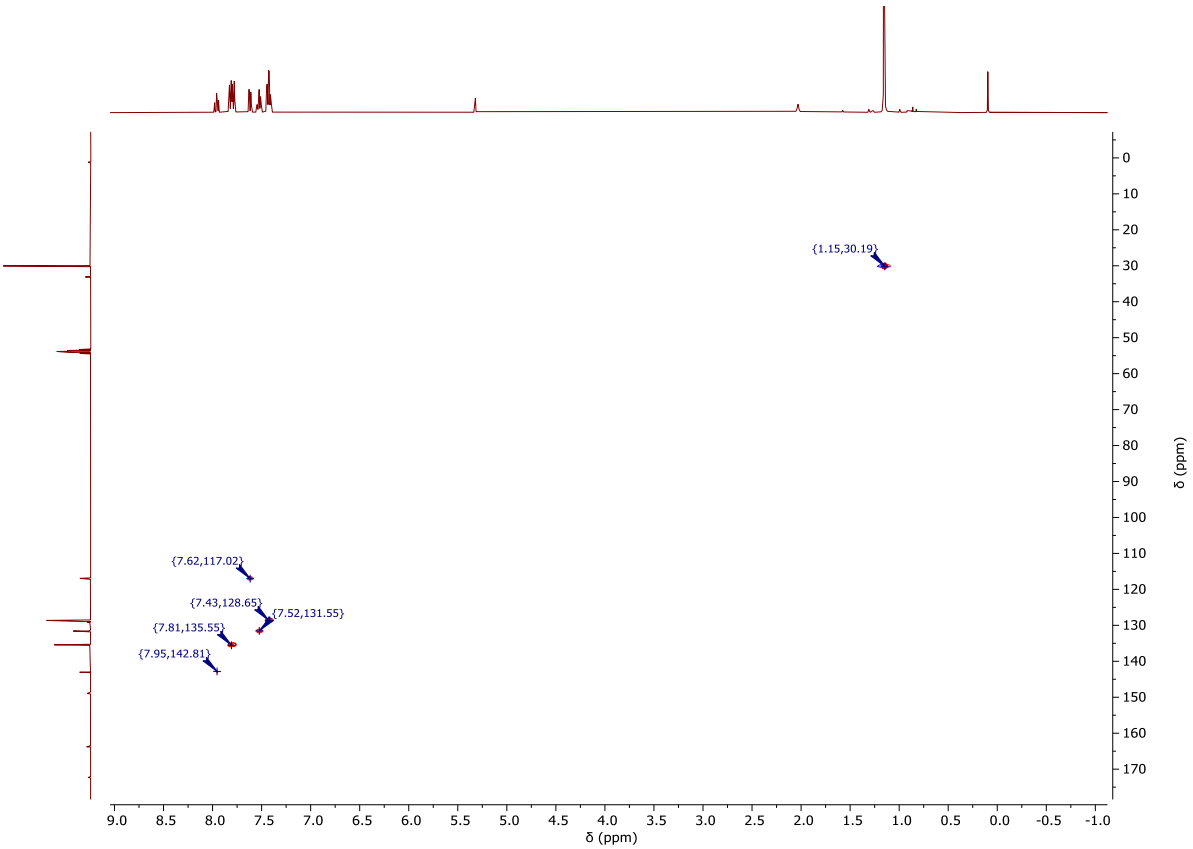

Figure S42. $^{1}H,^{13}C$-gHSQC-NMR spectrum (400 MHz, 101 MHz, DCM-d_2) of **^{t}bu-Pd-PPh$_3$**.

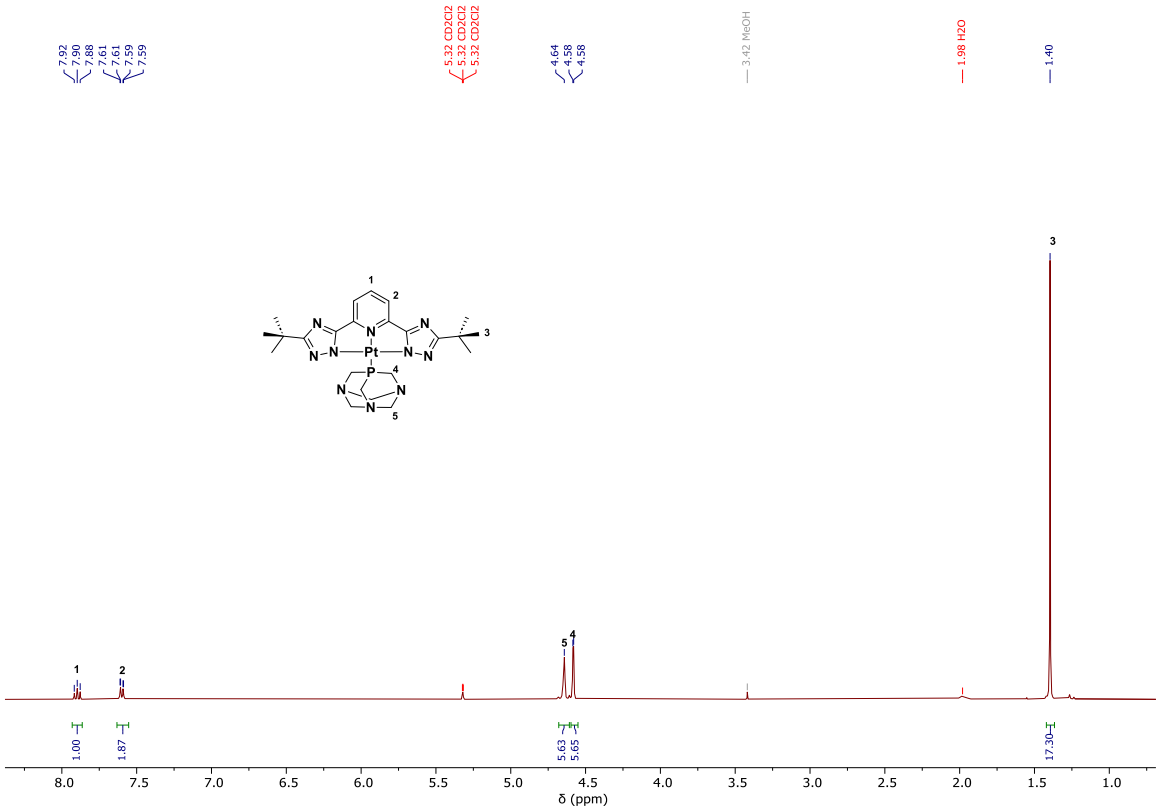

Figure S43. ^{1}H-NMR spectrum (400 MHz, DCM-d_2) of **^{t}bu-Pt-PTA**.

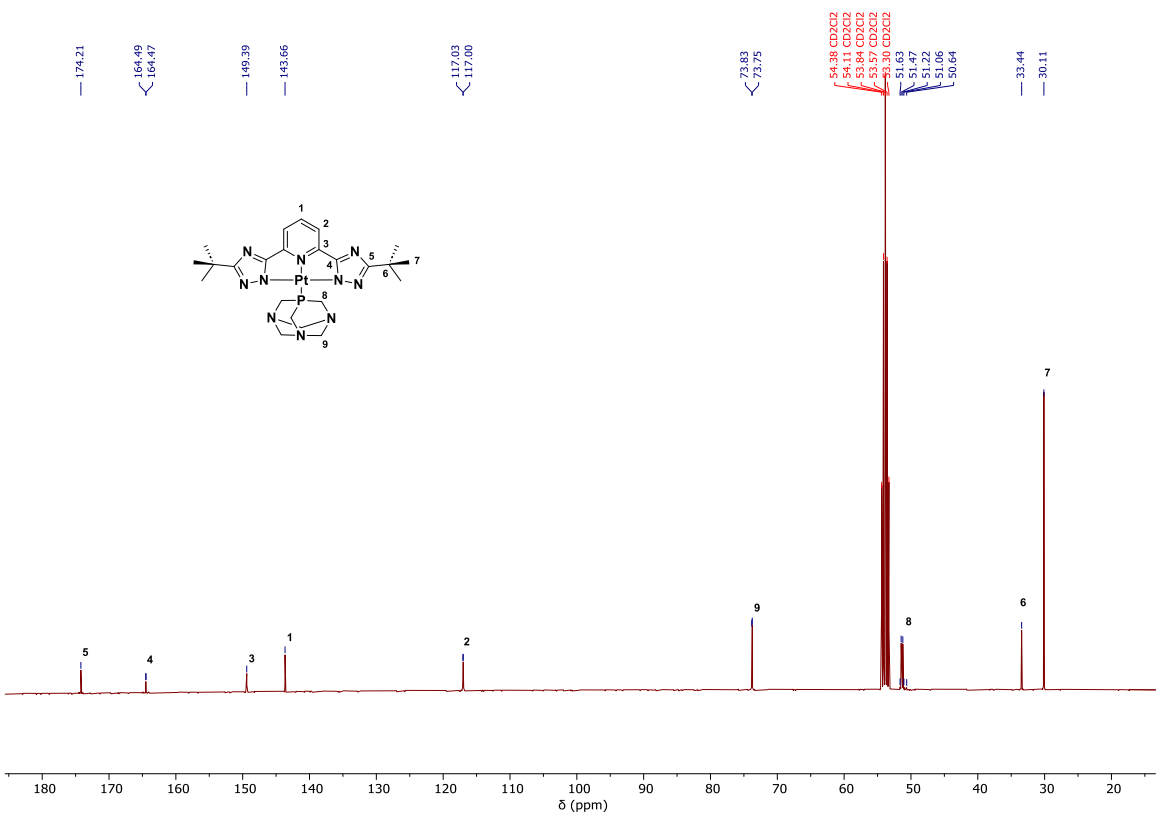

Figure S44. ^{13}C-{^{1}H}-NMR spectrum (101 MHz, DCM-d_2) of **^{t}bu-Pt-PTA**.

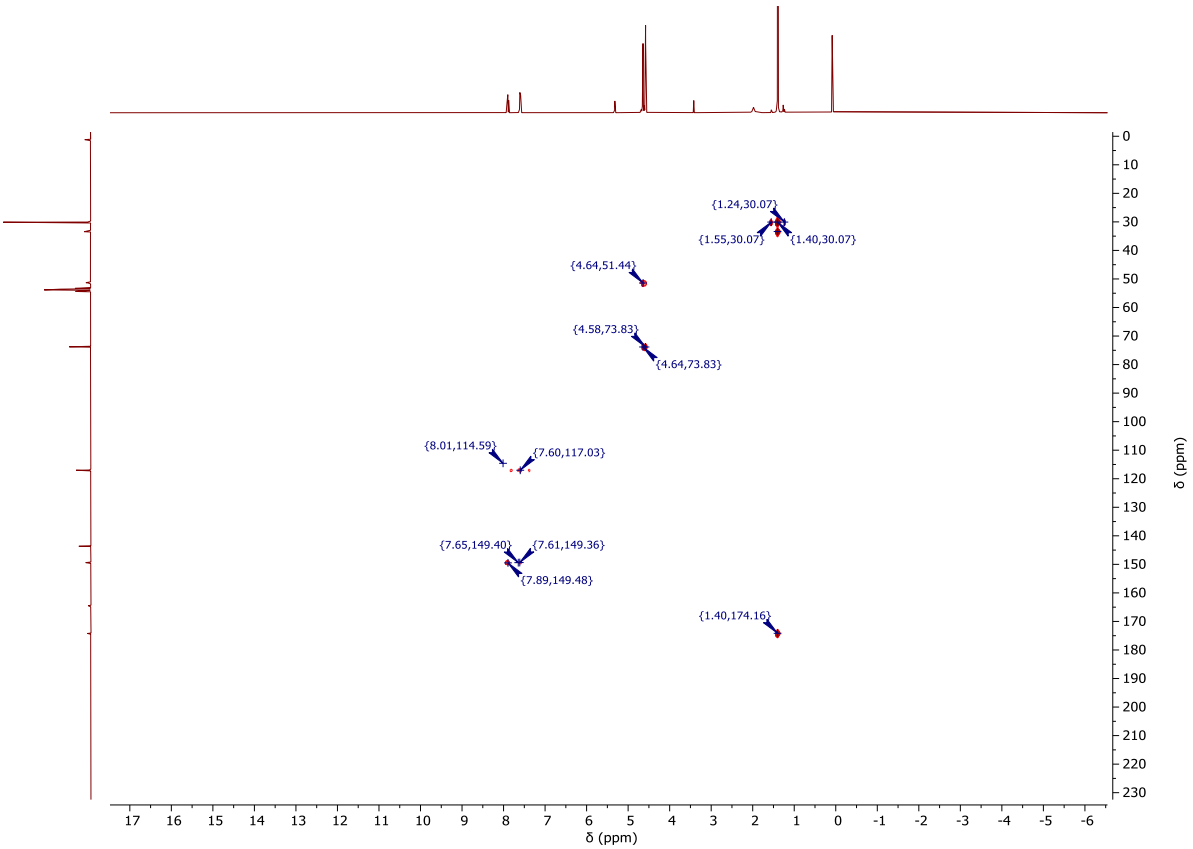

Figure S45. $^{1}H,^{13}C$-gHMBC-NMR spectrum (400 MHz, 101 MHz, DCM-d_2) of **^{t}bu-Pt-PTA**.

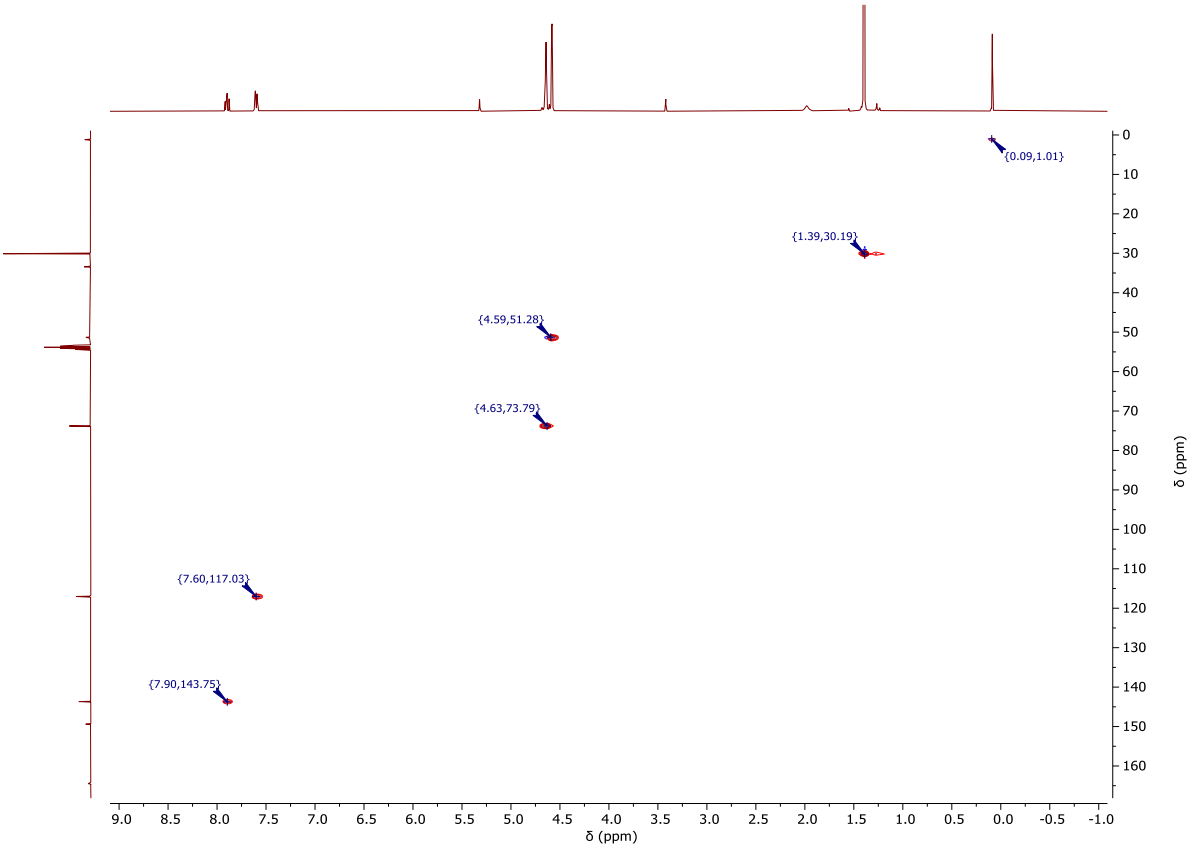

Figure S46. $^{1}H,^{13}C$-gHSQC-NMR spectrum (400 MHz, 101 MHz, DCM-d_2) of **^{t}bu-Pt-PTA**.

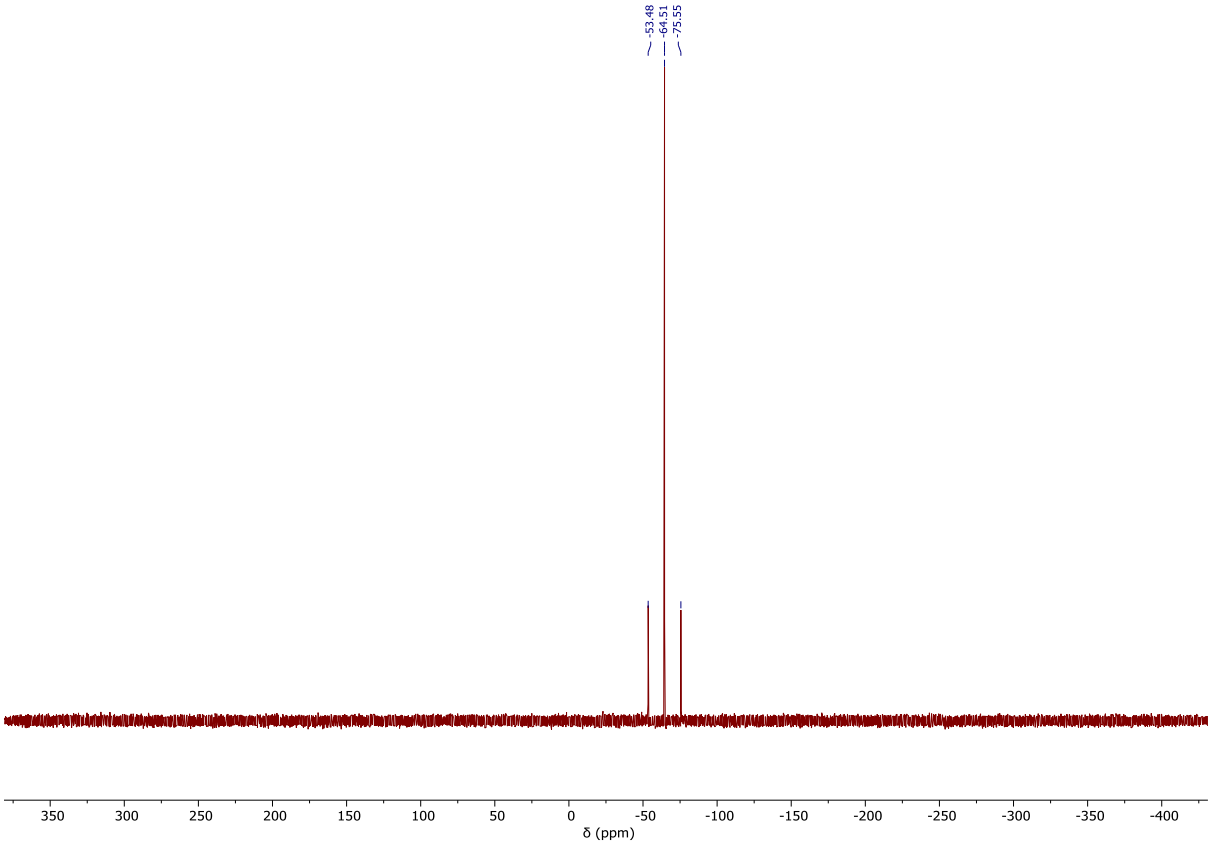

Figure S47. ^{31}P NMR spectrum (162 MHz, DCM-d_2) of **^{t}bu-Pt-PTA**.

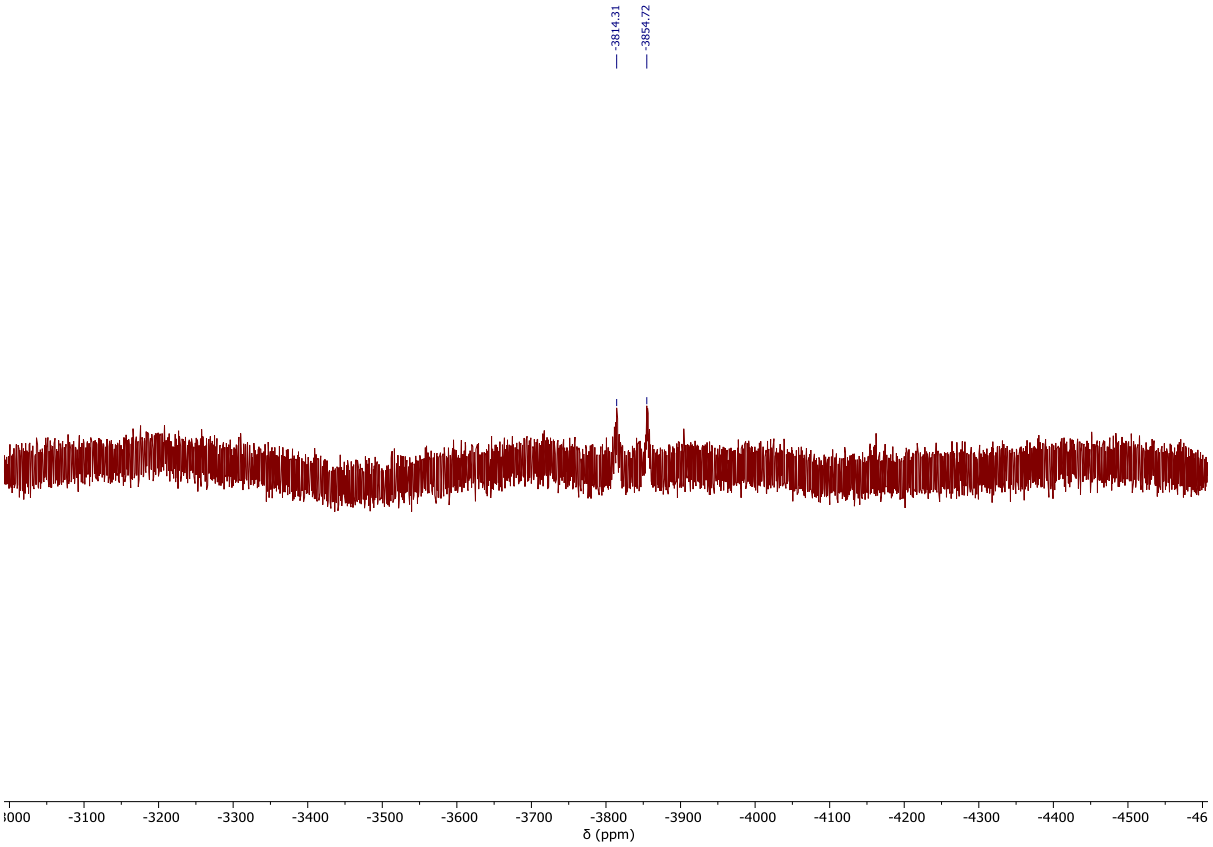

Figure S48. ^{195}Pt NMR spectrum (86 MHz, DCM-d_2) of **^{t}bu-Pt-PTA**.

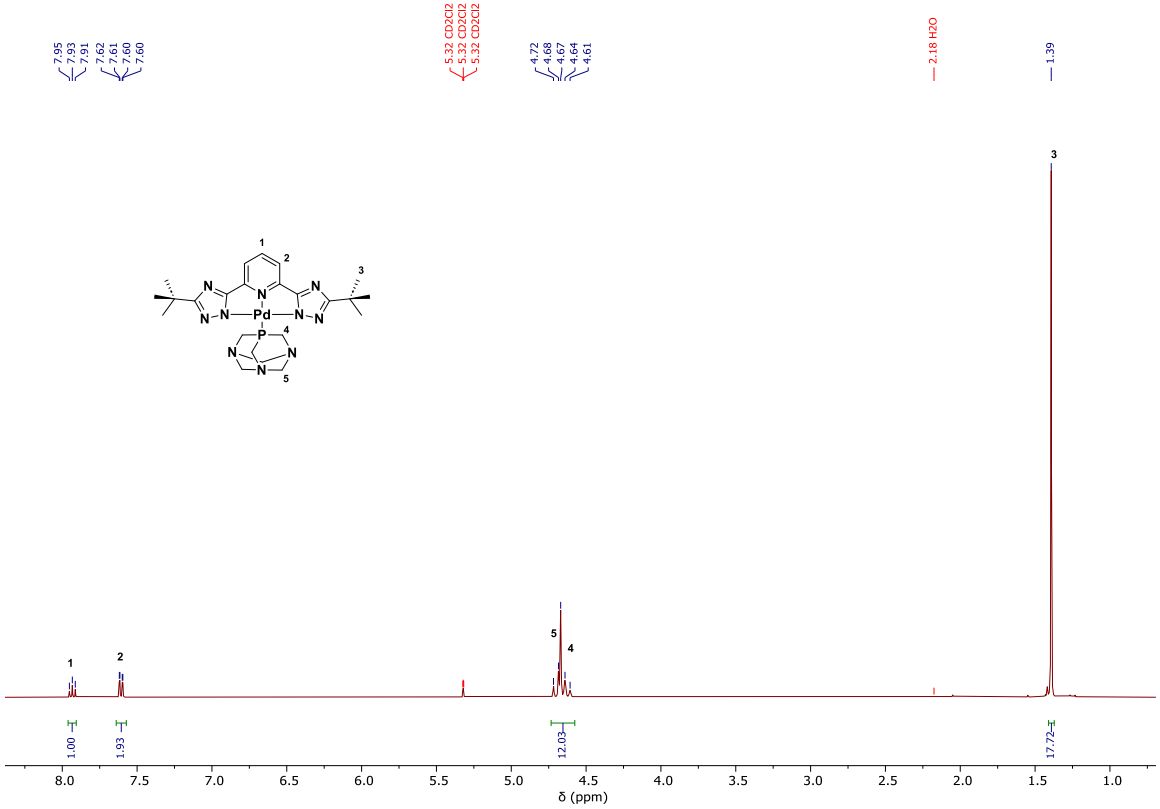

Figure S49. ^{1}H-NMR spectrum (400 MHz, DCM-d_2) of **^{t}bu-Pd-PTA**.

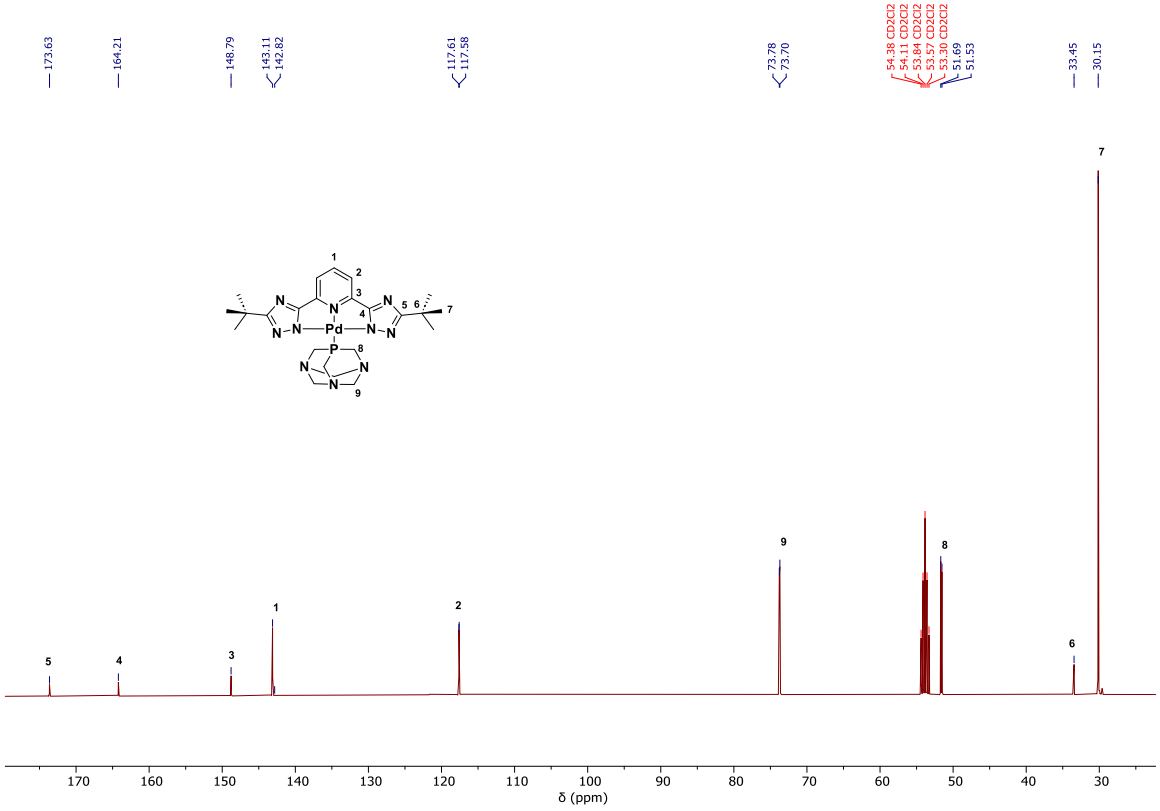

Figure S50. ^{13}C-{^{1}H}-NMR spectrum (101 MHz, DCM-d_2) of **^{t}bu-Pd-PTA**.

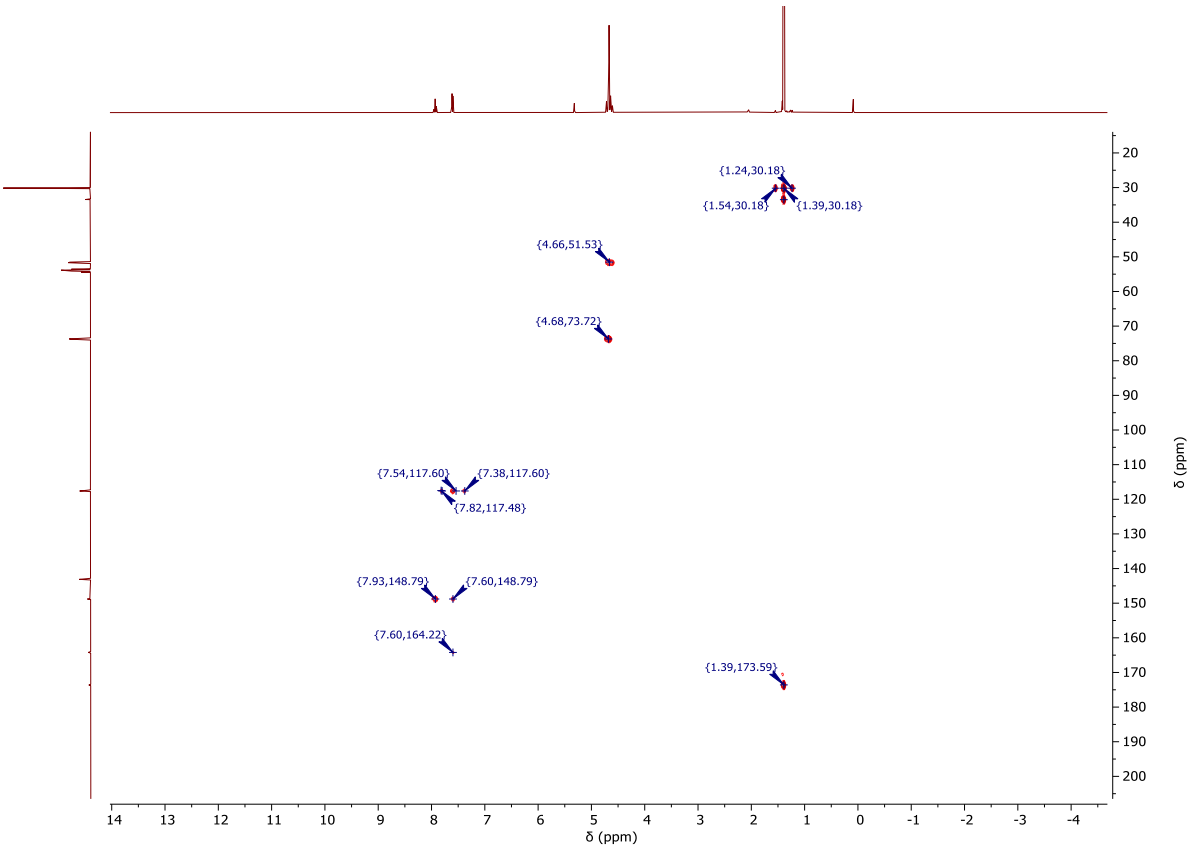

Figure S51. ^{1}H,^{13}C-gHMBC-NMR spectrum (400 MHz, 101 MHz, DCM-d_2) of **^{t}bu-Pd-PTA**.

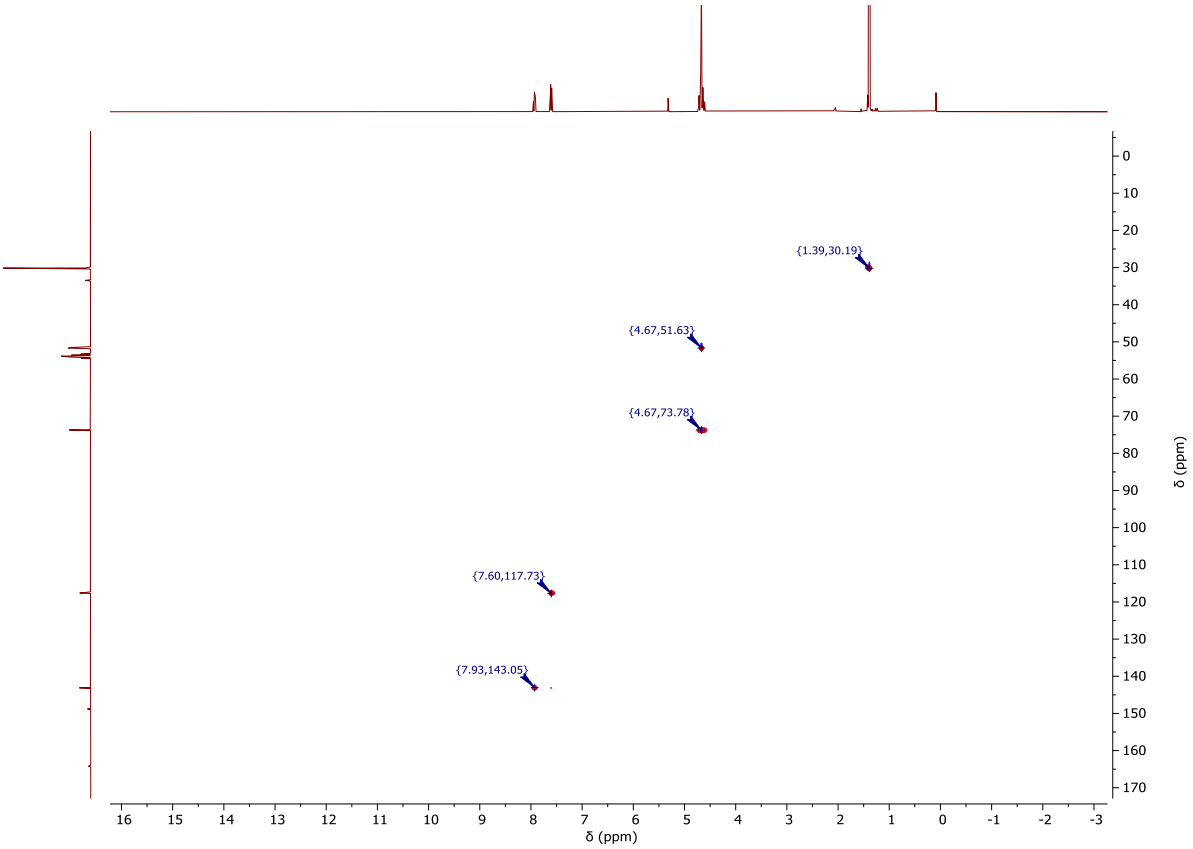

Figure S52. ^{1}H,^{13}C-gHSQC-NMR spectrum (400 MHz, 101 MHz, DCM-d_2) of **^{t}bu-Pd-PTA**.

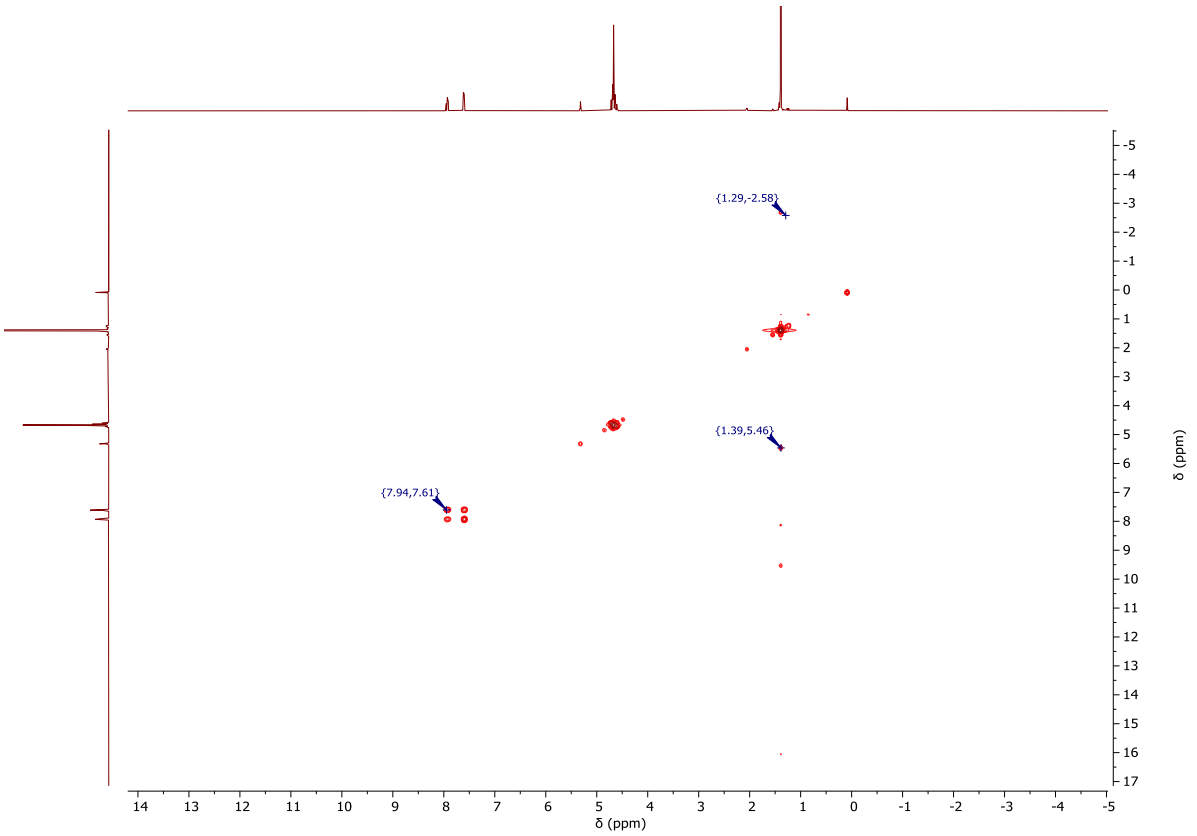

Figure S53. ^{1}H,^{1}H-COSY-NMR spectrum (101 MHz, DCM-d_2) of **^{t}bu-Pd-PTA**.

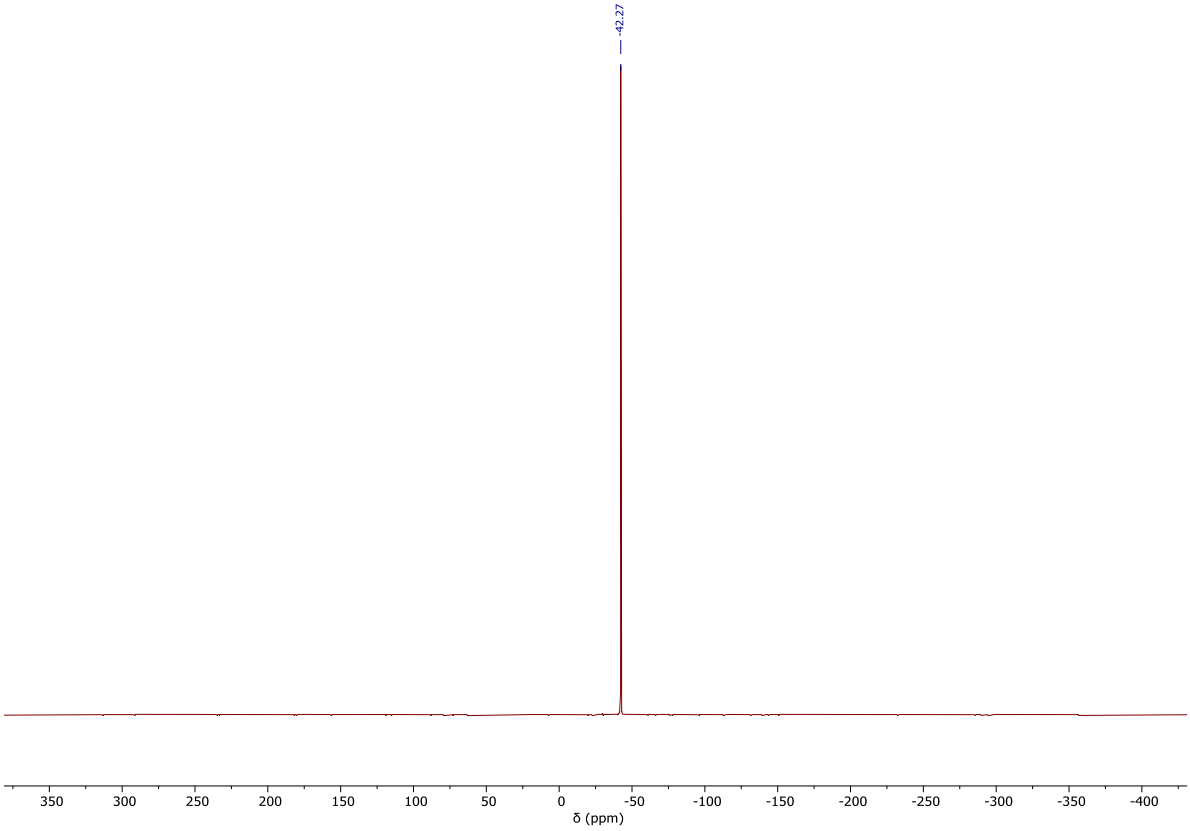

Figure S54. ^{31}P NMR spectrum (162 MHz, DCM-d_2) of **^{t}bu-Pd-PTA**.

Mass spectra of the N^N^N ligand precursors and of the complexes

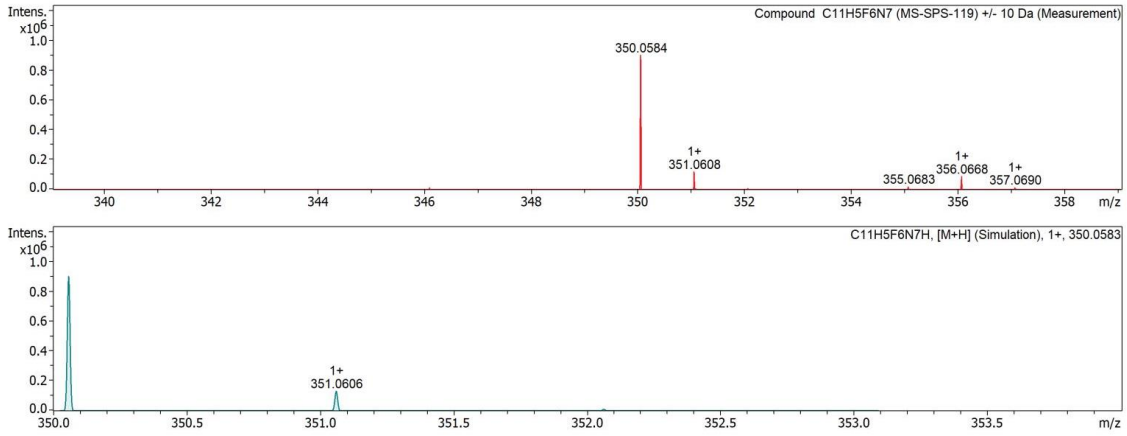

Figure S55. Mass spectrum of the **CF_3** ligand precursor (in MeOH, top). Additional simulation for the [**CF_3**+H]$^+$ adduct (bottom).

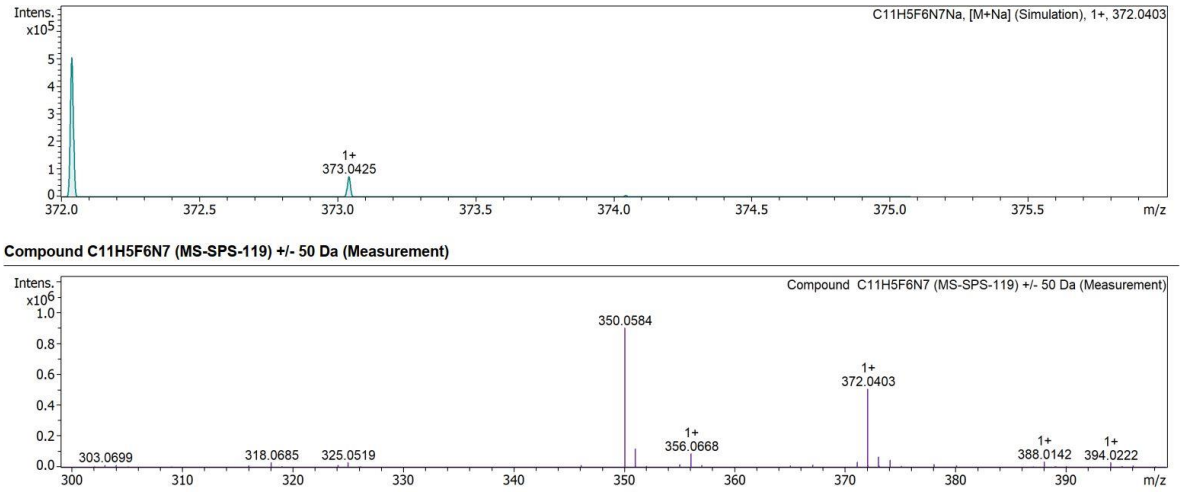

Figure S56. Mass spectrum of the **CF_3** ligand precursor (in MeOH, top). Additional simulation for the [**CF_3**+Na]$^+$ adduct (bottom).

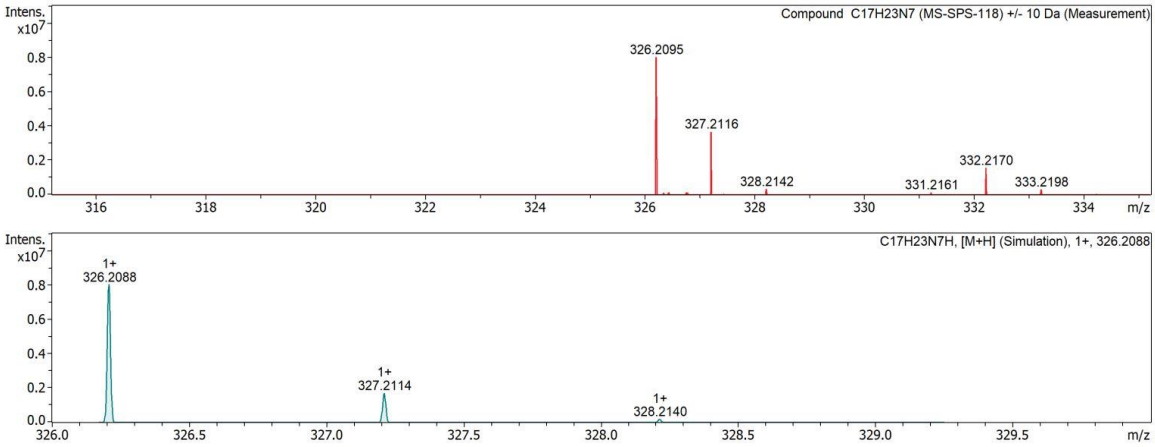

Figure S57. Mass spectrum of the **^{t}bu** ligand precursor (in MeOH, top). Additional simulation of the [**^{t}bu**+H]$^+$ adduct (bottom).

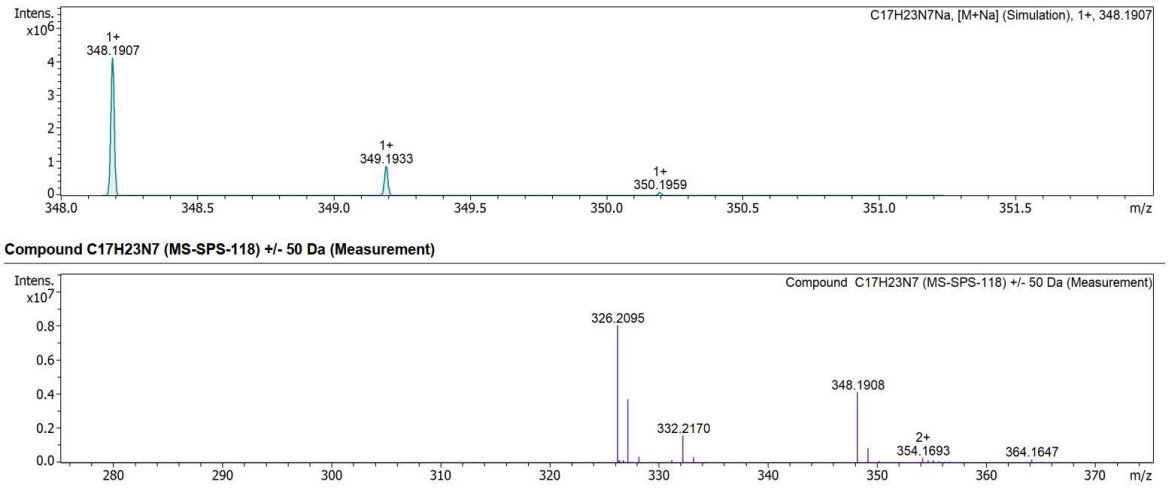

Figure S58. Mass spectrum of the **^{t}bu** ligand precursor (in MeOH, top). Additional simulation of the [**^{t}bu**+Na]$^+$ adduct (bottom).

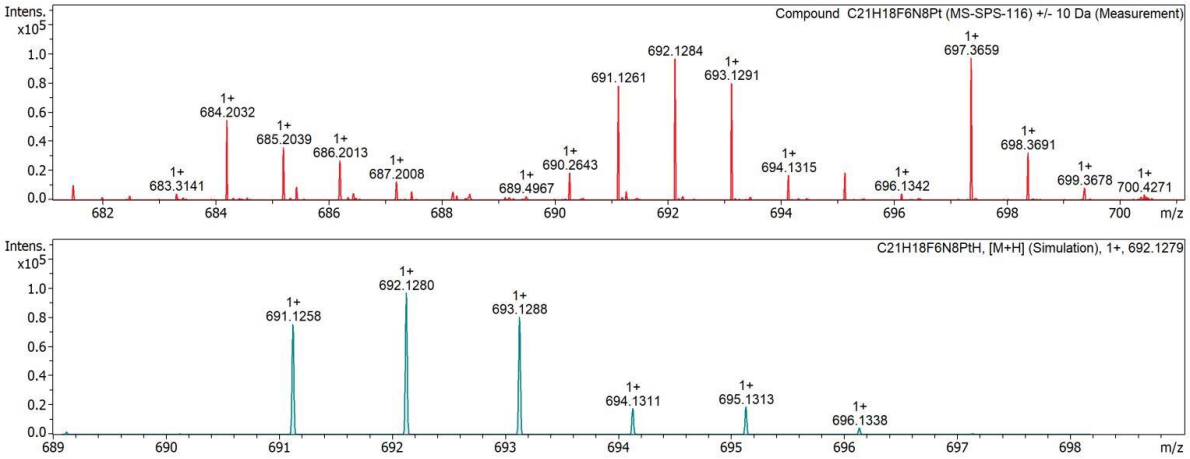

Figure S59. Mass spectrum of **CF$_3$-Pt-AmPy** (in MeOH, top). Additional simulation of the [**CF$_3$-Pt-AmPy**+H]$^+$ adduct (bottom).

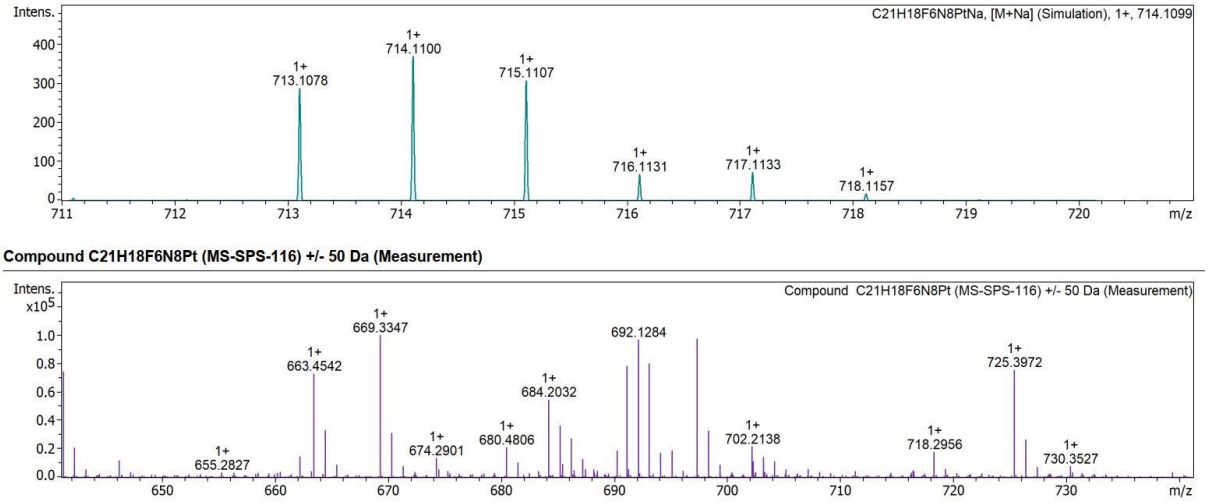

Figure S60. Mass spectrum of **CF$_3$-Pt-AmPy** (in MeOH, top). Additional simulation of the [**CF$_3$-Pt-AmPy**+Na]$^+$ adduct (bottom).

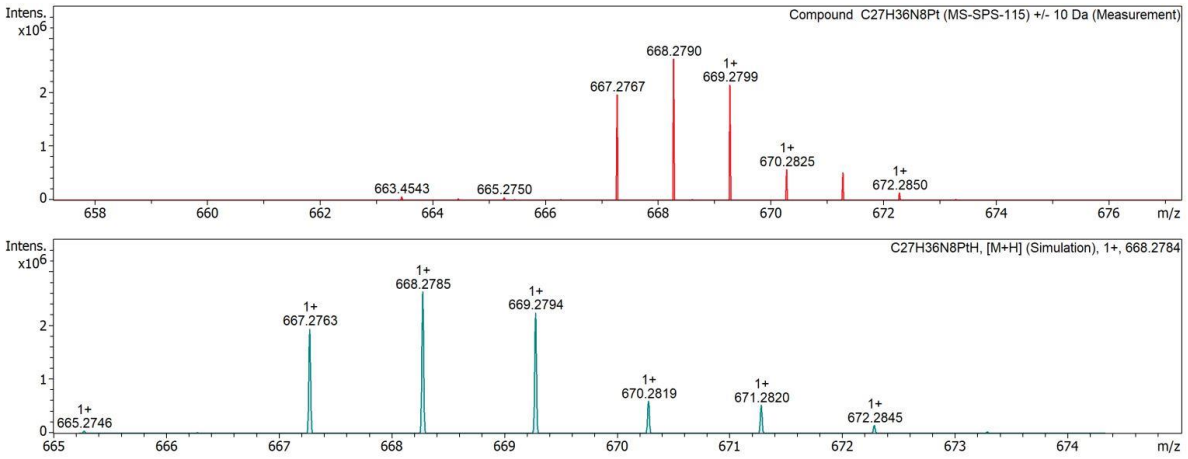

Figure S61. Mass spectrum of **^{t}bu-Pt-AmPy** (in MeOH, top). Additional simulation for the [**^{t}bu-Pt-AmPy**+H]$^+$ adduct (bottom).

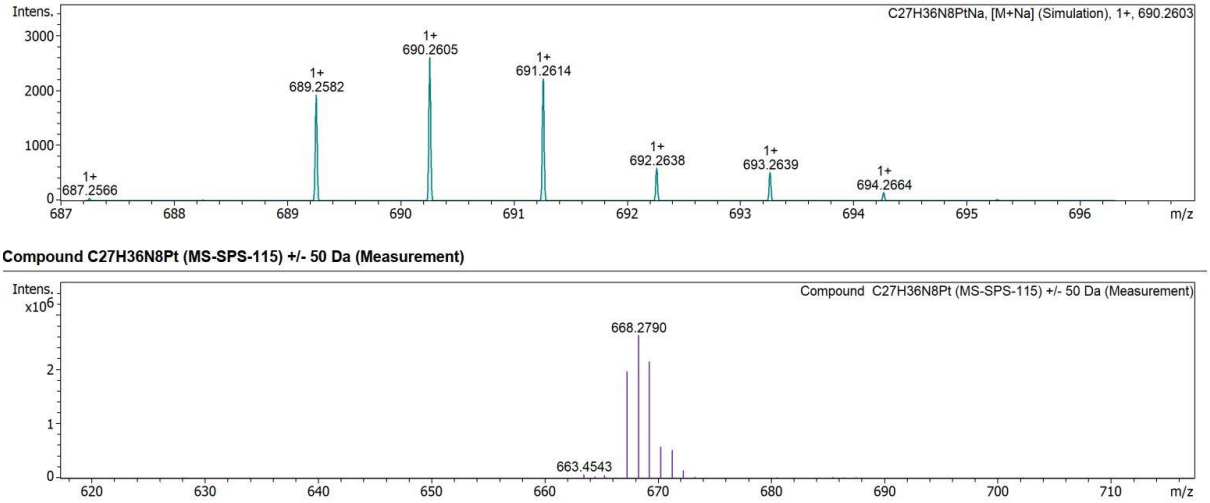

Figure S62. Mass spectrum of **^{t}bu-Pt-AmPy** (in MeOH, top). Additional simulation for the [**^{t}bu-Pt-AmPy**+Na]$^+$ adduct (bottom).

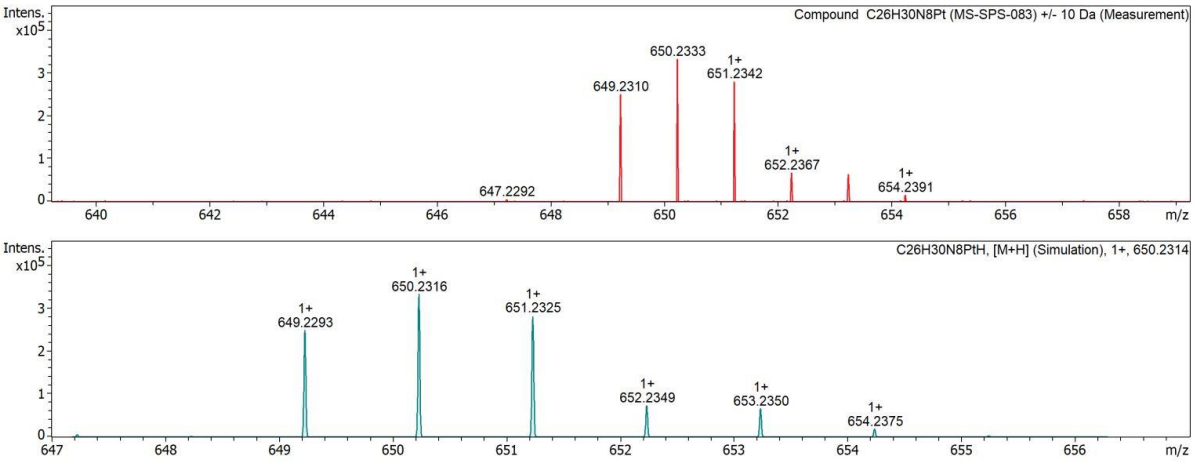

Figure S63. Mass spectrum of **^{t}bu-Pt-CNR** (in MeOH, top). Additional simulation for the [**^{t}bu-Pt-CNR**+H]$^+$ adduct (bottom).

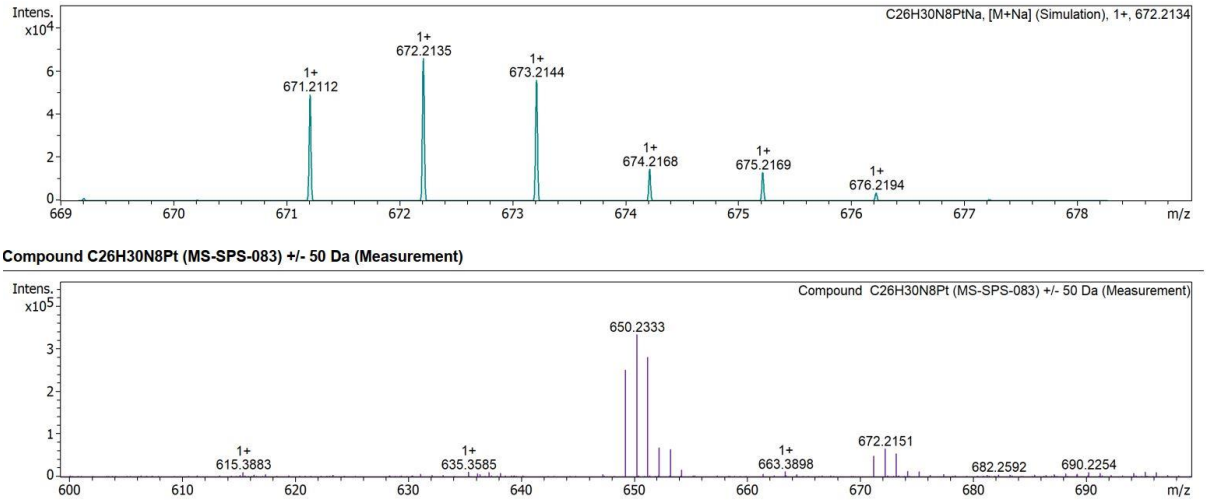

Figure S64. Mass spectrum of **^{t}bu-Pt-CNR** (in MeOH, top). Additional simulation for the [**^{t}bu-Pt-CNR**+Na]$^{+}$ adduct (bottom).

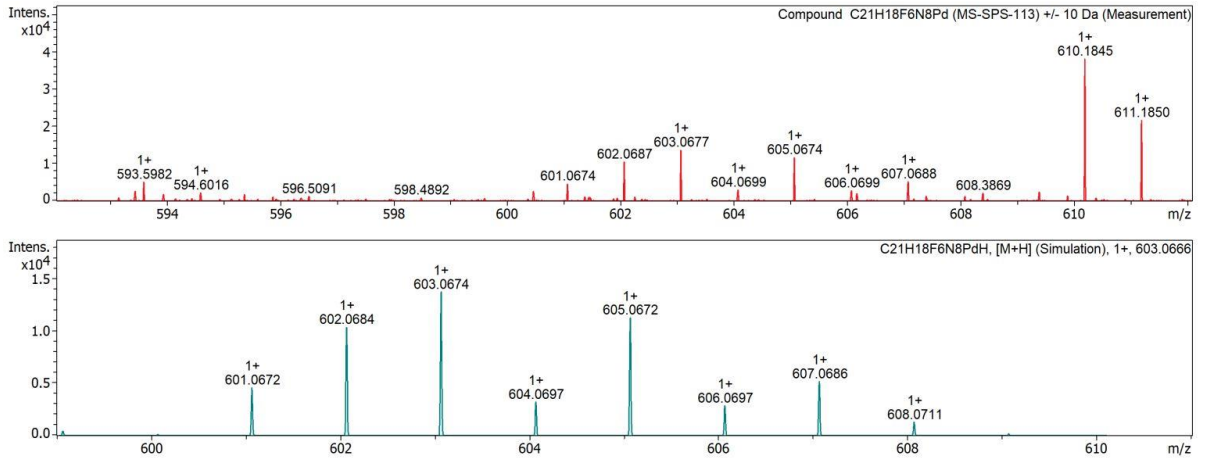

Figure S65. Mass spectrum of **CF_3-Pd-AmPy** (in MeOH, top). Additional simulation for the [**CF_3-Pd-AmPy**+H]$^{+}$ adduct (bottom).

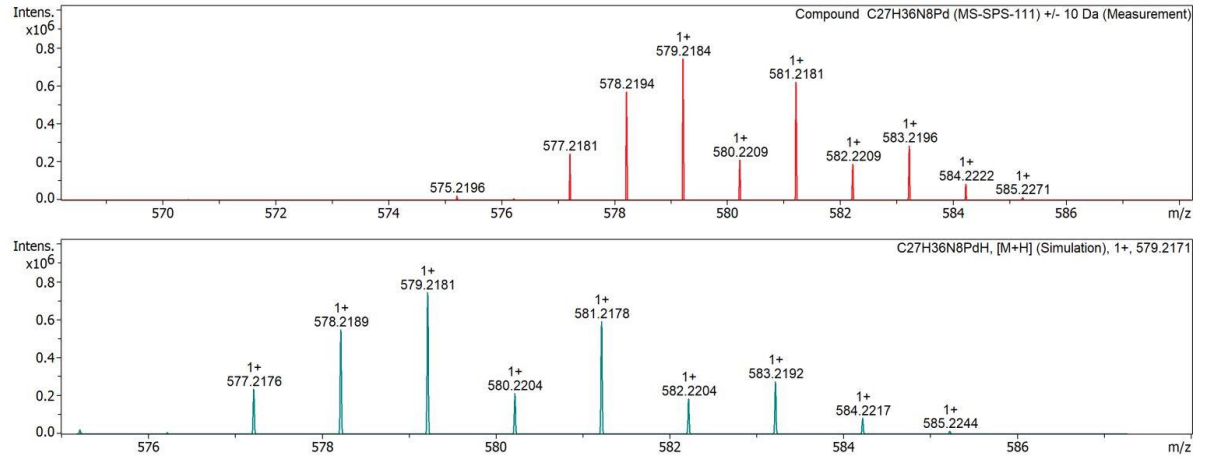

Figure S66. Mass spectrum of **^{t}bu-Pd-AmPy** (in MeOH, top). Additional simulation for the [**^{t}bu-Pd-AmPy**+H]$^{+}$ adduct (bottom).

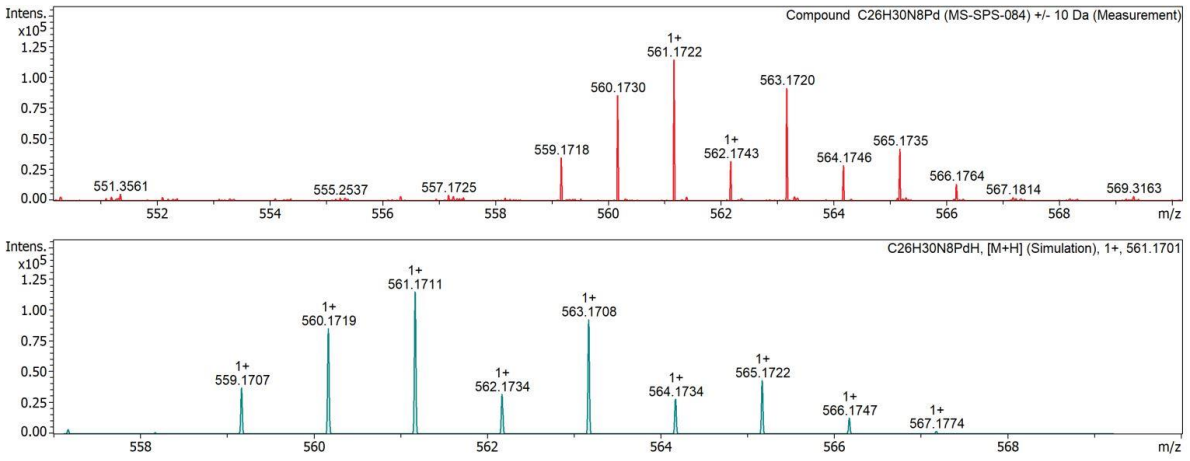

Figure S67. Mass spectrum of **^{t}bu-Pd-CNR** (in MeOH, top). Additional simulation for the [**^{t}bu-Pd-CNR**+H]$^+$ adduct (bottom).

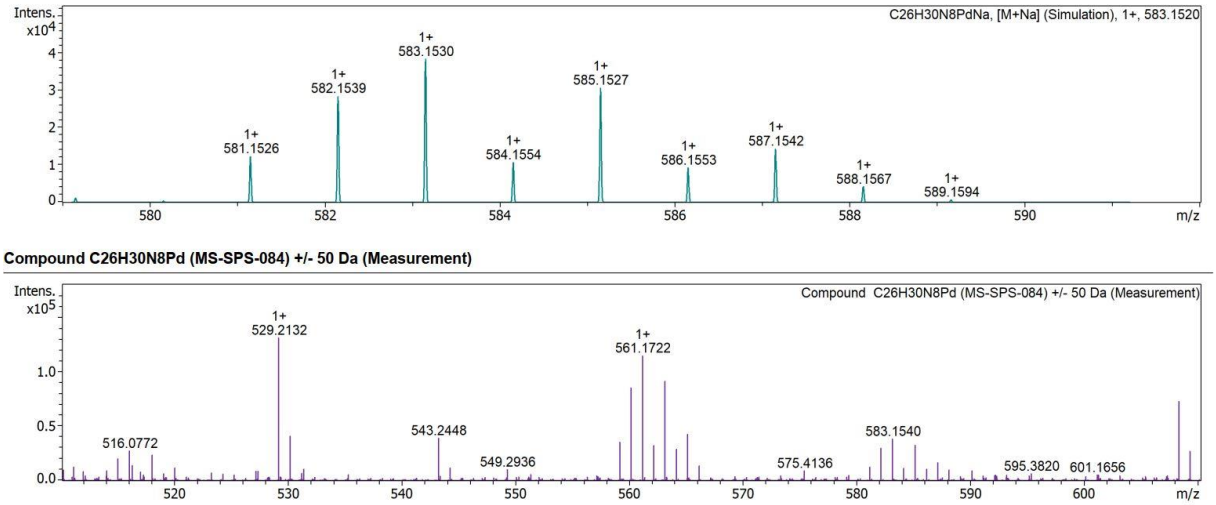

Figure S68. Mass spectrum of **^{t}bu-Pd-CNR** (in MeOH, top). Additional simulation for the [**^{t}bu-Pd-CNR**+Na]$^+$ adduct (bottom).

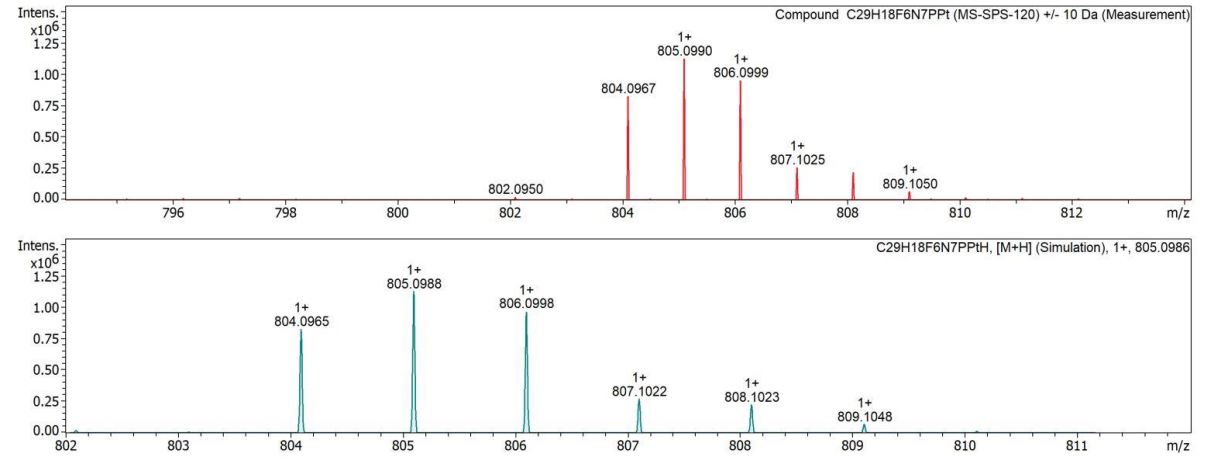

Figure S69. Mass spectrum of **CF_3-Pt-PPh_3** (in MeOH, top). Additional simulation of the [**CF_3-Pt-PPh_3**+H]$^+$ adduct (bottom).

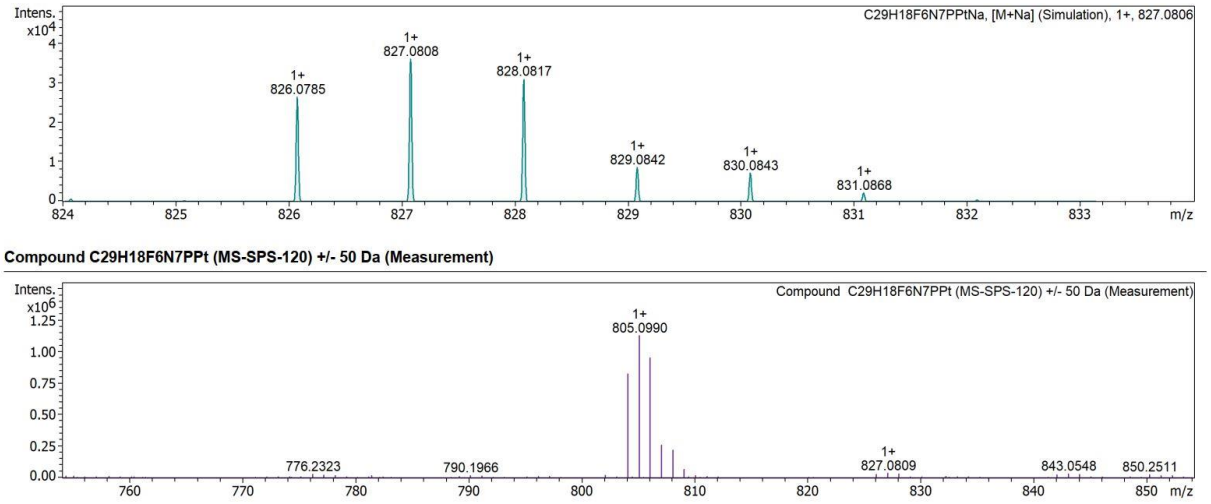

Figure S70. Mass spectrum of **CF_3-Pt-PPh_3** (in MeOH, top). Additional simulation of the [**CF_3-Pt-PPh_3**+Na]$^+$ adduct (bottom).

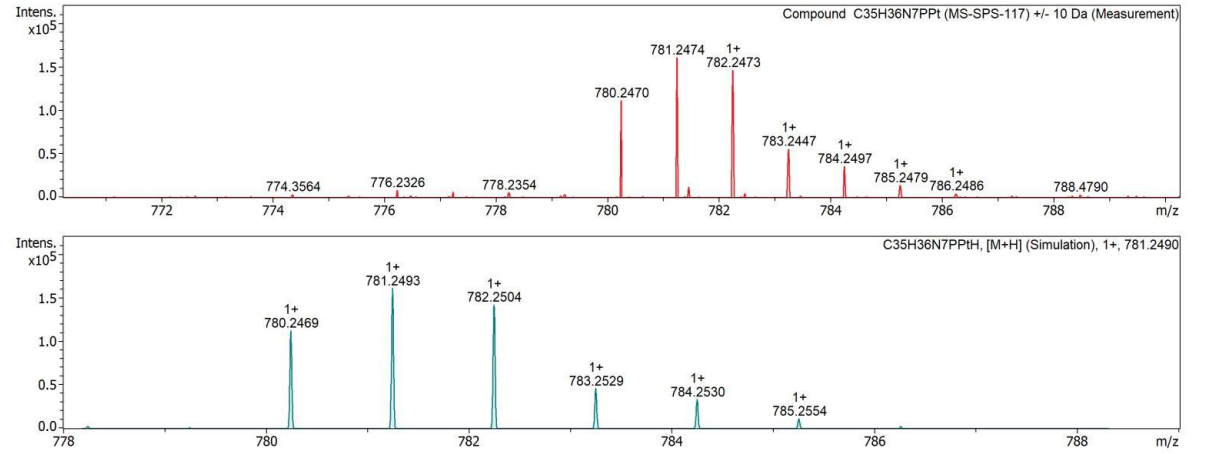

Figure S71. Mass spectrum of **^{t}bu-Pt-PPh_3** (in MeOH, top). Additional simulation of the [**^{t}bu-Pt-PPh_3**+H]$^+$ adduct (bottom).

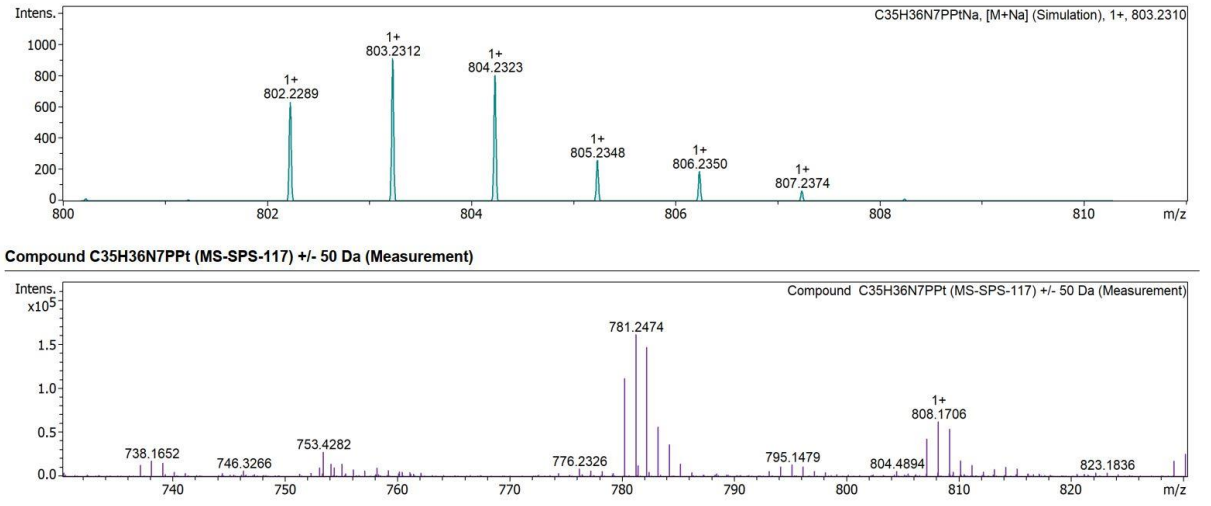

Figure S72. Mass spectrum of **^{t}bu-Pt-PPh_3** (in MeOH, top). Additional simulation of the [**^{t}bu-Pt-PPh_3**+Na]$^+$ adduct (bottom).

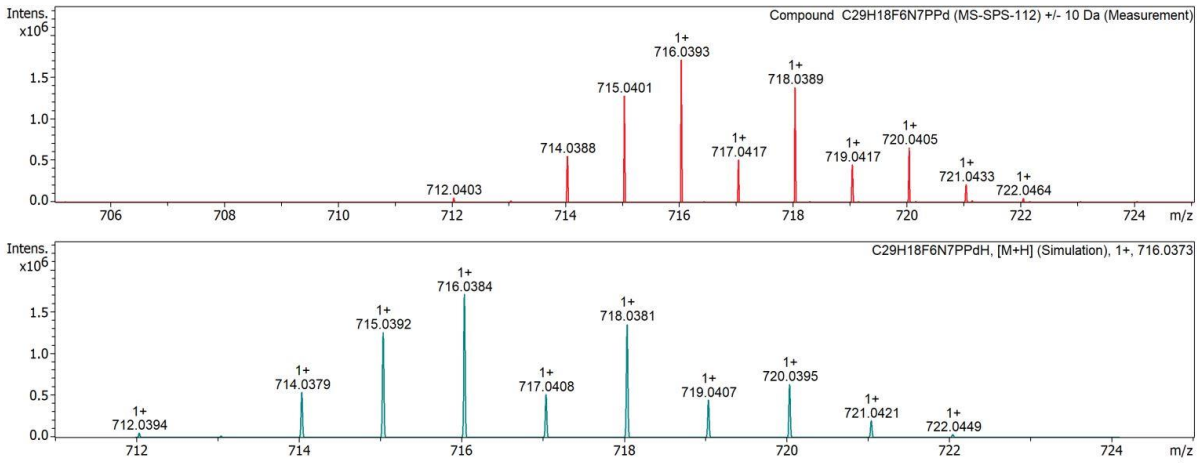

Figure S73. Mass spectrum of **CF_3-Pd-PPh_3** (in MeOH, top). Additional simulation of the [**CF_3-Pd-PPh_3**+H]$^+$ adduct (bottom).

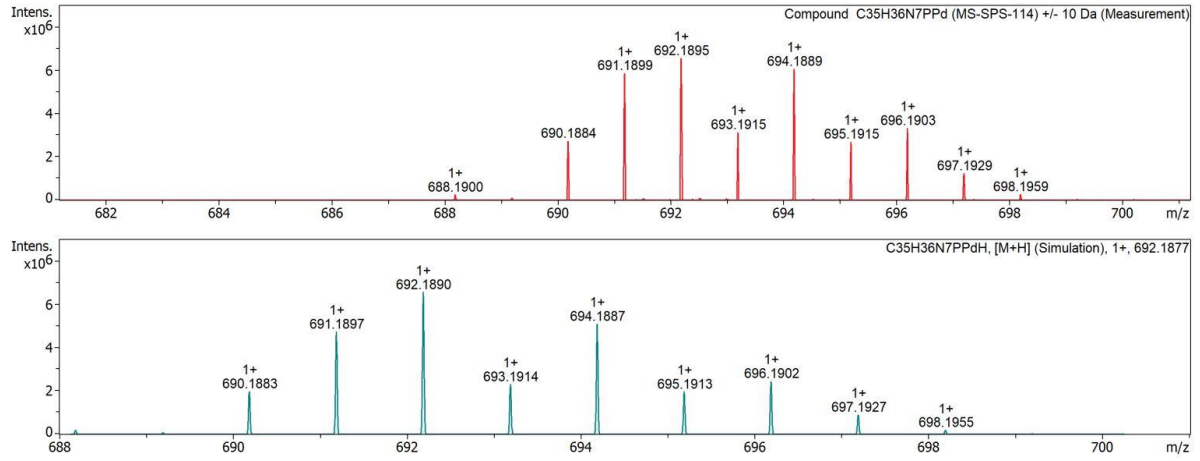

Figure S74. Mass spectrum of **^{t}bu-Pd-PPh_3** (in MeOH, top). Additional simulation of the [**^{t}bu-Pd-PPh_3**+H]$^+$ adduct (bottom).

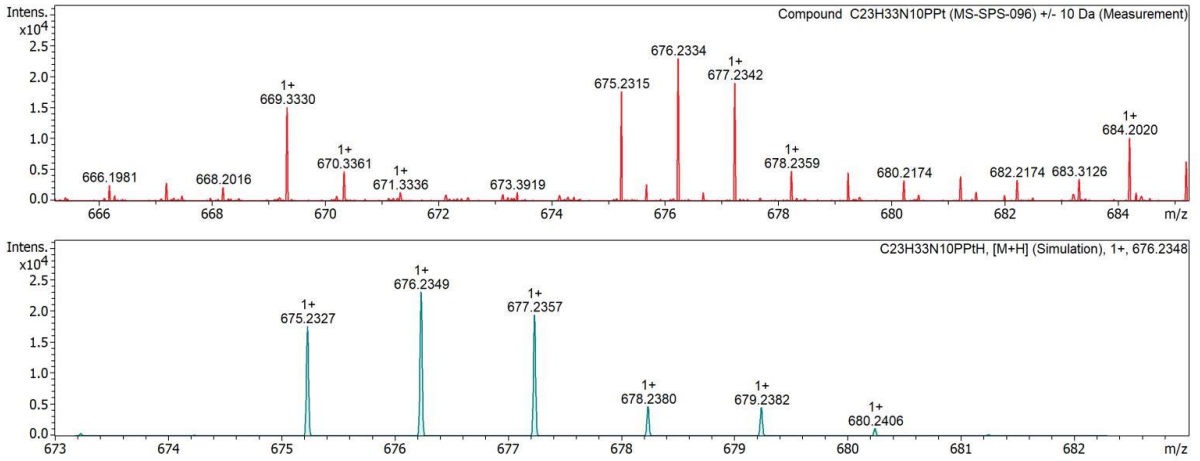

Figure S75. Mass spectrum of **^{t}bu-Pt-PTA** (in MeOH, top). Additional simulation of the [**^{t}bu-Pt-PTA**+H]$^+$ adduct (bottom).

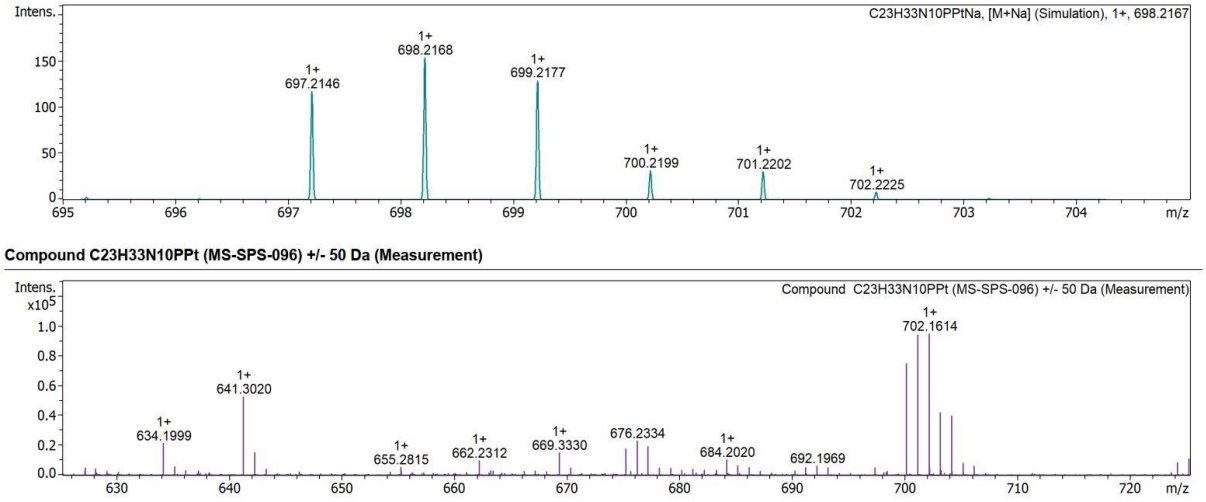

Figure S76. Mass spectrum of **^{t}bu-Pt-PTA** (in MeOH, top). Additional simulation of the [**^{t}bu-Pt-PTA**+Na]$^+$ adduct (bottom).

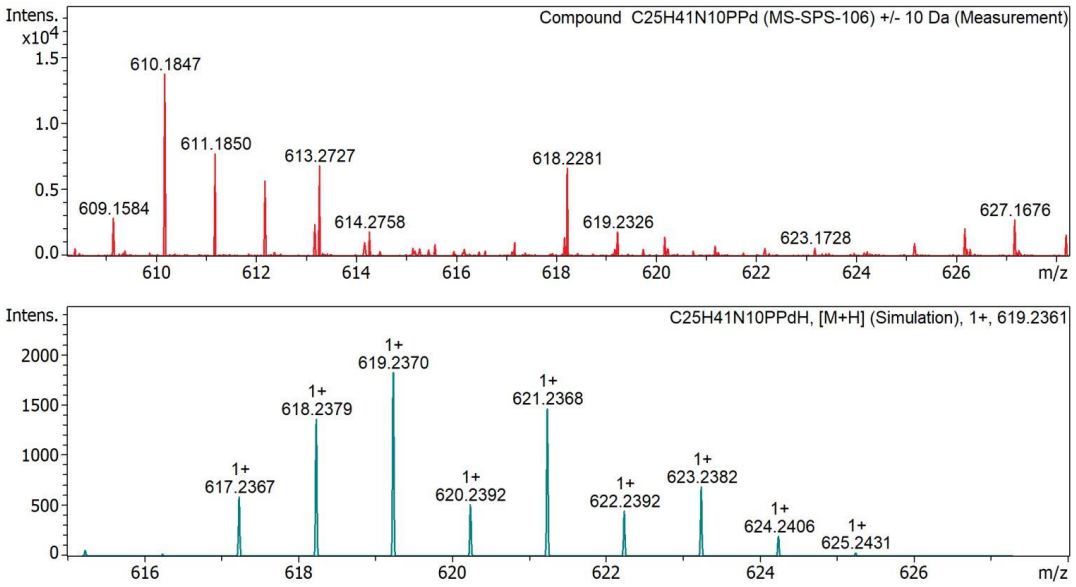

Figure S77. Mass spectrum of **^{t}bu-Pd-PTA** (in MeOH, top). Additional simulation of the [**^{t}bu-Pd-PTA**+H]$^+$ adduct (bottom).

UV-vis absorption and photoluminescence spectroscopies

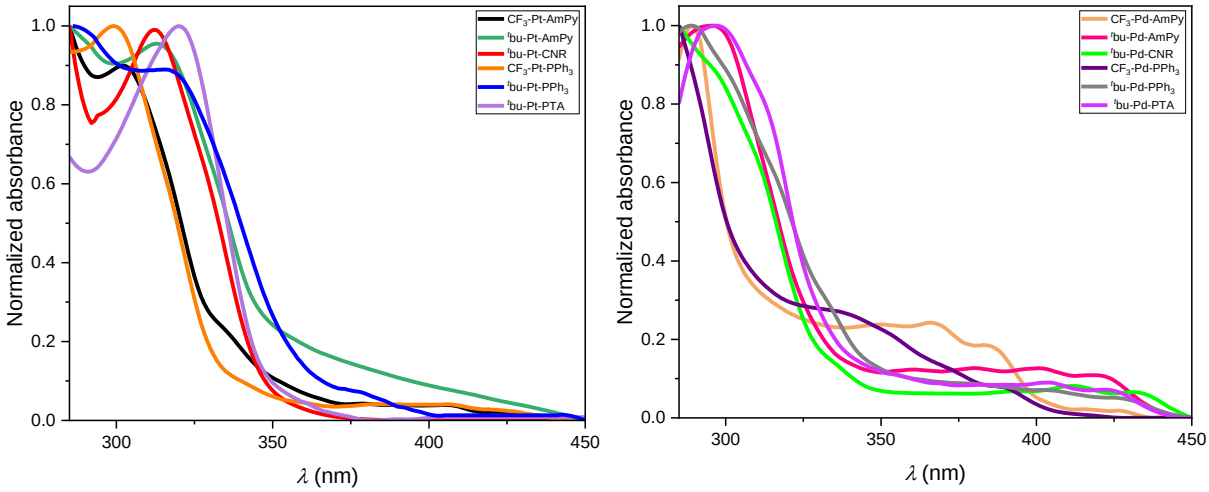

Figure S78. Normalized absorption spectra of the Pt(II) complexes (left) and of the Pd(II) complexes (right) at RT in liquid toluene. Molar absorption coefficients can be found in Table 1, Table 2 and Table S1.

Table S1. Molar absorption coefficients of Pd(II) complexes in liquid DCM and toluene.

Compound / Solvent	**CF_3-Pd-AmPy**	**^{t}bu-Pd-AmPy**	**^{t}bu-Pd-CNR**	**CF_3-Pd-PPh_3**	**^{t}bu-Pd-PPh_3**	**^{t}bu-Pd-PTA**
DCM	293 (27943)	263 (38653) 294 (20882) 400 (2957)	264 (27553) 404 (1827)	275 (24674) 336 (5561)	266 (26321) 401 (1833)	297 (15841) 263 (18831) 402 (1588)
Toluene	289 (14247) 369 (3258) 387 (2475)	295 (15632) 399 (2041)	286 (19473) 412 (1863)	285 (24342)	289 (29241)	297 (18026)

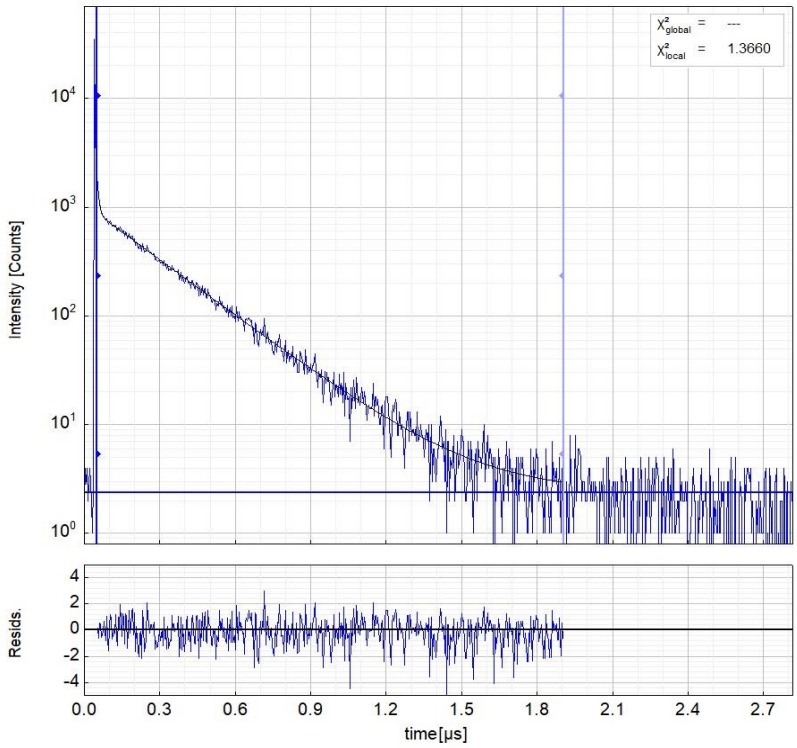

Parameter	Value	Δ	δ
A_1[kCnts/Chnl]	0.8693	±0.0100	1.1%
τ_1[ns]	252.9	±2.1	0.8%
I_1[kCnts]	54.94	±0.63	1.1%
A_{Rel1}[%]	55.7	±2.1	3.6%
I_{Rel1}[%]	97.6	±0.3	0.2%
A_2[kCnts/Chnl]	0.694	±0.057	8.1%
τ_2[ns]	7.82	±0.78	9.9%
I_2[kCnts]	1.36	±0.13	8.8%
A_{Rel2}[%]	44.4	±2.1	4.6%
I_{Rel2}[%]	2.5	±0.3	8.5%
$Bkgr_{Dec}$[kCnts]	0.0024	±0.0003	11%
τ_{AvInt}[ns]	247.0	±2.2	0.9%
τ_{AvAmp}[ns]	144.1	±6.3	4.4%

Figure S79. Left: Raw time-resolved photoluminescence decay of **CF_3-Pt-AmPy** in an air-equilibrated liquid solution at RT (DCM, $c \approx 10^{-5}$ M), including the residuals (λ_{ex} = 376 nm, λ_{em} = 462 nm). Right: Fitting parameters including pre-exponential factors and confidence limits.

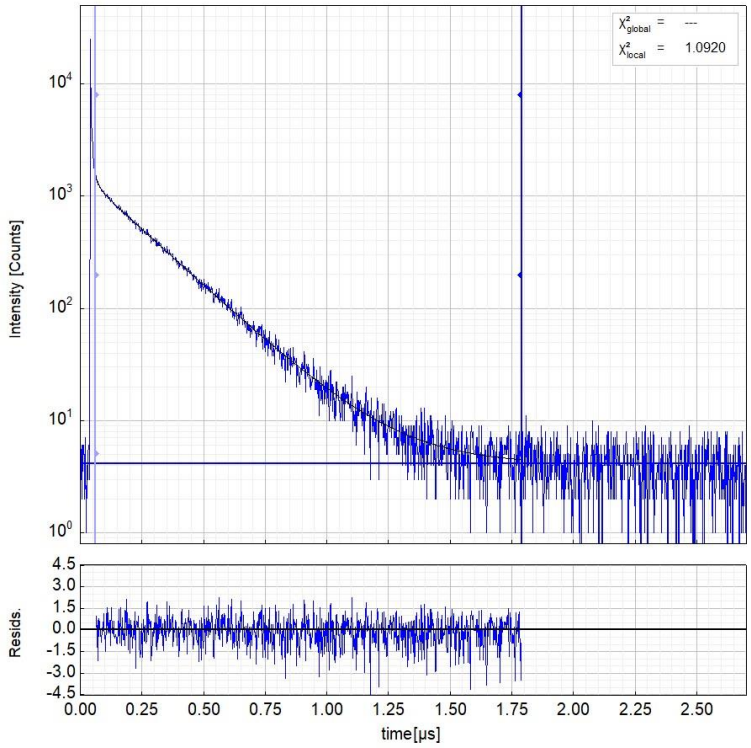

Parameter	Value	Δ	δ
A_1[kCnts/Chnl]	1.199	±0.012	0.9%
τ_1[ns]	214.9	±1.3	0.6%
I_1[kCnts]	128.76	±0.65	0.5%
A_{Rel1}[%]	82.3	±2.4	2.9%
I_{Rel1}[%]	98.6	±0.5	0.4%
A_2[kCnts/Chnl]	0.259	±0.042	16%
τ_2[ns]	15.1	±3.8	25%
I_2[kCnts]	1.96	±0.55	28%
A_{Rel2}[%]	17.8	±2.4	13%
I_{Rel2}[%]	1.5	±0.5	28%
$Bkgr_{Dec}$[kCnts]	0.0041	±0.0003	5.2%
τ_{AvInt}[ns]	211.9	±1.3	0.6%
τ_{AvAmp}[ns]	179.4	±4.2	2.3%

Figure S80. Left: Raw time-resolved photoluminescence decay of **CF_3-Pt-AmPy** in an Ar-purged liquid solution at RT (DCM, $c \approx 10^{-5}$ M), including the residuals (λ_{ex} = 376 nm, λ_{em} = 462 nm). Right: Fitting parameters including pre-exponential factors and confidence limits.

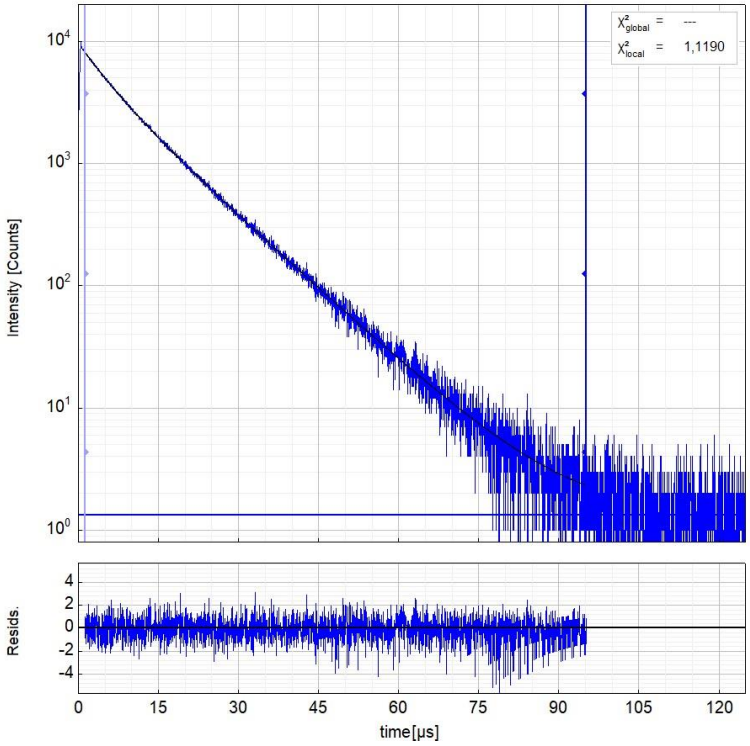

Parameter	Value	Δ	δ
A_1[kCnts/Chnl]	5,07	±0,12	2,2%
τ_1[ns]	10 986	±77	0,7%
I_1[kCnts]	1 739	±29	1,6%
A_{Rel1}[%]	62,8	±1,5	2,3%
I_{Rel1}[%]	79,0	±1,3	1,6%
A_2[kCnts/Chnl]	3,01	±0,13	4,0%
τ_2[ns]	4 930	±150	3,0%
I_2[kCnts]	463	±29	6,2%
A_{Rel2}[%]	37,3	±1,5	3,8%
I_{Rel2}[%]	21,1	±1,3	6,2%
$Bkgr_{Dec}$[kCnts]	0,0014	±0,0001	6,9%
τ_{AvInt}[ns]	9 714	±17	0,2%
τ_{AvAmp}[ns]	8 732	±21	0,2%

Figure S81. Left: Raw time-resolved photoluminescence decay of **CF_3-Pt-AmPy** in a frozen DCM/MeOH glassy matrix at 77 K ($c \approx 10^{-5}$ M), including the residuals (λ_{ex} = 376 nm, λ_{em} = 454 nm). Right: Fitting parameters including pre-exponential factors and confidence limits.

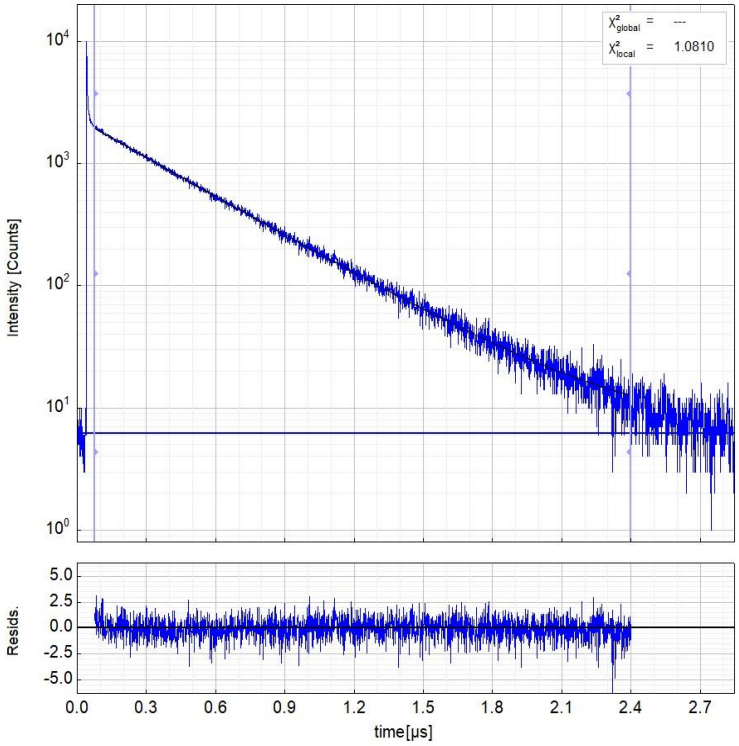

Parameter	Value	Δ	δ
A_1[kCnts/Chnl]	1.9360	±0.0026	0.1%
τ_1[ns]	406.92	±0.48	0.1%
I_1[kCnts]	787.76	±0.61	0.1%
A_{Rel1}[%]	100.0	---	---
I_{Rel1}[%]	100.0	---	---
$Bkgr_{Dec}$[kCnts]	0.0062	±0.0001	1.4%
τ_{AvInt}[ns]	406.92	±0.48	0.1%
τ_{AvAmp}[ns]	406.92	±0.48	0.1%

Figure S82. Left: Raw time-resolved photoluminescence decay of **^{t}bu-Pt-AmPy** in an air-equilibrated liquid solution at RT (DCM, $c \approx 10^{-5}$ M), including the residuals (λ_{ex} = 376 nm, λ_{em} = 510 nm). Right: Fitting parameters including pre-exponential factors and confidence limits.

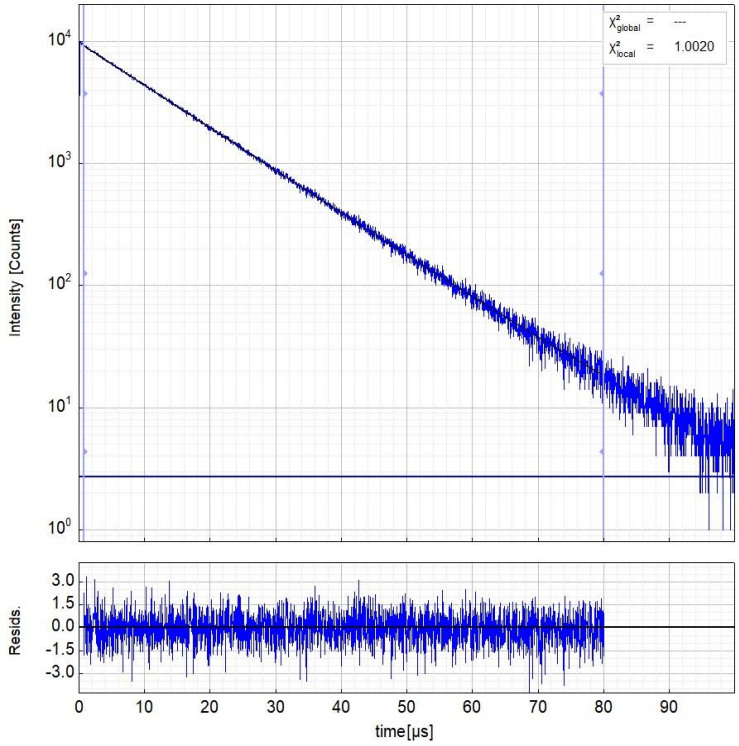

Parameter	Value	Δ	δ
A_1[kCnts/Chnl]	9.189	±0.012	0.1%
τ_1[ns]	12 440	±18	0.1%
I_1[kCnts]	3 572.1	±2.9	0.1%
A_{Rel1}[%]	100.0	---	---
I_{Rel1}[%]	100.0	---	---
$Bkgr_{Dec}$[kCnts]	0.0027	±0.0007	23%
τ_{AvInt}[ns]	12 440	±18	0.1%
τ_{AvAmp}[ns]	12 440	±18	0.1%

Figure S83. Left: Raw time-resolved photoluminescence decay of **^{t}bu-Pt-AmPy** in an Ar-purged liquid solution at RT (DCM, $c \approx 10^{-5}$ M), including the residuals (λ_{ex} = 376 nm, λ_{em} = 510 nm). Right: Fitting parameters including pre-exponential factors and confidence limits.

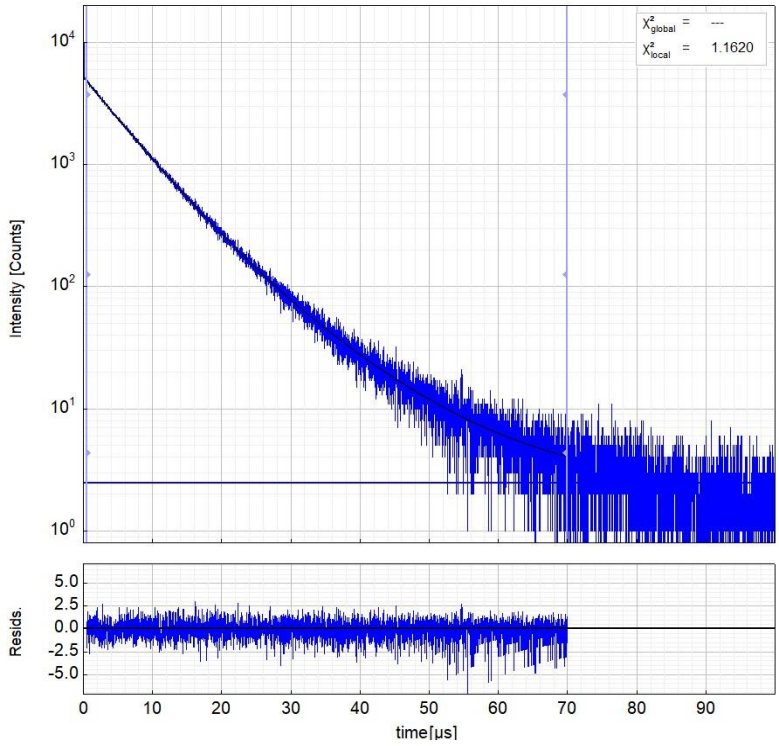

Parameter	Value	Δ	δ
A_1[kCnts/Chnl]	0.55	±0.19	33%
τ_1[ns]	11 870	±900	7.6%
I_1[kCnts]	405	±94	23%
A_{Rel1}[%]	11.4	±3.8	33%
I_{Rel1}[%]	20.4	±4.8	23%
A_2[kCnts/Chnl]	4.25	±0.18	4.1%
τ_2[ns]	5 970	±130	2.1%
I_2[kCnts]	1 582	±98	6.1%
A_{Rel2}[%]	88.7	±3.8	4.3%
I_{Rel2}[%]	79.7	±4.8	6.0%
$Bkgr_{Dec}$[kCnts]	0.0025	±0.0006	24%
τ_{AvInt}[ns]	7 168	±40	0.6%
τ_{AvAmp}[ns]	6 638	±25	0.4%

Figure S84. Left: Raw time-resolved photoluminescence decay of **^{t}bu-Pt-AmPy** in a frozen DCM/MeOH glassy matrix at 77 K ($c \approx 10^{-5}$ M), including the residuals (λ_{ex} = 376 nm, λ_{em} = 496 nm). Right: Fitting parameters including pre-exponential factors and confidence limits.

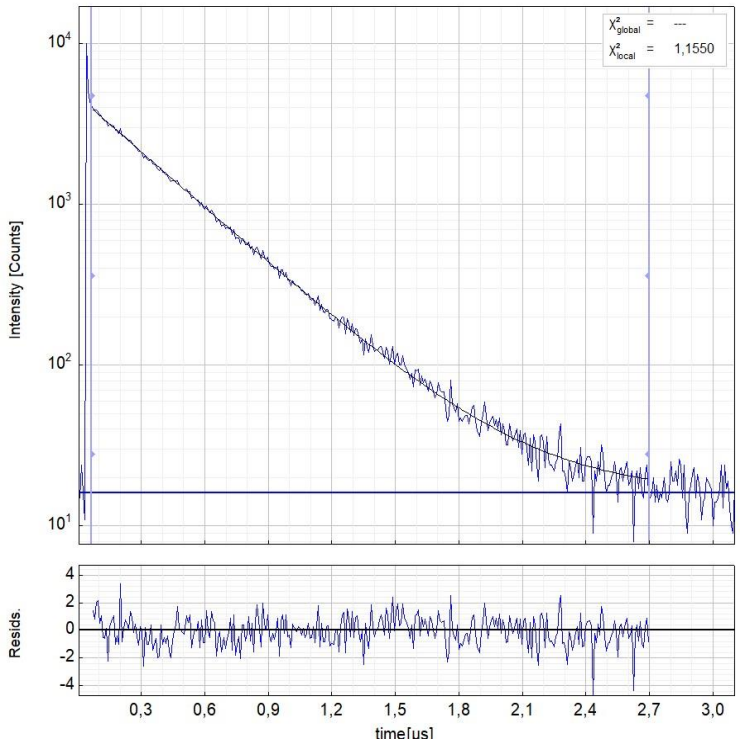

Parameter	Value	Δ	δ
A_1[kCnts/Chnl]	3,870	±0,037	0,9%
τ_1[ns]	374,1	±3,3	0,9%
I_1[kCnts]	180,92	±0,68	0,4%
A_{Rel1}[%]	100,0	---	---
I_{Rel1}[%]	100,0	---	---
$Bkgr_{Dec}$[kCnts]	0,0161	±0,0010	5,6%
τ_{AvInt}[ns]	374,1	±3,3	0,9%
τ_{AvAmp}[ns]	374,1	±3,3	0,9%

Figure S85. Left: Raw time-resolved photoluminescence decay of **^{t}bu-Pt-CNR** in an air-equilibrated liquid solution at RT (DCM, $c \approx 10^{-5}$ M), including the residuals (λ_{ex} = 376 nm, λ_{em} = 515 nm). Right: Fitting parameters including pre-exponential factors and confidence limits.

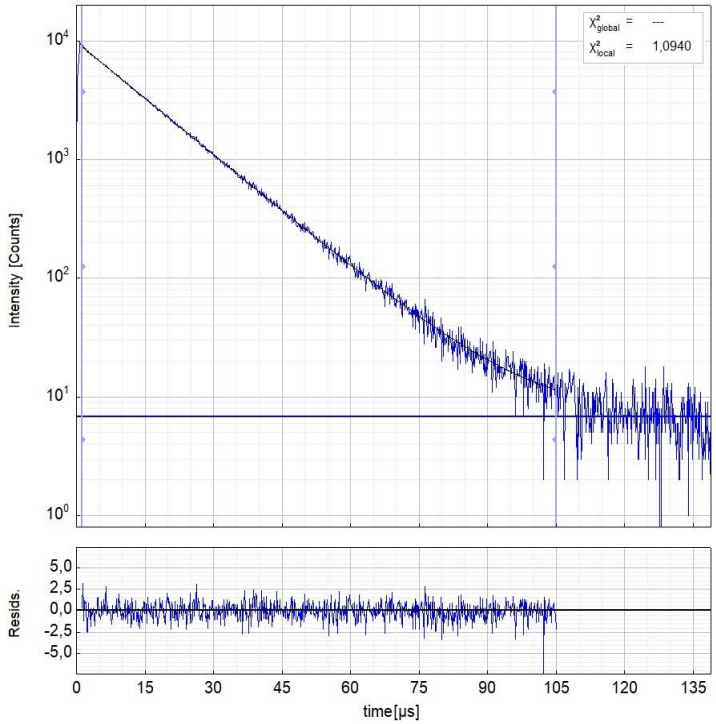

Parameter	Value	Δ	δ
A_1[kCnts/Chnl]	8,913	±0,028	0,3%
τ_1[ns]	13 693	±26	0,2%
I_1[kCnts]	953,5	±2,0	0,2%
A_{Rel1}[%]	100,0	---	---
I_{Rel1}[%]	100,0	---	---
$Bkgr_{Dec}$[kCnts]	0,0069	±0,0005	6,7%
τ_{AvInt}[ns]	13 693	±26	0,2%
τ_{AvAmp}[ns]	13 693	±26	0,2%

Figure S86. Left: Raw time-resolved photoluminescence decay of **^{t}bu-Pt-CNR** in an Ar-purged liquid solution at RT (DCM, $c \approx 10^{-5}$ M), including the residuals (λ_{ex} = 376 nm, λ_{em} = 515 nm). Right: Fitting parameters including pre-exponential factors and confidence limits.

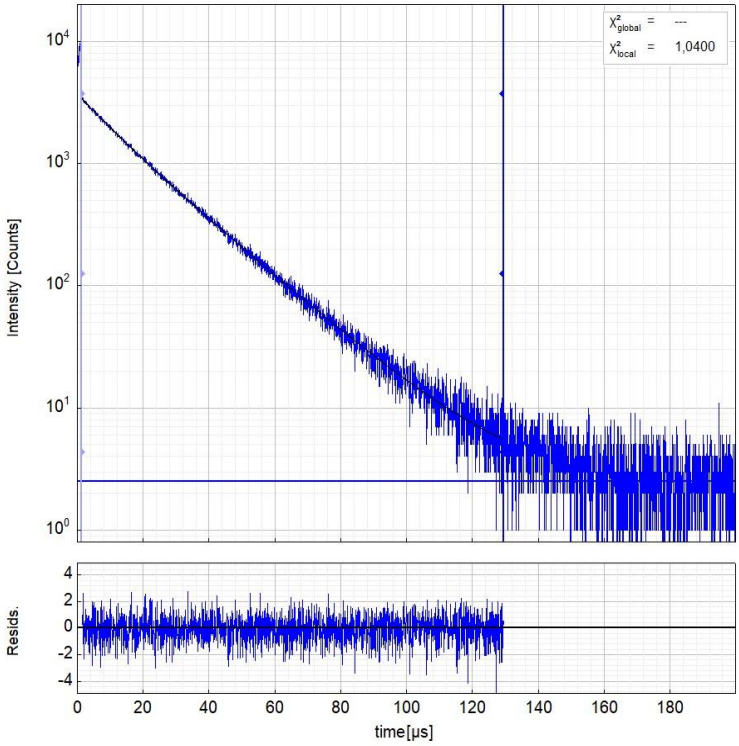

Parameter	Value	Δ	δ
A_1[kCnts/Chnl]	2,62	±0,11	4,2%
τ_1[ns]	18 940	±210	1,1%
I_1[kCnts]	773	±24	3,0%
A_{Rel1}[%]	77,3	±3,2	4,1%
I_{Rel1}[%]	87,4	±2,7	3,0%
A_2[kCnts/Chnl]	0,77	±0,11	14%
τ_2[ns]	9 310	±730	7,8%
I_2[kCnts]	112	±24	21%
A_{Rel2}[%]	22,8	±3,2	14%
I_{Rel2}[%]	12,7	±2,7	21%
$Bkgr_{Dec}$[kCnts]	0,0025	---	---
τ_{AvInt}[ns]	17 722	±38	0,2%
τ_{AvAmp}[ns]	16 748	±62	0,4%

Figure S87. Left: Raw time-resolved photoluminescence decay of **^{t}bu-Pt-CNR** in a frozen DCM/MeOH glassy matrix at 77 K ($c \approx 10^{-5}$ M), including the residuals (λ_{ex} = 376 nm, λ_{em} = 487 nm). Right: Fitting parameters including pre-exponential factors and confidence limits.

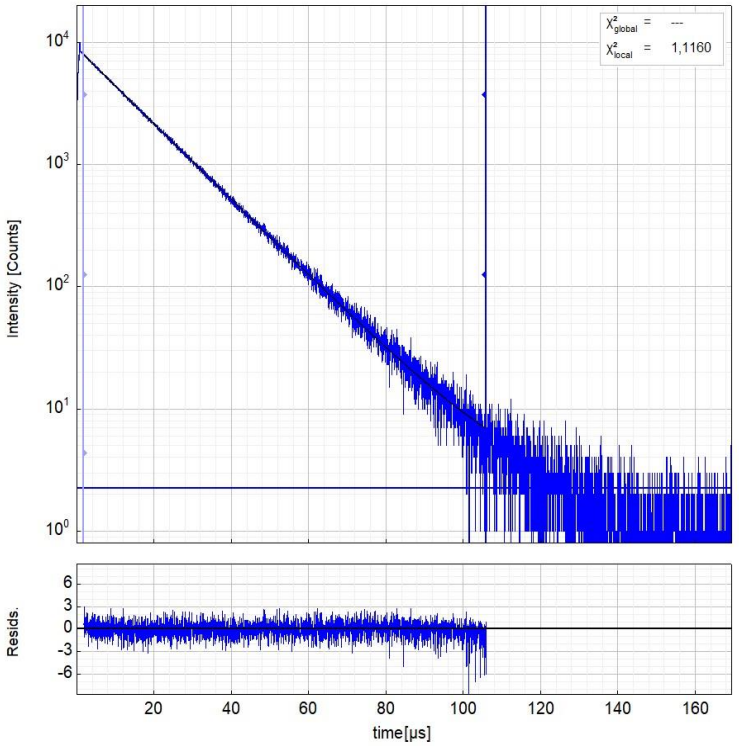

Parameter	Value	Δ	δ
A_1[kCnts/Chnl]	7,874	±0,014	0,2%
τ_1[ns]	14 010	±25	0,2%
I_1[kCnts]	3 447,0	±5,4	0,2%
A_{Rel1}[%]	100,0	---	---
I_{Rel1}[%]	100,0	---	---
$Bkgr_{Dec}$[kCnts]	0,0023	±0,0005	18%
τ_{AvInt}[ns]	14 010	±25	0,2%
τ_{AvAmp}[ns]	14 010	±25	0,2%

Figure S88. Left: Raw time-resolved photoluminescence decay of **CF_3-Pt-PPh_3** in a frozen DCM/MeOH glassy matrix at 77 K ($c \approx 10^{-5}$ M), including the residuals (λ_{ex} = 376 nm, λ_{em} = 455 nm). Right: Fitting parameters including pre-exponential factors and confidence limits.

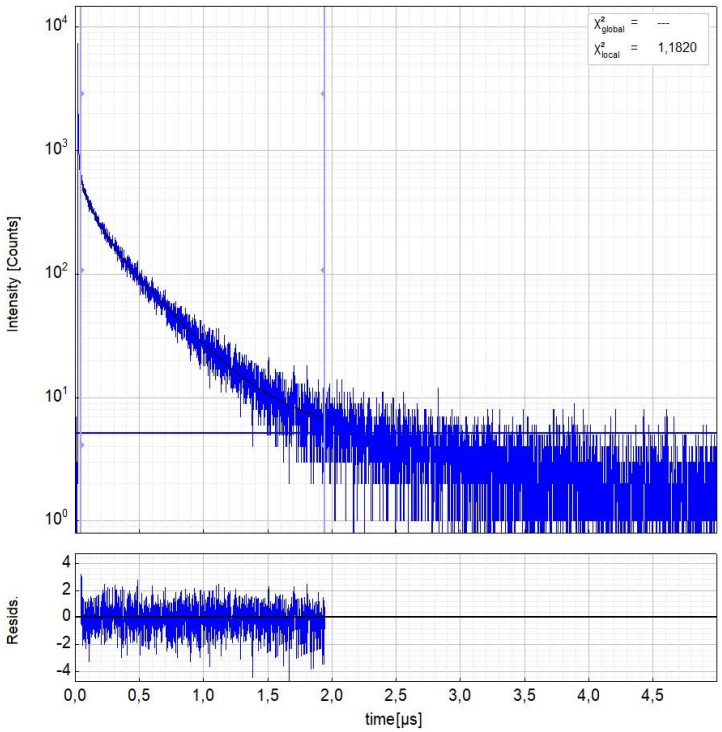

Parameter	Value	Δ	δ
A_1[kCnts/Chnl]	0,301	±0,040	13%
τ_1[ns]	367	±30	8,0%
I_1[kCnts]	110,3	±6,7	6,0%
A_{Rel1}[%]	53,0	±4,8	9,0%
I_{Rel1}[%]	83,0	±5,9	7,1%
A_2[kCnts/Chnl]	0,268	±0,016	5,7%
τ_2[ns]	85	±25	29%
I_2[kCnts]	22,7	±8,2	36%
A_{Rel2}[%]	47,1	±4,8	10%
I_{Rel2}[%]	17,1	±5,9	35%
$Bkgr_{Dec}$[kCnts]	0,0052	±0,0009	16%
τ_{AvInt}[ns]	319	±12	3,7%
τ_{AvAmp}[ns]	234	±14	5,8%

Figure S89. Left: Raw time-resolved photoluminescence decay of **^{t}bu-Pt-PPh$_3$** in an air-equilibrated liquid solution at RT (DCM, $c \approx 10^{-5}$ M), including the residuals (λ_{ex} = 376 nm, λ_{em} = 517 nm). Right: Fitting parameters including pre- exponential factors and confidence limits.

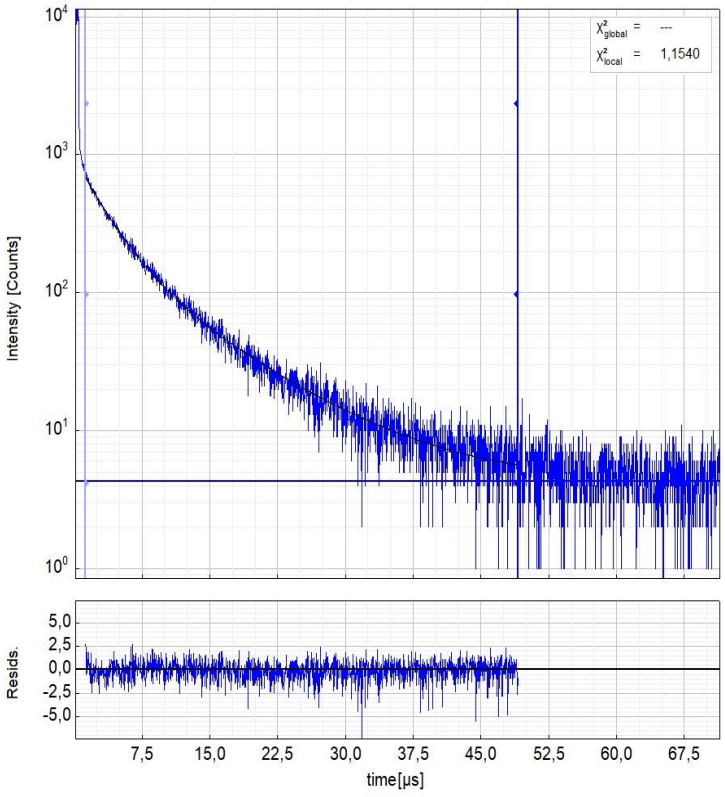

Parameter	Value	Δ	δ
A_1[kCnts/Chnl]	0,196	±0,025	13%
τ_1[ns]	9 620	±570	5,8%
I_1[kCnts]	58,7	±4,4	7,5%
A_{Rel1}[%]	28,5	±3,4	12%
I_{Rel1}[%]	56,0	±4,2	7,4%
A_2[kCnts/Chnl]	0,491	±0,022	4,3%
τ_2[ns]	3 010	±180	5,7%
I_2[kCnts]	46,2	±4,4	9,3%
A_{Rel2}[%]	71,6	±3,4	4,6%
I_{Rel2}[%]	44,1	±4,2	9,4%
$Bkgr_{Dec}$[kCnts]	0,0043	---	---
τ_{AvInt}[ns]	6 703	±100	1,5%
τ_{AvAmp}[ns]	4 886	±72	1,5%

Figure S90. Left: Raw time-resolved photoluminescence decay of **^{t}bu-Pt-PPh$_3$** in an Ar-purged liquid solution at RT (DCM, $c \approx 10^{-5}$ M), including the residuals (λ_{ex} = 376 nm, λ_{em} = 517 nm). Right: Fitting parameters including pre-exponential factors and confidence limits.

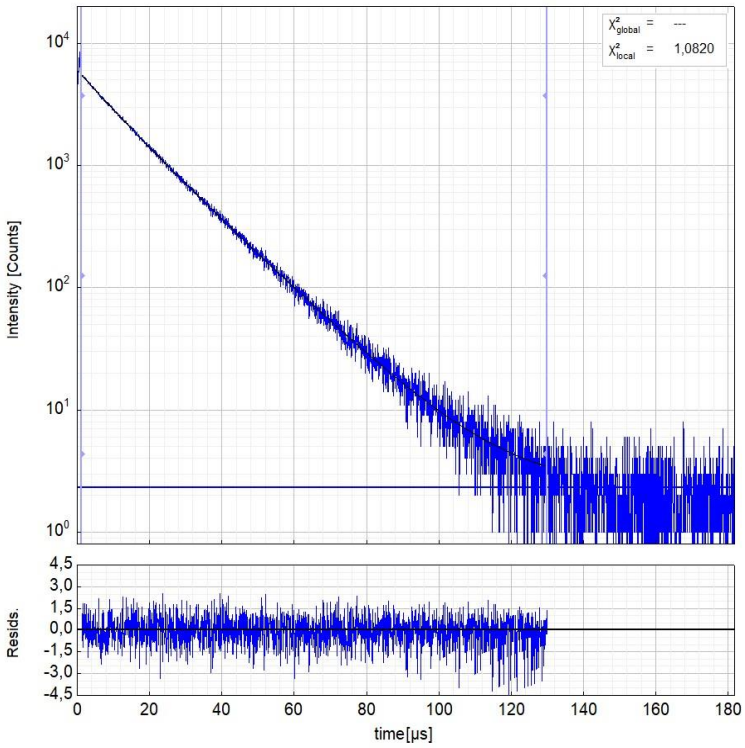

Parameter	Value	Δ	δ
A_1[kCnts/Chnl]	4,07	±0,31	7,5%
τ_1[ns]	15 690	±310	1,9%
I_1[kCnts]	996	±60	6,0%
A_{Rel1}[%]	74,2	±5,5	7,3%
I_{Rel1}[%]	83,4	±5,0	6,0%
A_2[kCnts/Chnl]	1,43	±0,30	21%
τ_2[ns]	8 940	±690	7,7%
I_2[kCnts]	199	±60	30%
A_{Rel2}[%]	25,9	±5,5	21%
I_{Rel2}[%]	16,7	±5,0	30%
$Bkgr_{Dec}$[kCnts]	0,0024	±0,0004	17%
τ_{AvInt}[ns]	14 561	±43	0,3%
τ_{AvAmp}[ns]	13 935	±41	0,3%

Figure S91. Left: Raw time-resolved photoluminescence decay of **^{t}bu-Pt-PPh$_3$** in a frozen DCM/MeOH glassy matrix at 77 K ($c \approx 10^{-5}$ M), including the residuals (λ_{ex} = 376 nm, λ_{em} = 495 nm). Right: Fitting parameters including pre-exponential factors and confidence limits.

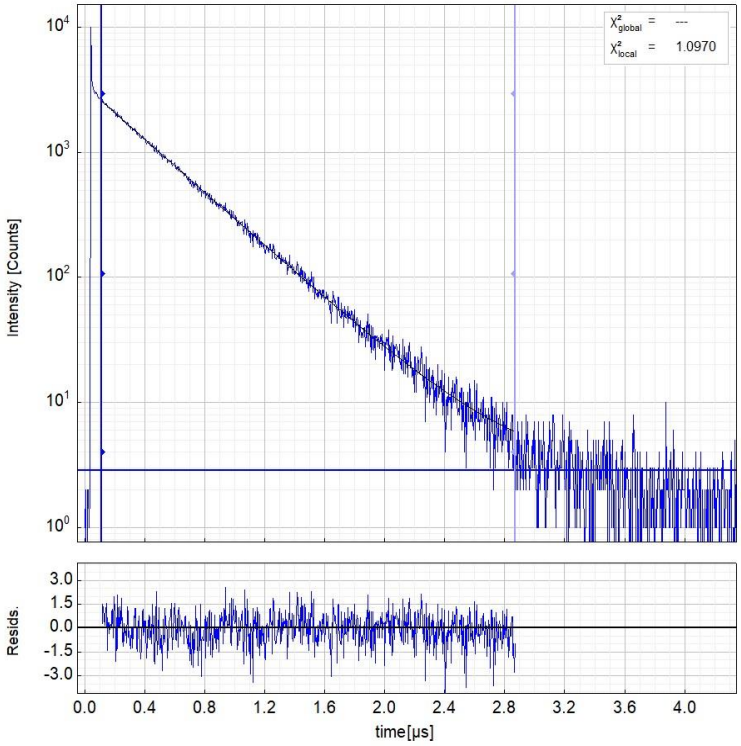

Parameter	Value	Δ	δ
A_1[kCnts/Chnl]	2.543	±0.015	0.6%
τ_1[ns]	408.0	±2.7	0.6%
I_1[kCnts]	259.34	±0.99	0.4%
A_{Rel1}[%]	100.0	---	---
I_{Rel1}[%]	100.0	---	---
$Bkgr_{Dec}$[kCnts]	0.0029	±0.0004	12%
τ_{AvInt}[ns]	408.0	±2.7	0.6%
τ_{AvAmp}[ns]	408.0	±2.7	0.6%

Figure S92. Left: Raw time-resolved photoluminescence decay of **^{t}bu-Pt-PTA** in an air-equilibrated liquid solution at RT (DCM, $c \approx 10^{-5}$ M), including the residuals (λ_{ex} = 376 nm, λ_{em} = 512 nm). Right: Fitting parameters including pre-exponential factors and confidence limits.

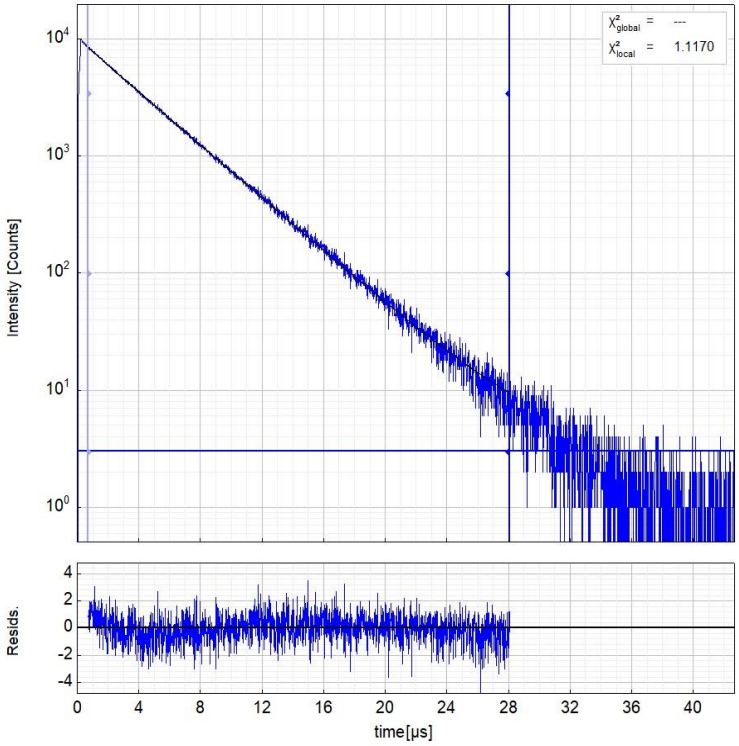

Parameter	Value	Δ	δ
A_1[kCnts/Chnl]	8.367	±0.020	0.2%
τ_1[ns]	3 819.2	±3.4	0.1%
I_1[kCnts]	1 997.1	±3.2	0.2%
A_{Rel1}[%]	100.0	---	---
I_{Rel1}[%]	100.0	---	---
$Bkgr_{Dec}$[kCnts]	0.0030	±0.0006	18%
τ_{AvInt}[ns]	3 819.2	±3.4	0.1%
τ_{AvAmp}[ns]	3 819.2	±3.4	0.1%

Figure S93. Left: Raw time-resolved photoluminescence decay of **^{t}bu-Pt-PTA** in an Ar-purged liquid solution at RT (DCM, $c \approx 10^{-5}$ M), including the residuals (λ_{ex} = 376 nm, λ_{em} = 512 nm). Right: Fitting parameters including pre-exponential factors and confidence limits.

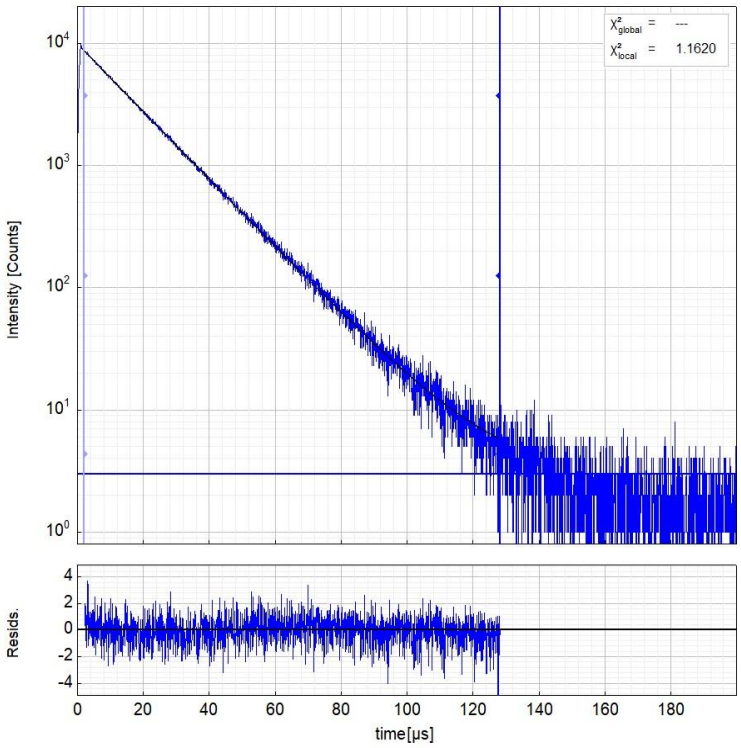

Parameter	Value	Δ	δ
A_1[kCnts/Chnl]	8.578	±0.017	0.2%
τ_1[ns]	15 703	±24	0.2%
I_1[kCnts]	2 104.4	±2.1	0.1%
A_{Rel1}[%]	100.0	---	---
I_{Rel1}[%]	100.0	---	---
$Bkgr_{Dec}$[kCnts]	0.0030	±0.0003	7.3%
τ_{AvInt}[ns]	15 703	±24	0.2%
τ_{AvAmp}[ns]	15 703	±24	0.2%

Figure S94. Left: Raw time-resolved photoluminescence decay of **^{t}bu-Pt-PTA** in a frozen DCM/MeOH glassy matrix at 77 K ($c \approx 10^{-5}$ M), including the residuals (λ_{ex} = 376 nm, λ_{em} = 490 nm). Right: Fitting parameters including pre-exponential factors and confidence limits.

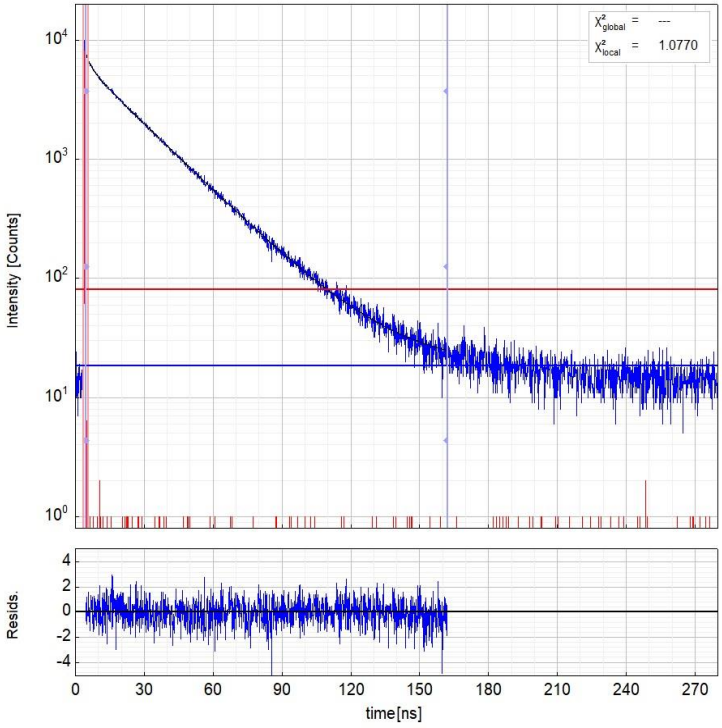

Parameter	Value	Δ	δ
A_1[kCnts/Chnl]	6.92	±0.33	4.7%
τ_1[ns]	23.123	±0.043	0.2%
I_1[kCnts]	1 249	±61	4.9%
A_{Rel1}[%]	74.9	±2.4	3.2%
I_{Rel1}[%]	95.8	±0.4	0.4%
A_2[kCnts/Chnl]	2.33	±0.30	13%
τ_2[ns]	3.04	±0.38	12%
I_2[kCnts]	55.1	±6.0	11%
A_{Rel2}[%]	25.2	±2.4	9.5%
I_{Rel2}[%]	4.3	±0.4	9.4%
$Bkgr_{Dec}$[kCnts]	0.0184	±0.0008	4.2%
$Bkgr_{IRF}$[Cnts/Chnl]	81	±31	38%
$Shift_{IRF}$[ps]	190	±170	88%
τ_{AvInt}[ns]	22.274	±0.091	0.4%
τ_{AvAmp}[ns]	18.07	±0.54	2.9%

Figure S95. Left: Raw time-resolved photoluminescence decay (in blue) of **CF_3-Pt-AmPy** in an air-equilibrated liquid solution at RT (toluene, $c \approx 10^{-5}$ M; λ_{ex} = 376 nm, λ_{em} = 493 nm), including the residuals (in blue) and the instrument response function (IRF, in red). Right: Fitting parameters including pre-exponential factors and confidence limits.

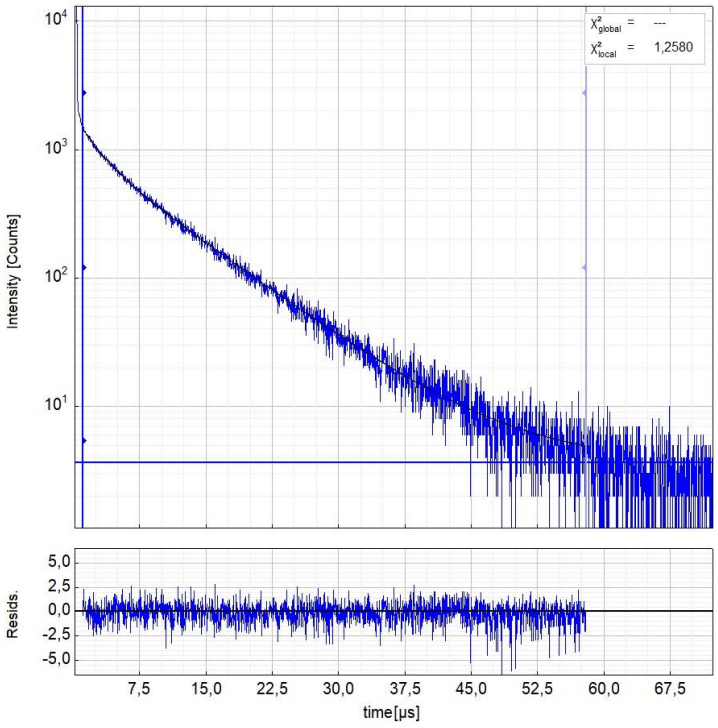

Parameter	Value	Δ	δ
A_1[kCnts/Chnl]	0,912	±0,022	2,4%
τ_1[ns]	8 686	±85	1,0%
I_1[kCnts]	247,3	±3,6	1,4%
A_{Rel1}[%]	62,9	±1,5	2,3%
I_{Rel1}[%]	86,8	±1,5	1,6%
A_2[kCnts/Chnl]	0,538	±0,021	3,8%
τ_2[ns]	2 250	±160	6,9%
I_2[kCnts]	37,8	±4,1	11%
A_{Rel2}[%]	37,2	±1,5	3,9%
I_{Rel2}[%]	13,3	±1,5	11%
$Bkgr_{Dec}$[kCnts]	0,0037	±0,0004	11%
τ_{AvInt}[ns]	7 833	±55	0,7%
τ_{AvAmp}[ns]	6 296	±52	0,8%

Figure S96. Left: Raw time-resolved photoluminescence decay of **CF_3-Pt-AmPy** in an Ar-purged liquid solution at RT (toluene, $c \approx 10^{-5}$ M), including the residuals (λ_{ex} = 376 nm, λ_{em} = 493 nm). Right: Fitting parameters including pre-exponential factors and confidence limits.

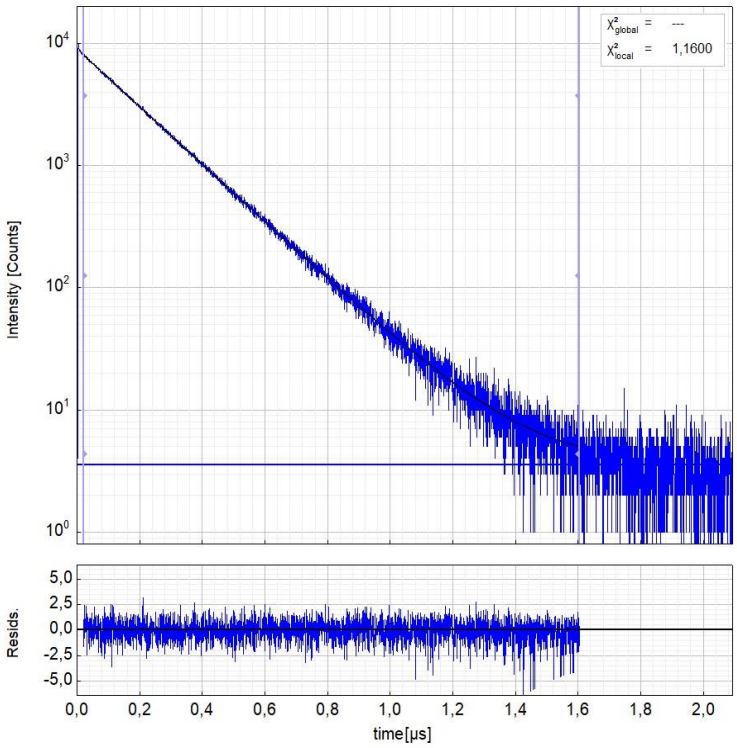

Parameter	Value	Δ	δ
A_1[kCnts/Chnl]	7,9894	±0,0085	0,1%
τ_1[ns]	184,28	±0,14	0,1%
I_1[kCnts]	2 875,5	±2,3	0,1%
A_{Rel1}[%]	100,0	---	---
I_{Rel1}[%]	100,0	---	---
$Bkgr_{Dec}$[kCnts]	0,0036	±0,0003	6,3%
τ_{AvInt}[ns]	184,28	±0,14	0,1%
τ_{AvAmp}[ns]	184,28	±0,14	0,1%

Figure S97. Left: Raw time-resolved photoluminescence decay of **^{t}bu-Pt-AmPy** in an air-equilibrated liquid solution at RT (toluene, $c \approx 10^{-5}$ M), including the residuals (λ_{ex} = 376 nm, λ_{em} = 507 nm). Right: Fitting parameters including pre-exponential factors and confidence limits.

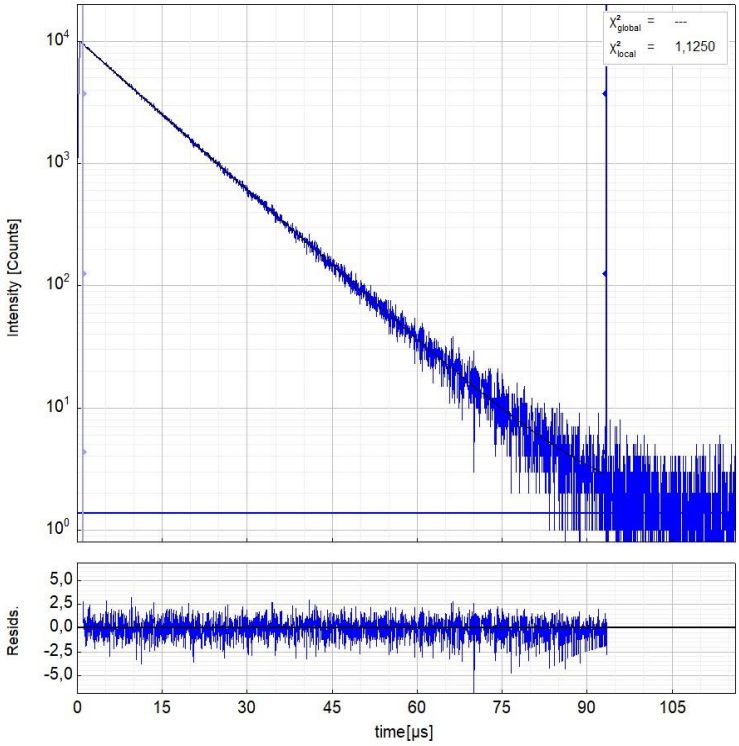

Parameter	Value	Δ	δ
A_1[kCnts/Chnl]	9,416	±0,013	0,1%
τ_1[ns]	10 548,4	±7,8	0,1%
I_1[kCnts]	3 103,9	±4,1	0,1%
A_{Rel1}[%]	100,0	---	---
I_{Rel1}[%]	100,0	---	---
$Bkgr_{Dec}$[kCnts]	0,0014	±0,0002	8,7%
τ_{AvInt}[ns]	10 548,4	±7,8	0,1%
τ_{AvAmp}[ns]	10 548,4	±7,8	0,1%

Figure S98. Left: Raw time-resolved photoluminescence decay of **^{t}bu-Pt-AmPy** in an Ar-purged liquid solution at RT (toluene, $c \approx 10^{-5}$ M), including the residuals (λ_{ex} = 376 nm, λ_{em} = 507 nm). Right: Fitting parameters including pre-exponential factors and confidence limits.

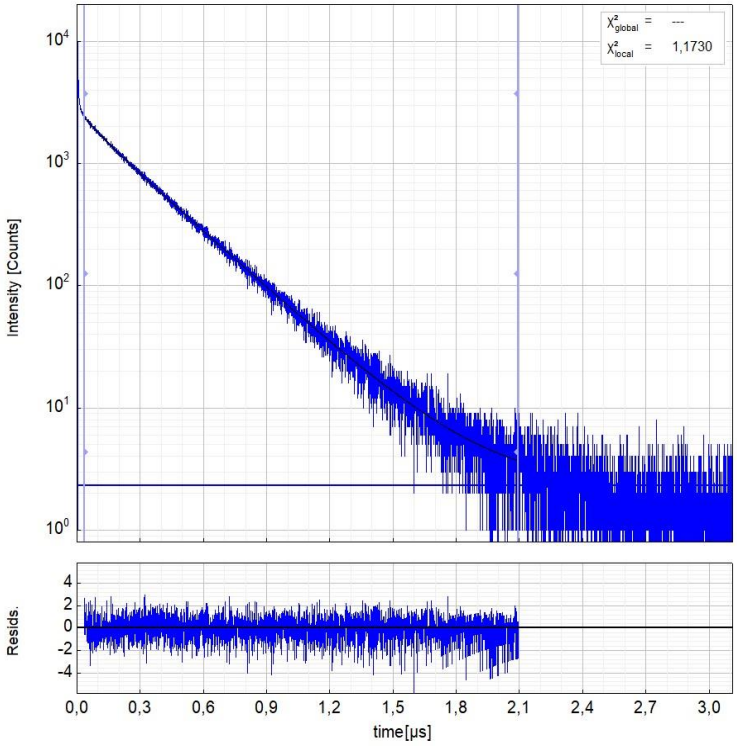

Parameter	Value	Δ	δ
A_1[kCnts/Chnl]	2,057	±0,053	2,5%
τ_1[ns]	281,5	±2,9	1,0%
I_1[kCnts]	1 131	±18	1,6%
A_{Rel1}[%]	87,0	±2,1	2,3%
I_{Rel1}[%]	95,1	±1,7	1,7%
A_2[kCnts/Chnl]	0,308	±0,047	15%
τ_2[ns]	99	±16	16%
I_2[kCnts]	59	±20	33%
A_{Rel2}[%]	13,1	±2,1	15%
I_{Rel2}[%]	5,0	±1,7	33%
$Bkgr_{Dec}$[kCnts]	0,0024	±0,0002	6,7%
τ_{AvInt}[ns]	272,41	±0,67	0,2%
τ_{AvAmp}[ns]	257,7	±1,3	0,5%

Figure S99. Left: Raw time-resolved photoluminescence decay of **^{t}bu-Pt-CNR** in an air-equilibrated liquid solution at RT (toluene, $c \approx 10^{-5}$ M), including the residuals (λ_{ex} = 376 nm, λ_{em} = 515 nm). Right: Fitting parameters including pre-exponential factors and confidence limits.

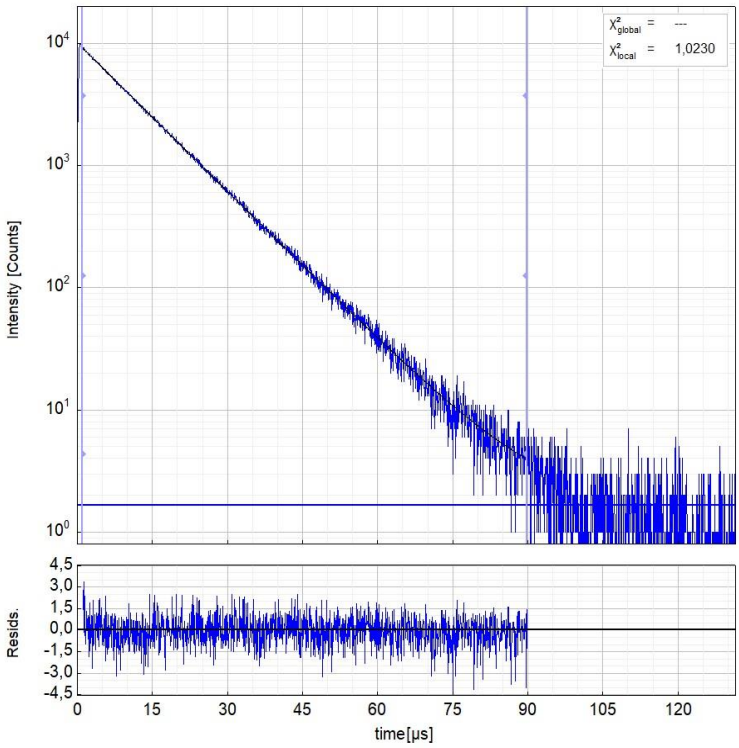

Parameter	Value	Δ	δ
A_1[kCnts/Chnl]	9,089	±0,027	0,3%
τ_1[ns]	10 717	±18	0,2%
I_1[kCnts]	1 521,9	±2,3	0,1%
A_{Rel1}[%]	100,0	---	---
I_{Rel1}[%]	100,0	---	---
$Bkgr_{Dec}$[kCnts]	0,0017	±0,0004	18%
τ_{AvInt}[ns]	10 717	±18	0,2%
τ_{AvAmp}[ns]	10 717	±18	0,2%

Figure S100. Raw time-resolved photoluminescence decay of **^{t}bu-Pt-CNR** in an Ar-purged liquid solution at RT (toluene, $c \approx 10^{-5}$ M), including the residuals (λ_{ex} = 376 nm, λ_{em} = 515 nm). Right: Fitting parameters including pre-exponential factors and confidence limits.

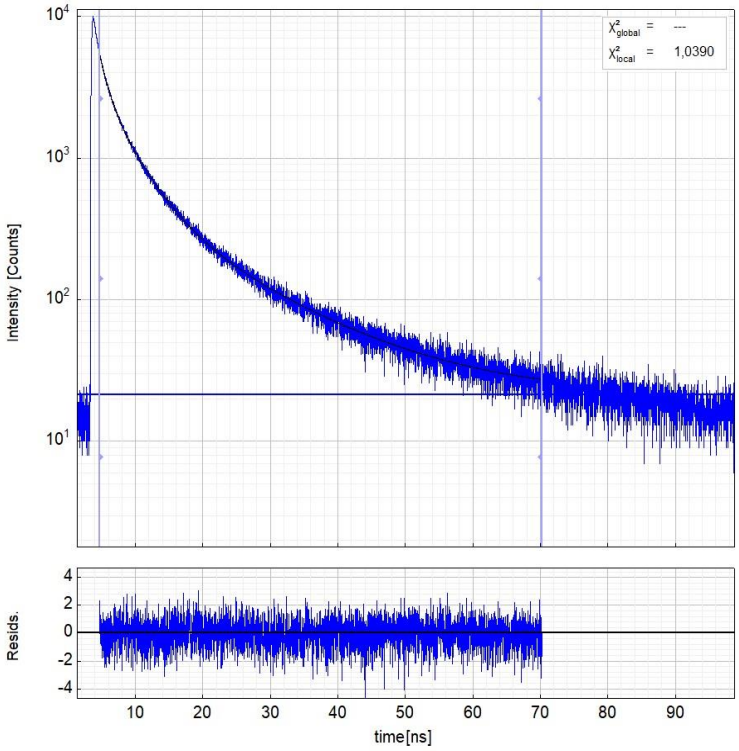

Parameter	Value	Δ	δ
A_1[kCnts/Chnl]	0,533	±0,063	12%
τ_1[ns]	14,56	±0,89	6,1%
I_1[kCnts]	485	±26	5,3%
A_{Rel1}[%]	9,8	±1,1	11%
I_{Rel1}[%]	37,2	±2,2	5,7%
A_2[kCnts/Chnl]	2,50	±0,11	4,1%
τ_2[ns]	4,10	±0,26	6,2%
I_2[kCnts]	639	±16	2,4%
A_{Rel2}[%]	45,7	±1,7	3,7%
I_{Rel2}[%]	49,1	±1,0	1,9%
A_3[kCnts/Chnl]	2,44	±0,13	4,9%
τ_3[ns]	1,183	±0,073	6,2%
I_3[kCnts]	180	±23	13%
A_{Rel3}[%]	44,6	±2,7	5,9%
I_{Rel3}[%]	13,8	±1,7	12%
$Bkgr_{Dec}$[kCnts]	0,0215	±0,0017	7,5%
τ_{AvInt}[ns]	7,58	±0,21	2,7%
τ_{AvAmp}[ns]	3,817	±0,040	1,0%

Figure S101. Left: Raw time-resolved photoluminescence decay of **^{t}bu-Pd-AmPy** in an air-equilibrated liquid solution at RT (toluene, $c \approx 10^{-5}$ M), including the residuals (λ_{ex} = 376 nm, λ_{em} = 513 nm). Right: Fitting parameters including pre-exponential factors and confidence limits.

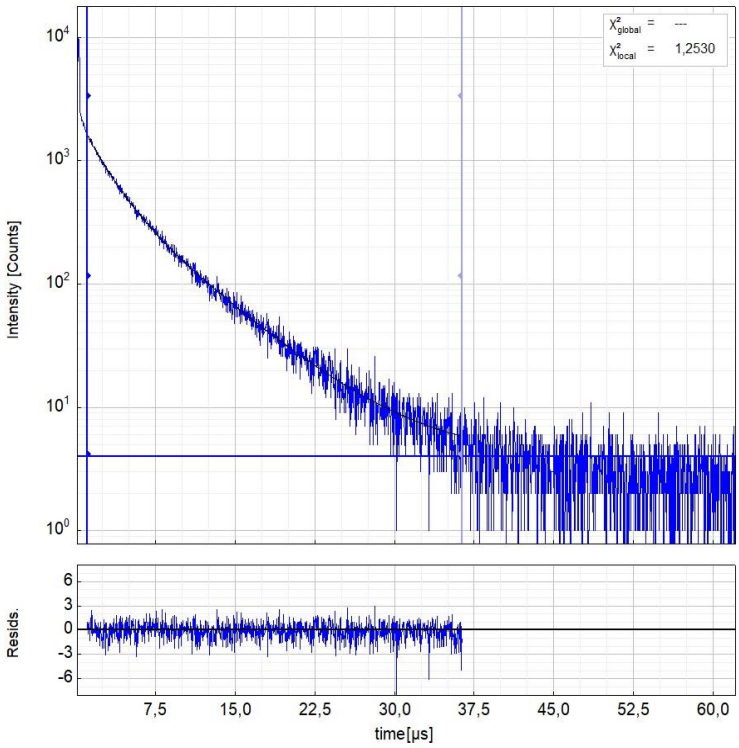

Parameter	Value	Δ	δ
A_1[kCnts/Chnl]	0,603	±0,048	7,8%
τ_1[ns]	6 090	±190	3,1%
I_1[kCnts]	114,7	±5,9	5,1%
A_{Rel1}[%]	37,7	±2,8	7,2%
I_{Rel1}[%]	63,8	±3,2	4,9%
A_2[kCnts/Chnl]	0,999	±0,037	3,6%
τ_2[ns]	2 090	±120	5,5%
I_2[kCnts]	65,2	±5,6	8,5%
A_{Rel2}[%]	62,4	±2,8	4,3%
I_{Rel2}[%]	36,3	±3,2	8,7%
$Bkgr_{Dec}$[kCnts]	0,0041	±0,0006	13%
τ_{AvInt}[ns]	4 639	±68	1,4%
τ_{AvAmp}[ns]	3 592	±44	1,2%

Figure S102. Left: Raw time-resolved photoluminescence decay of **^{t}bu-Pd-AmPy** in an Ar-purged liquid solution at RT (toluene, $c \approx 10^{-5}$ M), including the residuals (λ_{ex} = 376 nm, λ_{em} = 515 nm). Right: Fitting parameters including pre-exponential factors and confidence limits.

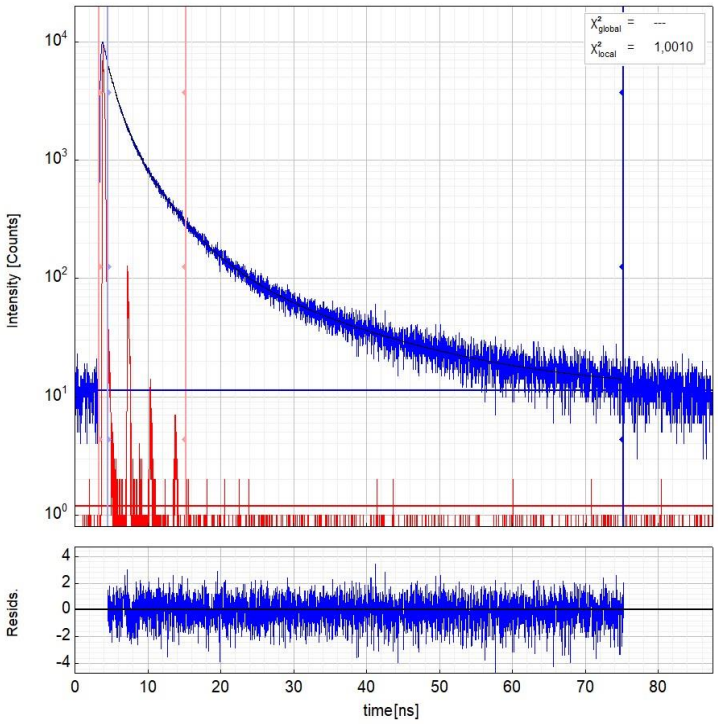

Parameter	Value	Δ	δ
A_1[kCnts/Chnl]	0,230	±0,034	14%
τ_1[ns]	16,2	±1,4	8,6%
I_1[kCnts]	232	±17	7,1%
A_{Rel1}[%]	2,6	±0,4	16%
I_{Rel1}[%]	16,3	±1,7	9,9%
A_2[kCnts/Chnl]	2,27	±0,13	5,5%
τ_2[ns]	4,37	±0,26	5,8%
I_2[kCnts]	620	±33	5,3%
A_{Rel2}[%]	24,8	±2,4	9,4%
I_{Rel2}[%]	43,6	±1,7	3,8%
A_3[kCnts/Chnl]	6,7	±1,2	18%
τ_3[ns]	1,369	±0,043	3,1%
I_3[kCnts]	580	±110	18%
A_{Rel3}[%]	72,8	±2,8	3,7%
I_{Rel3}[%]	40,3	±3,3	8,1%
$Bkgr_{Dec}$[kCnts]	0,0114	±0,0009	7,5%
$Bkgr_{IRF}$[Cnts/Chnl]	1,19	±0,80	67%
$Shift_{IRF}$[ps]	360	±230	61%
τ_{AvInt}[ns]	5,07	±0,22	4,3%
τ_{AvAmp}[ns]	2,48	±0,11	4,2%

Figure S103. Left: Raw time-resolved photoluminescence decay (in blue) of **^{t}bu-Pd-CNR** in an air-equilibrated liquid solution at RT (toluene, $c \approx 10^{-5}$ M; λ_{ex} = 376 nm, λ_{em} = 512 nm), including the residuals (in blue), and the instrument response function (IRF, in red). Right: Fitting parameters including pre-exponential factors and confidence limits.

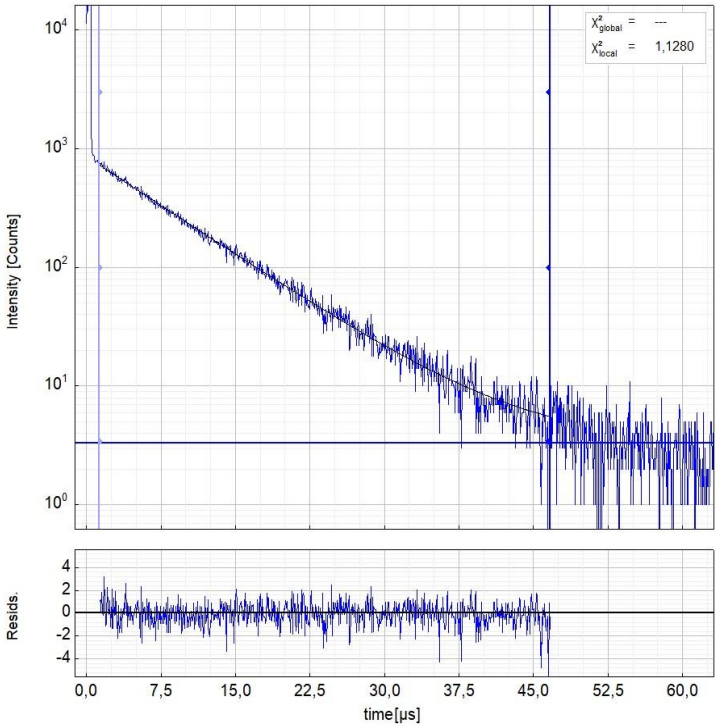

Parameter	Value	Δ	δ
A_1[kCnts/Chnl]	0,7196	±0,0039	0,5%
τ_1[ns]	7 846	±22	0,3%
I_1[kCnts]	88,21	±0,32	0,4%
A_{Rel1}[%]	100,0	---	---
I_{Rel1}[%]	100,0	---	---
$Bkgr_{Dec}$[kCnts]	0,0034	±0,0002	4,7%
τ_{AvInt}[ns]	7 846	±22	0,3%
τ_{AvAmp}[ns]	7 846	±22	0,3%

Figure S104. Left: Raw time-resolved photoluminescence decay of **^{t}bu-Pd-CNR** in an Ar-purged liquid solution at RT (toluene, $c \approx 10^{-5}$ M), including the residuals (λ_{ex} = 376 nm, λ_{em} = 512 nm). Right: Fitting parameters including pre-exponential factors and confidence limits.

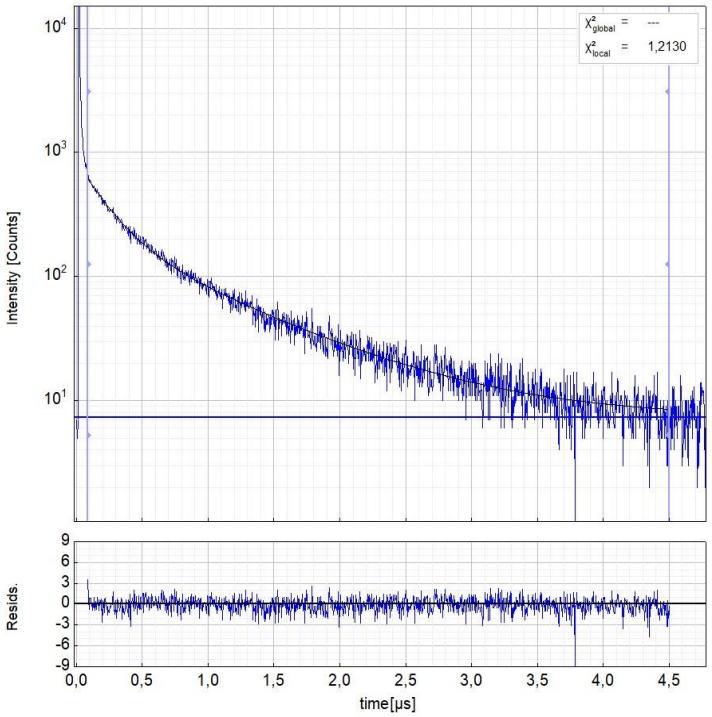

Parameter	Value	Δ	δ
A_1[kCnts/Chnl]	0,207	±0,013	6,3%
τ_1[ns]	852	±28	3,2%
I_1[kCnts]	44,0	±1,5	3,3%
A_{Rel1}[%]	34,2	±1,6	4,5%
I_{Rel1}[%]	68,7	±2,6	3,8%
A_2[kCnts/Chnl]	0,399	±0,014	3,5%
τ_2[ns]	203	±17	8,3%
I_2[kCnts]	20,2	±1,8	8,8%
A_{Rel2}[%]	65,9	±1,6	2,3%
I_{Rel2}[%]	31,4	±2,6	8,3%
$Bkgr_{Dec}$[kCnts]	0,0074	±0,0004	5,2%
τ_{AvInt}[ns]	648,1	±9,9	1,5%
τ_{AvAmp}[ns]	425	±11	2,4%

Figure S105. Left: Raw time-resolved photoluminescence decay of **CF_3-Pt-PPh_3** in an air-equilibrated liquid solution at RT (toluene, $c \approx 10^{-5}$ M), including the residuals (λ_{ex} = 376 nm, λ_{em} = 507 nm). Right: Fitting parameters including pre-exponential factors and confidence limits.

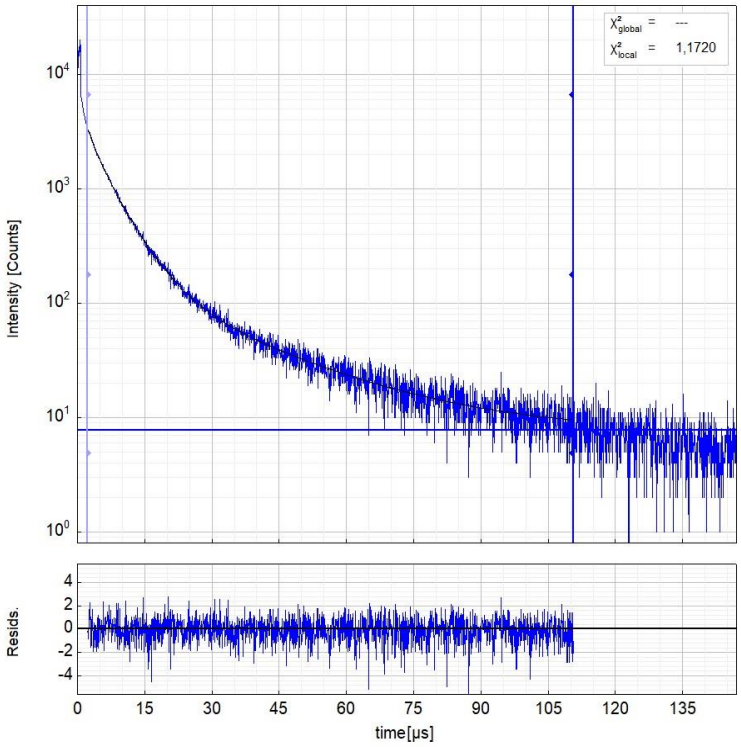

Parameter	Value	Δ	δ
A_1[kCnts/Chnl]	0,189	±0,030	16%
τ_1[ns]	23 400	±2 000	8,5%
I_1[kCnts]	68,8	±4,0	5,8%
A_{Rel1}[%]	5,7	±0,9	15%
I_{Rel1}[%]	23,6	±1,6	6,6%
A_2[kCnts/Chnl]	2,39	±0,24	9,9%
τ_2[ns]	5 420	±350	6,4%
I_2[kCnts]	201,7	±5,7	2,8%
A_{Rel2}[%]	71,6	±6,8	9,4%
I_{Rel2}[%]	69,1	±2,6	3,6%
A_3[kCnts/Chnl]	0,76	±0,26	33%
τ_3[ns]	1 820	±620	34%
I_3[kCnts]	22	±12	56%
A_{Rel3}[%]	22,8	±7,7	33%
I_{Rel3}[%]	7,4	±4,1	55%
$Bkgr_{Dec}$[kCnts]	0,0078	±0,0009	11%
τ_{AvInt}[ns]	9 380	±350	3,6%
τ_{AvAmp}[ns]	5 616	±68	1,2%

Figure S106. Left: Raw time-resolved photoluminescence decay of **CF_3-Pt-PPh_3** in an Ar-purged liquid solution at RT (toluene, $c \approx 10^{-5}$ M), including the residuals (λ_{ex} = 376 nm, λ_{em} = 507 nm). Right: Fitting parameters including pre-exponential factors and confidence limits.

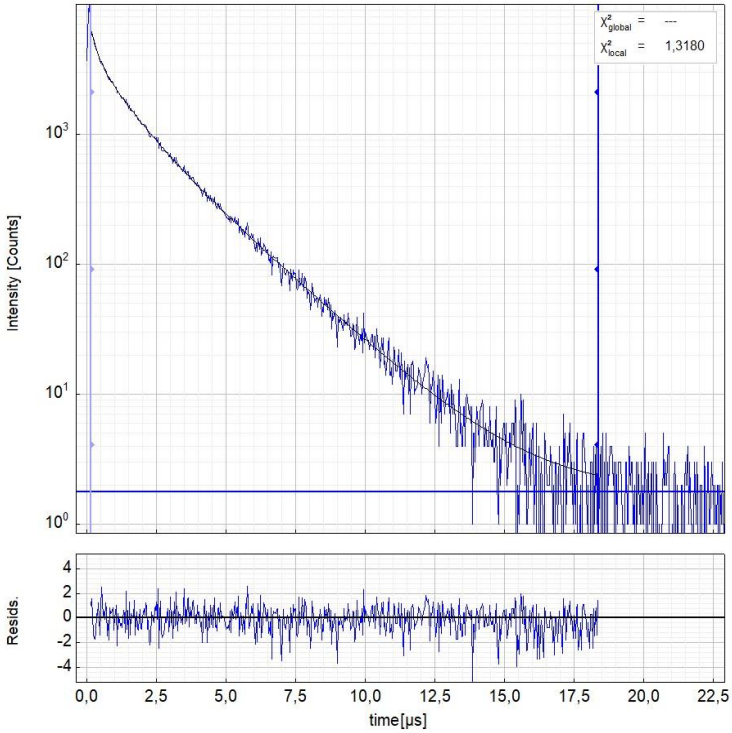

Parameter	Value	Δ	δ
A_1[kCnts/Chnl]	1,97	±0,34	17%
τ_1[ns]	2 250	±110	4,6%
I_1[kCnts]	139	±19	13%
A_{Rel1}[%]	31,1	±4,8	15%
I_{Rel1}[%]	63,0	±8,4	13%
A_2[kCnts/Chnl]	2,30	±0,16	6,7%
τ_2[ns]	970	±170	17%
I_2[kCnts]	69	±15	21%
A_{Rel2}[%]	36,2	±2,2	5,9%
I_{Rel2}[%]	31,4	±6,6	21%
A_3[kCnts/Chnl]	2,09	±0,34	16%
τ_3[ns]	192	±49	26%
I_3[kCnts]	12,6	±4,2	33%
A_{Rel3}[%]	32,9	±3,9	12%
I_{Rel3}[%]	5,8	±1,9	33%
$Bkgr_{Dec}$[kCnts]	0,0018	±0,0004	21%
τ_{AvInt}[ns]	1 724,5	±6,3	0,4%
τ_{AvAmp}[ns]	1 107	±56	5,0%

Figure S107. Left: Raw time-resolved photoluminescence decay of **^{t}bu-Pt-PPh$_3$** in an air-equilibrated liquid solution at RT (toluene, $c \approx 10^{-5}$ M), including the residuals (λ_{ex} = 376 nm, λ_{em} = 511 nm). Right: Fitting parameters including pre-exponential factors and confidence limits.

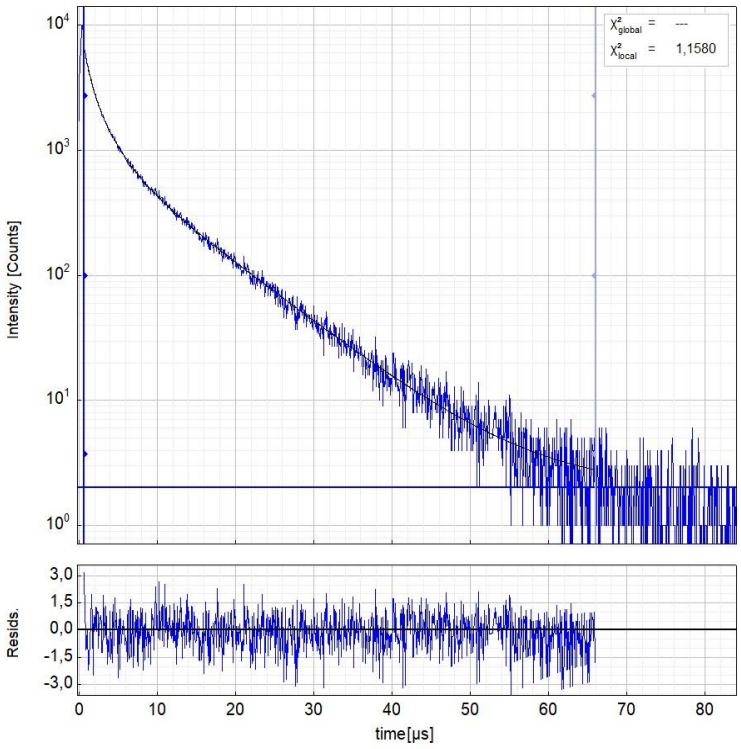

Parameter	Value	Δ	δ
A_1[kCnts/Chnl]	1,05	±0,12	11%
τ_1[ns]	9 070	±340	3,7%
I_1[kCnts]	149	±12	8,0%
A_{Rel1}[%]	16,4	±2,0	12%
I_{Rel1}[%]	53,7	±4,7	8,7%
A_2[kCnts/Chnl]	2,49	±0,83	33%
τ_2[ns]	2 420	±790	32%
I_2[kCnts]	94	±13	14%
A_{Rel2}[%]	39	±14	34%
I_{Rel2}[%]	33,9	±4,7	14%
A_3[kCnts/Chnl]	2,87	±0,99	35%
τ_3[ns]	770	±220	27%
I_3[kCnts]	35	±25	71%
A_{Rel3}[%]	45	±16	34%
I_{Rel3}[%]	12,5	±8,8	70%
$Bkgr_{Dec}$[kCnts]	0,0021	±0,0006	25%
τ_{AvInt}[ns]	5 783	±48	0,8%
τ_{AvAmp}[ns]	2 770	±44	1,6%

Figure S108. Left: Raw time-resolved photoluminescence decay of **^{t}bu-Pt-PPh$_3$** in an Ar-purged liquid solution at RT (toluene, $c \approx 10^{-5}$ M), including the residuals (λ_{ex} = 376 nm, λ_{em} = 511 nm). Right: Fitting parameters including pre-exponential factors and confidence limits.

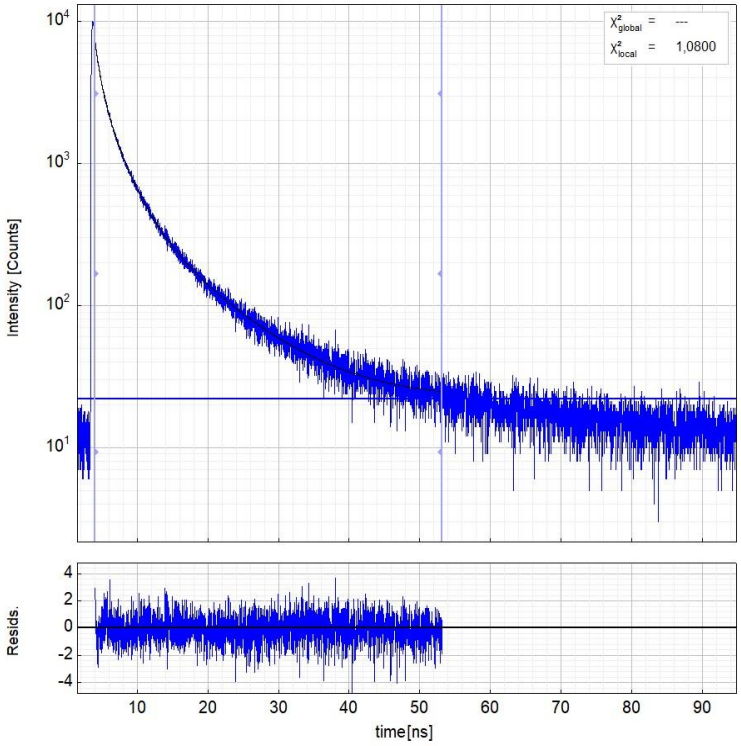

Parameter	Value	Δ	δ
A_1[kCnts/Chnl]	0,663	±0,099	15%
τ_1[ns]	9,01	±0,66	7,2%
I_1[kCnts]	373	±33	8,8%
A_{Rel1}[%]	9,3	±1,4	15%
I_{Rel1}[%]	36,7	±3,4	9,1%
A_2[kCnts/Chnl]	3,10	±0,26	8,3%
τ_2[ns]	2,56	±0,26	9,8%
I_2[kCnts]	494,4	±6,6	1,3%
A_{Rel2}[%]	43,3	±3,5	7,9%
I_{Rel2}[%]	48,6	±0,5	1,0%
A_3[kCnts/Chnl]	3,40	±0,33	9,6%
τ_3[ns]	0,708	±0,077	11%
I_3[kCnts]	151	±33	22%
A_{Rel3}[%]	47,5	±4,8	10%
I_{Rel3}[%]	14,8	±3,2	21%
$Bkgr_{Dec}$[kCnts]	0,0219	±0,0009	3,8%
τ_{AvInt}[ns]	4,648	±0,081	1,7%
τ_{AvAmp}[ns]	2,276	±0,035	1,5%

Figure S109. Left: Raw time-resolved photoluminescence decay of **^{t}bu-Pd-PPh$_3$** in an air-equilibrated liquid solution at RT (toluene, $c \approx 10^{-5}$ M), including the residuals (λ_{ex} = 376 nm, λ_{em} = 516 nm). Right: Fitting parameters including pre-exponential factors and confidence limits.

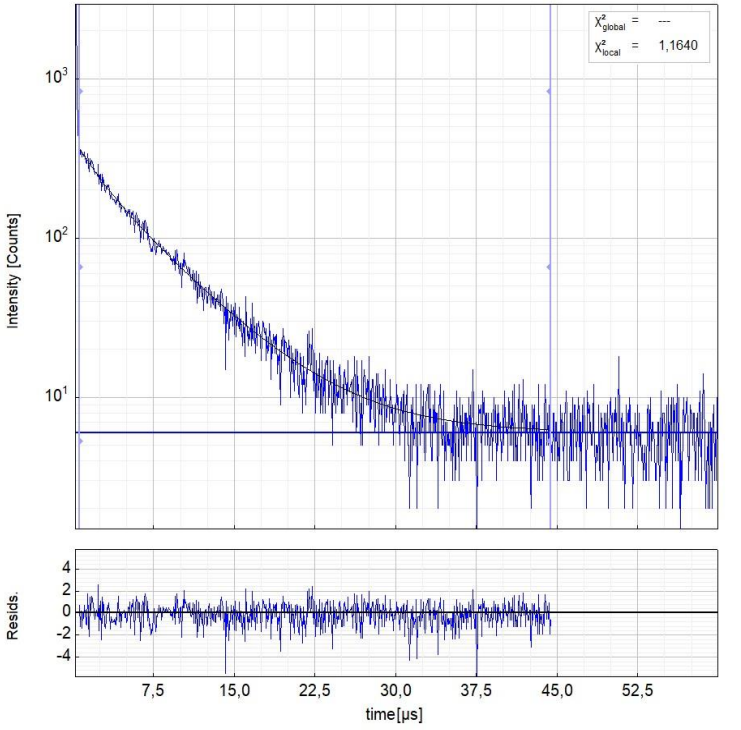

Parameter	Value	Δ	δ
A_1[kCnts/Chnl]	0,258	±0,043	16%
τ_1[ns]	6 330	±560	8,8%
I_1[kCnts]	25,5	±2,4	9,1%
A_{Rel1}[%]	72	±12	16%
I_{Rel1}[%]	88,9	±9,3	10%
A_2[kCnts/Chnl]	0,101	±0,040	39%
τ_2[ns]	2 040	±780	38%
I_2[kCnts]	3,2	±2,8	85%
A_{Rel2}[%]	29	±12	40%
I_{Rel2}[%]	11,2	±9,3	83%
$Bkgr_{Dec}$[kCnts]	0,0061	±0,0005	8,1%
τ_{AvInt}[ns]	5 850	±190	3,1%
τ_{AvAmp}[ns]	5 120	±160	3,0%

Figure S110. Left: Raw time-resolved photoluminescence decay of **^{t}bu-Pd-PPh$_3$** in an Ar-purged liquid solution at RT (toluene, $c \approx 10^{-5}$ M), including the residuals (λ_{ex} = 376 nm, λ_{em} = 516 nm). Right: Fitting parameters including pre-exponential factors and confidence limits.

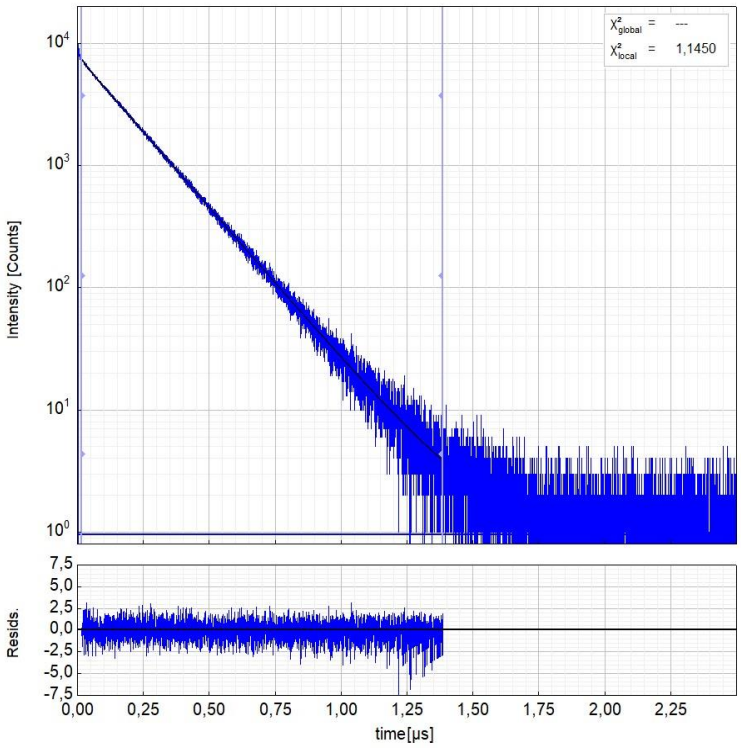

Parameter	Value	Δ	δ
A_1[kCnts/Chnl]	7,1284	±0,0087	0,1%
τ_1[ns]	175,39	±0,14	0,1%
I_1[kCnts]	4 883,8	±3,8	0,1%
A_{Rel1}[%]	96,9	±0,6	0,6%
I_{Rel1}[%]	99,7	±0,1	0,1%
A_2[kCnts/Chnl]	0,231	±0,046	20%
τ_2[ns]	17,1	±2,5	14%
I_2[kCnts]	15,4	±2,9	19%
A_{Rel2}[%]	3,2	±0,6	19%
I_{Rel2}[%]	0,4	±0,1	19%
$Bkgr_{Dec}$[kCnts]	0,0010	±0,0002	13%
τ_{AvInt}[ns]	174,90	±0,13	0,1%
τ_{AvAmp}[ns]	170,44	±0,89	0,5%

Figure S111. Left: Raw time-resolved photoluminescence decay of **^{t}bu-Pt-PTA** in an air-equilibrated liquid solution at RT (toluene, $c \approx 10^{-5}$ M), including the residuals (λ_{ex} = 376 nm, λ_{em} = 510 nm). Right: Fitting parameters including pre-exponential factors and confidence limits.

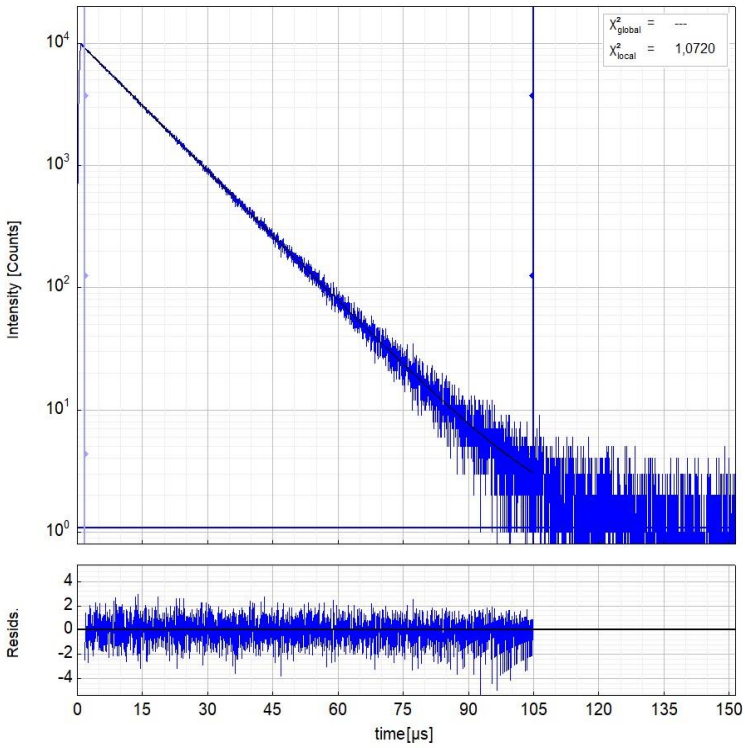

Parameter	Value	Δ	δ
A_1[kCnts/Chnl]	9,118	±0,026	0,3%
τ_1[ns]	12 214	±25	0,2%
I_1[kCnts]	3 479,8	±4,7	0,1%
A_{Rel1}[%]	100,0	---	---
I_{Rel1}[%]	100,0	---	---
$Bkgr_{Dec}$[kCnts]	0,0011	±0,0002	17%
τ_{AvInt}[ns]	12 214	±25	0,2%
τ_{AvAmp}[ns]	12 214	±25	0,2%

Figure S112. Left: Raw time-resolved photoluminescence decay of **^{t}bu-Pt-PTA** in an Ar-purged liquid solution at RT (toluene, $c \approx 10^{-5}$ M), including the residuals (λ_{ex} = 376 nm, λ_{em} = 510 nm). Right: Fitting parameters including pre-exponential factors and confidence limits.

References

(1) Mydlak, M.; Mauro, M.; Polo, F.; Felicetti, M.; Leonhardt, J.; Diener, G.; De Cola, L.; Strassert, C. A. Controlling Aggregation in Highly Emissive Pt(II) Complexes Bearing Tridentate Dianionic N^N^N Ligands. Synthesis, Photophysics, and Electroluminescence. *Chem. Mater.* **2011**, *23* (16), 3659.

(2) Sanning, J.; Ewen, P. R.; Stegemann, L.; Schmidt, J.; Daniliuc, C. G.; Koch, T.; Doltsinis, N. L.; Wegner, D.; Strassert, C. A. Scanning-Tunneling-Spectroscopy-Directed Design of Tailored Deep-Blue Emitters. *Angew. Chemie Int. Ed.* **2015**, *54* (3), 786–791. https://doi.org/https://doi.org/10.1002/anie.201407439.

(3) Gangadharappa, S. C.; Maisuls, I.; Schwab, D. A.; Kösters, J.; Doltsinis, N. L.; Strassert, C. A. Compensation of Hybridization Defects in Phosphorescent Complexes with Pnictogen-Based Ligands—A Structural, Photophysical, and Theoretical Case-Study with Predictive Character. *J. Am. Chem. Soc.* **2020**, *142* (51), 21353–21367. https://doi.org/10.1021/jacs.0c09467.